The role of GPR111 in adipose tissue

Dissertation

zur

Erlangung des Doktorgrades (Dr. rer. nat.)

der

Mathematisch-Naturwissenschaftlichen Fakultät

der

Rheinischen Friedrich-Wilhelms-Universität Bonn

vorgelegt von

Jelena Zurkovic

aus

Sombor, Serbien

Bonn, 2020

Angefertigt mit Genehmigung der Mathematisch-Naturwissenschaftlichen Fakultät der Rheinischen Friedrich-Wilhelms-Universität Bonn

1. Gutachter: Prof. Dr. Alexander Pfeifer

2. Gutachter: Prof. Dr. Christa Müller

Tag der Promotion: 24.03.2021

Erscheinungsjahr: 2021

Acknowledgements

First of all, I would like to thank Prof. Dr. Alexander Pfeifer for his support, tolerance and guidance throughout my doctoral studies. I am grateful for everything he did for me. It was my honor to do my PhD under his supervision. I would like to thank Dr. Meis-Klomfass for proofreading my thesis and for her guidance and help with the graduate school. Also, I would like to thank Prof. Dr. Christa Müller for her comments, questions and help during my Colloquiums and retreats. Besides them, I would like to thank DFG (Deutsche Forschungsgemeinschaft) for funding.

Furthermore, I would like to thank my supervisors, Aga and Katarina, with them I made my first experiments at this institute. After those amazing girls, for almost two years, Dr. Abhishek Sanyal took care of me. He was my lab-father. He taught me all tricks and thanks to him I had always perfect Western blot and the best white adipocytes. I am thankful for his help and support and I hope that one day I will supervise students like he supervised me. After Dr.Sanyal, Dr. Hildebrand and Dr.Reverte, adopted me. Dr Hildebrant solved all my cloning problems and Dr. Reverte was always there when I had questions regarding signaling pathways. Both of them had a great impact on me and my work and I will never forget how much they did for me.

Specially I would like to thank Dani for teaching me how to work with mice, how to be perfectly organized and always positive.

On my thank you list are my office mates Juhee and Bini. Those girls were always ready to help. They made my life during the studies much easier and today they are one of my best friends.

However, nothing of this wouldn’t happened without Prof. Dr. Miroslav Savic. I am more than thankful for every advice, suggestion and support that he gave me. He is my role model and I hope that one day I will be at least as half good as he is. Without him I would never fall in love in pharmacology.

On a personal note, I would like to thank my parents for all the sacrifice that they made for me. I hope that one day I will somehow return everything that they did for me.

Lastly, I would like to thank my Stefan for proofreading my thesis and for everything that he did for me. His constant support and encouragement helped me to go through the most difficult time. I am sure that I wouldn’t be here without him.

Table of contents

Acknowledgements ..... ***I***
Table of contents ..... ***II***
Abbreviations ..... ***VII***
1. Introduction ***1***

1.1. G-protein coupled receptors **1**

1.1.2. The signaling of GPCRs *1*

1.2. Adhesion G protein coupled receptors **3**

1.2.1. Classification and nomenclature of adhesion G protein coupled receptors *3*

1.2.2. The structure of aGPCRs *3*

1.2.3. Activation and signaling of aGPCRs *5*

1.2.4. The structure of Gpr111 ..... *5*

1.2.5. Physiological role of aGPCRs *6*

1.2.6. Physiological role of Gpr111 ..... *7*

1.3. Obesity **7**

1.3.1. Adipose tissue (AT) *8*

1.3.1.1. Brown adipose tissue (BAT) *10*

1.3.1.2. White adipose tissue (WAT) *11*

1.3.1.3. Beige/brite adipocytes *12*

1.4. Cilia and ciliopathies **13**

1.4.1. Structure of primary cilium *14*

1.4.2. Canonical and non-canonical Hedgehog signaling (HH) *15*

1.5. Aim of the PhD thesis **16**

2. Material and methods ***17***

2.1. Chemicals and compounds 17

2.2. In vivo experiments 17

2.2.1. Animals 17

2.2.2. Diet induced obesity (DIO) experiments 17

2.2.3. Long term cold exposure 18

2.3. Cell culture methods 18

2.3.1. Materials in cell culture 18

2.3.2. Equipment in cell culture 20

2.3.3. Isolation and culture of stromal vascular fraction (SVF) from BAT 20

2.3.3.1. Immortalization procedure 22

2.3.3.2. Trypsinization and cryo preservation of BAs 22

2.3.3.3. Differentiation of immortalized brown adipocytes 22

2.3.4. Isolation and culture of stromal vascular fraction (SVF) from WATi 23

2.3.4.1. Differentiation of white adipocytes 24

2.3.5. Oil Red O staining of differentiated adipocytes 25

2.3.6. Glycerol assay (lipolysis) 26

2.3.6.1. Ex vivo lipolysis 27

2.3.7. Measurement of mitochondrial respiration 27

2.3.7.1. Preparation and calibration of oxygraph 28

2.3.7.2. Cell preparation for oxygraph measurements 28

2.3.7.3. Adipose tissue preparation for oxygraph measurement 29

2.4. Immunological methods 30

2.4.1. Materials 30

2.4.2. Equipment 30

2.4.3. EdU Proliferaton assay and microscopy *30*

2.4.4. Immunofluorescence (IF) staining of cilia *31*

2.4.5. Phalloidin staining of stress fibers *32*

2.4.6. Serum leptin level measurement (Leptin ELISA) *32*

2.4.7. cAMP concentration (cAMP ELISA) *32*

2.5. Biochemical methods 32

2.5.1. Materials *32*

2.5.2. Equipment *33*

2.5.3. Western blotting *33*

2.5.3.1. Protein extraction from fat tissues *33*

2.5.3.2. Protein extraction from cells *34*

2.5.3.3. Quantification of proteins with the Bradford protein assay *34*

2.5.3.4. Sample preparation for Western blot *35*

2.5.3.5. Sodium dodecyl-sulphate polyacrylamide gel electrophoresis (SDS-PAGE) *35*

2.5.3.6. Western blotting *36*

2.6. Molecuar biology methods 38

2.6.1. Materials *38*

2.6.2. Equipment *38*

2.6.3. Preparation of genomic DNA and genotyping *39*

2.6.4. Agarose gel electrophoresis *39*

2.7. RNA isolation and reverse transcription 40

2.7.1. RNA extraction from the tissue with high lipid content *40*

2.7.1.2. RNA extraction from cells *40*

2.7.1.3. cDNA synthesis *41*

2.7.1.4. Quantitative real-time polymerase chain reaction (qRT-PCR) 41

2.8. Immunohistochemistry 42

2.8.1. Materials 42

2.8.2. Equipment 43

2.8.3. Sample preparation 43

2.8.4. Hematoxylin/Eosin staining (H&E) 43

2.8.5. UCP1 staining 44

2.9. Statistical analysis 45

3. Results 45

3.1. Expression pattern of Gpr111 45

3.2. Role of Gpr111 in BAs 48

3.2.1. Loss of Gpr111 promotes differentiation of BAs 48

3.2.2. Effects of Gpr111 ablation on BAs function 48

3.2.3. Lack of Gpr111 has no effect on proliferation of BAs 50

3.3. Role of Gpr111 in WAs 52

3.3.1. Loss of Gpr111 promotes differentiation and browning of WAs 52

3.3.2. Effects of Gpr111 deletion on function of WAs 53

3.3.3. Lack of Gpr111 increases proliferation of WAs 56

3.4. Lack of Gpr111 in adult mice increases energy expenditure (EE) 57

3.4.1. Lack of Gpr111 in adult mice promotes browning of WAT 59

3.5. Cold exposure of Gpr111$^{-/-}$ mice cause metabolic changes 61

3.5.1. Cold exposure of Gpr111$^{-/-}$ mice induces massive browning of WAT ... 63

3.6. Analysis of the effect of DIO in GPR111 KO mice 65

3.6.1. Analysis of UCP1 in AT of Gpr111 KO mice on HFD 68

3.7. Molecular mechanism of Gpr111 signaling 73

3.7.1. Gpr111 signaling is related to HH signaling in cilia 73

3.7.2. Interplay between GPR111, cAMP signaling and mechanical force 76

4. Discussion 79

4.1. Role of Gpr111 in differentiation, proliferation and function of brown and white adipocytes 79

4.2. Potential Gpr111 signaling 80

4.3. Role of Gpr111 in AT of adult mice 82

4.4. Metabolic changes of KO mice after cold exposure 83

4.5. Changes in Gpr111 KO mice upon HFD 84

5. Summary 85

6. References 87

List of Figures 98

List of Tables 100

Abbreviations

ABP-L-Ascorbate, d-Biotin, Panthothenate
AcCoA- acetyl coenzyme A
Acaca1a-Acyl-Coenzyme A carboxylase gene (*Mus musculus*)
Adrb3-Adrenergic Beta-3 Receptor gene (*Mus musculus*)
aGPCRs-adhesion G protein coupled receptors
aP2-Adipocyte protein 2 (same as FABP4)
AT-Adipose tissue
ATP-Adenosine triphosphate
β-ox-beta oxidation
BA-Brown adipocyte
BAT-Brown adipose tissue
BBS-Bardet-Biedl Syndrome
BSA-Bovine serum albumin
CAC-citric acid cycle
Ccl2-chemokine (C-C motif) ligand 2 gene (*Mus musculus*)
cAMP-Cyclic 3',5'- adenosine monophosphate
cDNA-complementary DNA
cGMP-Cyclic 3'-5' guanosine monophosphate
CTF-C terminal fragment
DAB-3-3' diaminobenzidine
Dhh-desert hedgehog signaling
DIO-Diet-induced obesity
DMEM-Dulbecco's Modified Eagle Medium
DMSO-dimethyl sulfoxide
DNA-deoxyribonucleic acid
ECD-extracellular domain
EDTA-ethylene diamine tetraaceitic acid
EE-energy expenditure
ECM-extracellular matrix
EGTA-Ethylene glycol-bis (β-aminoethyl ether) - N, N, N', N'-tetraacetic acid
EtOH-ethanol
EPAC-exchange factor directly activated by cAMP
Fabp4-Fatty acid binding protein 4 (aP2/ FABP4) gene (*Mus musculus*)
Fasn-Fatty acid synthase gene (*Mus musculus*)
FBS-foetal bovine serum
FFA-free fatty acids
FADH-flavine adenine dinucleotide
FACS-fluorescence-activated cell sorting
Gapdh-glycerol aldehyde-3-phosphate dehydrogenase (*Mus musculus*)
Glut4-Glucose Transporter Type 4 gene (*Mus musculus*)
GMP-Guanosine monophosphate
GTP-Guanosine triphosphate
GDP-Guanosine diphosphate
Gli1,2,3-glioma-associated oncogene

Gli-FL- transcriptional repressor full-length Gli
GliA-active form of Gli
Gpr111-G protein coupled receptor 111
Gpr111- G protein coupled receptor 111 gene (*Mus musculus*)
h-hours
HBSS-Hanks' balanced salt solution
H&E-hematoxylin/eosin staining
HFD-high fat diet
HRP-horseradish peroxidase
Hprt-hypoxanthine-guanine-phosphoribosyltransferas (*Mus musculus*)
HSL- hormone sensitive lipase
HH- hedgehog signaling
IBMX-3-isobutyl-1-methylxanthine
ICD-intracellular domain
Ihh- Indian hedgehog signaling
IF- immunofluorescence
i.p- intraperitoneal
KO-knock out
Lep-leptin gene (*Mus musculus*)
LepR-leptin receptor (*Mus musculus*)
Lpl-Lipoprotein lipase gene (*Mus musculus*)
M/mM/µM-molar/millimolar/micromolar
ml/µl-milliliter/microliter
mg/µg-milligram/microgram
min-minutes
mRNA–messenger ribonucleic acid
MSCs-mesenchymal stem cells
Nm-nanometer
nM-nanomolar
NaCl-sodium chloride
NADH-nicotinamide adenine dinucleotide
NaF-sodium fluoride
Na2HPO4-disodium hydrogenphosphate
NaN3-sodium azid
Na3VO4-sodium orthovanadate
ND-normal diet
NE-norepinephrine
NGS-normal goat serum
NH4OAc-ammonium acetate
NMR-nuclear magnetic resonance
NST-Non-shivering thermogenesis
NTF-N terminal fragment
o/n-over night
P/S-Penicillin/ Streptomycin
PBS-Phosphate buffered saline
PCR-polymerase chain reaction

PGC1α-Peroxisome proliferator associated protein gamma (PPARγ cofactor 1 alpha)
PFA-paraformaldehyde
PKA- protein kinase A
***Plin1*-**Perilipin 1 gene (*Mus musculus*)
***Pparγ*-**Peroxisome proliferator associated protein gamma (PPARγ gene (*Mus musculus*)
***Ppargc1α*-**Peroxisome proliferator associated protein gamma (PPARγ cofactor 1 alpha gene (*Mus musculus*)
PPARγ-Peroxisome proliferator associated protein gamma
PRDM16-PR-Domain Zinc Finger Protein 16
Ptch1-Protein patched homolog 1
RT-room temperature
RhoA- Ras homology gene family, member A
ROCKs-Ras homology gene family, member A (RhoA) associated protein kinases
rpm-rotations per minute
qRT-PCR-Quantitative real-time polymerase chain reaction
SAG-Smoothened agonist
SDS-PAGESodium dodecyl-sulphate polyacrylamide gel electrophoresis
SEM-standard error of the mean
Shh-sonic hedgehog signaling
Smo-Smoothened
SV40-simian virus 40
SVF-stromal vascular fraction
7TM- seven transmembrane domin
T2DM-Type 2 diabetes mellitus
T3-Triiodothyronine
TAg SV40-large tumor antigen
TBS-T-Tris buffered saline – Tween 20 (0.1%)
TCA- tricarboxylic acid cycle
TEMEDN, N, N', N'-Tetramethyl ethylene diamine
TG-Triglyceride
***Tnfα*-**Tumor necrosis factor alpha (TNFα) gene (*Mus musculus*)
UCP1-Uncoupling protein 1
Ucp1-Uncoupling protein 1 gene (*Mus musculus*)
WA-White adipocytes
WAT-White adipose tissue
WATg-Gonadal white adipose tissue
WATi-Inguinal white adipose tissue
WB-Western blot
WHO-world health organisation
WT-wild type

1. Introduction

1.1. G-protein coupled receptors

G protein coupled receptors (GPCRs) are the largest family of membrane proteins and they mediate most cellular responses to hormones and neurotransmitters, as well as being responsible for vision, olfaction and taste (Rosenbaum et al., 2009). They are always in the research focus because, GPCRs are the most common targets for therapeutic drugs for a large number of diseases in humans (Sriram and Insel, 2018). In mammals GPCRs are divided according to their sequence and structural similarity into 5 groups (Rosenbaum et al., 2009): the largest being the rhodopsin family, or class A, with about 284 members (plus about 380 olfactory receptors) in humans, followed by the adhesion GPCR family with 33 members, and then the glutamate family (class C), secretin family (class B), and frizzled family, with 22, 15, and 11 members, respectively (Yona et al., 2008).The main characteristic of all GPCRs is a 7 transmembrane domain (7TM) or α-helix that is associating extra and intracellular loop regions (Rosenbaum et al. 2009). Although GPCRs are very similar, some GPCRs have a unique molecular structure and exclusive signal transduction (Rosenbaum et al. 2009). Canonical GPCR activation begins with the binding of extracellular ligands/agonists, which causes conformational changes in the receptor and consequently activation of G proteins (Yona et al. 2008) which in return leads to the modulation of downstream proteins. GPCR signaling is complex, because many receptors possess constitutive activity. For some of them β-arrestin-mediated internalization, oligomerisation, compartmentalization etc. is characteristic (Yona et al. 2008).

Ligands that are activating GPCRs are classified into agonists, inverse agonists, and antagonists. Agonists binding to GPCRs promote active conformational changes of GPCR, which increases the signaling. Inverse agonists inhibit constitutive activity by stabilizing an inactive conformation of GPCRs. Antagonists have no effect on the active and inactive conformations of GPCRs, but they prevent binding of both agonists and inverse agonists (Syrovatkina et al., 2016).

1.1.2. The signaling of GPCRs

The main role in signal transduction from GPCRs on the plasma membrane to the inside of the cell belongs to heterotrimeric G proteins (Syrovatkina et al., 2016). G proteins belong to a family of GTP hydrolases. Each G protein has three subunits α, β and γ and a nucleotide binding pocket, which is located on α subunit (Syrovatkina et al., 2016). Activation of G proteins starts after binding of a ligand for GPCR. This event leads to a fast nucleotide exchange from GDP to GTP. This exchange causes a dissociation of G protein from GPCR. Further on, G protein dissociates into free, active α subunit and βγ complex, which activate different proteins that will, in the end, cause physiological responses (Jastrzebska, 2013) (Figure1).

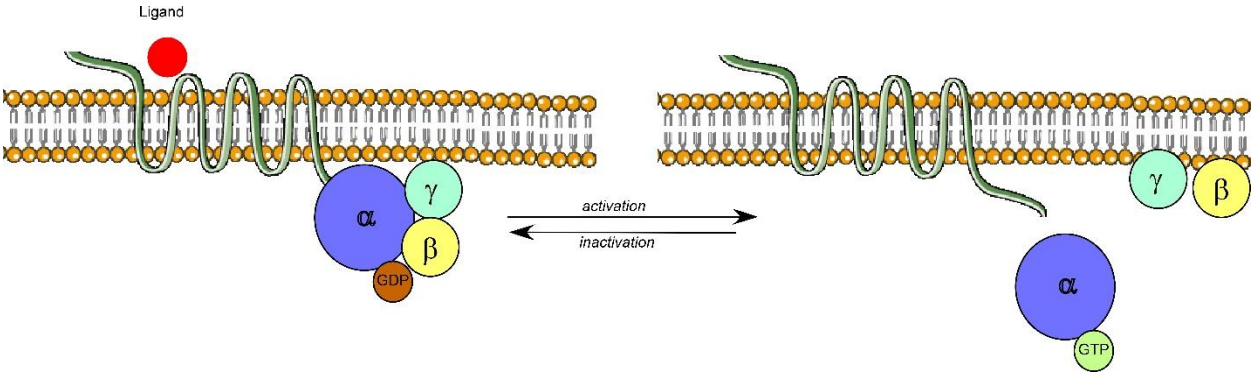

Figure 1: Activation of GPCRs
Simplified mechanism of GPCRs activation. Picture was generated using online available tools **https://smart.servier.com/page/17/?s=protein+coupled+receptor**. GDP, guanosine diphosphate; GTP, guanosine triphosphate.

Gα subunit signaling is limited by the intrinsic GTPase activity of this subunit which hydrolyzes the bound GTP to GDP; on the other hand the Gβγ signaling is limited by re-association with α subunit (Syrovatkina et al., 2016).

Gα subunit can interact with many proteins and according to that, G proteins are divided into 4 groups $G\alpha_s$, $G\alpha_i$, $G\alpha_q$ and $G\alpha_{12/13}$ (Syrovatkina et al., 2016).Target protein for $G\alpha_s$ and $G\alpha_i$ is adenylyl cyclase. $G\alpha_s$ stimulates adenylyl cyclase and $G\alpha_i$ is inhibiting this enzyme, which leads to elevation ($G\alpha_s$) or reduction ($G\alpha_i$) of cyclic adenosine monophosphate (cAMP) levels (Wettschureck and Offermanns, 2005). Elevated cAMP in case of $G\alpha_s$ signaling will activate cAMP-regulated proteins, such as protein kinase A (PKA), cyclic nucleotide-gated channels, and exchange factor directly activated by cAMP (EPAC). On the other hand, $G\alpha_i$ will have an opposite effect on cAMP levels (Syrovatkina et al., 2016).

$G\alpha_q$ family of G-proteins activates the β-isoforms of phospholipase C (PLC-β1-4), which cleaves phosphatidylinositol 4,5-bisphosphate (PP2) into inositol trisphosphate (IP_3) and membrane-bound diacylglycerol (DAG) (Rhee and Bae, 1997). IP_3 then opens the calcium channel IP_3 receptor on the membrane of the endoplasmic reticulum (ER), and DAG activates protein kinase C (PKC) (Syrovatkina et al., 2016).

$G\alpha_{13}$ increases the activity of different RhoGEF proteins, tyrosine kinase, cadherin and some integrins (Syrovatkina et al., 2016).

Several proteins, such as Btk-family tyrosine kinases, Gap1, RasGAP, cadherins, α-SNAP, and p120-caterin, were reported to interact with $G\alpha_{12}$ (Jiang et al., 1998).

Additionally, Gβγ subunit can also signal further and regulate adenylyl cyclase, phospholipase Cβ, K^+ channel, and voltage-gated Ca^{2+}channels (Khan et al., 2013).

1.2. Adhesion G protein coupled receptors

1.2.1. Classification and nomenclature of adhesion G protein coupled receptors

Human adhesion G protein coupled receptors (aGPCRs) are divided into 9 subfamilies and each subfamily is assigned with roman numbers (I-IX). Nomenclature of aGPCR is highly diverse. Initial names of the receptors were given without any harmonization, later all receptors in their name had prefix GPR and appropriate number. The International Union of Basic and Clinical Pharmacology (IUPHAR) Committee on Receptor Nomenclature and Drug Classification (NC-IUPHAR) together with the Adhesion GPCR Consortium proposed a new nomenclature that is suitable for any aGPCRs, independent of species and subfamily. The common prefix for all members is ADGR and it comes from Adhesion G protein-coupled Receptors, each subfamily is additionally assigned with a letter, related to the previous nomenclature, i.e. latrophilin receptors (ADGRL) (Hamann et al., 2015).

TABLE 1
Proposed new nomenclature for Adhesion GPCRs

Subfamily		Receptor		
Current Number	Proposed New Name	Current Gene Name	Current Protein Name (Alternative Names)	Proposed New Name
I	L (Latrophilin)	*LPHN1*	Latrophilin 1 (CIRL-1, CL1, LEC2)	*ADGRL1*
		LPHN2	Latrophilin 2 (CIRL-2, CL2, LPHH1, LEC1)	*ADGRL2*
		LPHN3	Latrophilin 3 (CIRL-3, CL3, LEC3)	*ADGRL3*
		ELTD1	ELTD1 (ETL)	*ADGRL4*
II	E (EGF-TM7)	*EMR1*	EMR1 (F4/80)	*ADGRE1*
		EMR2	EMR2 (CD312)	*ADGRE2*
		EMR3	EMR3	*ADGRE3*
		EMR4	EMR4 (FIRE, GPR127)	*ADGRE4*
		CD97	CD97 (BL-Ac(F2))	*ADGRE5*
III	A	*GPR123*	GPR123	*ADGRA1*
		GPR124	GPR124 (TEM5)	*ADGRA2*
		GPR125	GPR125	*ADGRA3*
IV	C (CELSR)	*CELSR1*	CELSR1	*ADGRC1*
		CELSR2	CELSR2 (MEGF3)	*ADGRC2*
		CELSR3	CELSR3 (MEGF2, Fm1, EGFL1)	*ADGRC3*
V	D	*GPR133*	GPR133	*ADGRD1*
		GPR144	GPR144	*ADGRD2*
VI	F	*GPR110*	GPR110	*ADGRF1*
		GPR111	GPR111	*ADGRF2*
		GPR113	GPR113	*ADGRF3*
		GPR115	GPR115	*ADGRF4*
		GPR116	GPR116 (Ig-Hepta)	*ADGRF5*
VII	B (BAI)	*BAI1*	BAI1	*ADGRB1*
		BAI2	BAI2	*ADGRB2*
		BAI3	BAI3	*ADGRB3*
VIII	G	*GPR56*	GPR56 (TM7XN1)	*ADGRG1*
		GPR64	GPR64 (HE6)	*ADGRG2*
		GPR97	GPR97 (Pb99)	*ADGRG3*
		GPR112	GPR112	*ADGRG4*
		GPR114	GPR114	*ADGRG5*
		GPR126	GPR126 (VIGR, DREG)	*ADGRG6*
		GPR128	GPR128	*ADGRG7*
IX	V	*GPR98*	VLGR1 (GPR98, MASS1, USH2C, FEB4)	*ADGRV1*

BAI, brain-specific angiogenesis inhibitor; CD, cluster of differentiation; CELSR, cadherin EGF LAG seven-pass G-type receptor; CIRL, calcium-independent receptor of a-latrotoxin; CL, CIRL/latrophilin; DREG, developmentally regulated GPCR; EGFL, epidermal growth factor–like; EGF-TM7, epidermal growth factor–seven-span transmembrane; ELTD, EGF, latrophilin and seven transmembrane domain–containing protein; EMR, EGF-like molecule containing mucin-like hormone receptor; ETL, EGF-TM7-latrophilin–related protein; FEB, febrile seizures gene disease locus; FIRE, F4/80-like receptor; Fm, Flamingo; HE, human epididymal; LEC, lectomedin; LPHH, latrophilin homolog in humans; MASS, monogenic audiogenic seizure susceptibility; MEGF, multiple epidermal growth factor–like domains; TEM, tumor endothelial marker; VIGR, vascular inducible GPCR; VLGR, very large GPCR.

Table 1: Nomenclature of aGPCRs (Hamann et al., 2015)

1.2.2. The structure of aGPCRs

Most of the aGPCRs are orphan receptors and they are characterized by their enormous size and complex structure. These receptors undergo autoproteolytic cleavage in the endoplasmic reticulum during receptor biosynthesis and it is completely mediated by GPCR proteolysis site (GPS) (Chang et al., 2003), which is the part of a

larger GPCR autoproteolysis-inducing (GAIN) domain. This cleavage event divides the receptor into an N-terminal fragment (NTF) and a C-terminal fragment (CTF) and these fragments stay non-covalently attached. An autoproteolysis reaction is based on a reaction between aliphatic residue (usually leucine) and threonine, serine, or cysteine, in which an ester is generated that is easily hydrolyzing in two products NTF and CTF. (Figure 2B). Autoproteolysis is one of the main characteristics of aGPCRs. This reaction is stated as the most important for maturation, trafficking, stability and the function of aGPCRs (Yona et al., 2008). This reaction is also reversible and GPS motif mediates non-covalent re-association of the cleaved fragments (Araç et al., 2012). The larger NTF often contains conserved domains: the GAIN domain and the majority of the extracellular domain (ECD). The smaller CTF consists of a residual part of the GAIN domain/ECD, the 7TM domain, and the intracellular domain (ICD) (Monk et al., 2015). A very important role in signal-transduction is that of the *Stachel* sequence, which is located within the residual ECD (Liebscher et al., 2014) (Figure 2A). The NTF is responsible for the enormous size of most aGPCRs and presents characteristic modular protein domains. Many of the about 20 different protein domains found in aGPCR NTFs can mediate contacts with cellular or extracellular matrix (ECM) (Hamann et al., 2015).

Only several ligands for aGPCR have been described over the years. Mainly these receptors interact with cellular and extracellular molecules (Langenhan et al., 2013). A characteristic of aGPCRs is high promiscuity in ligand recognition: one receptor can bind multiple ligands. A good example for this case is the first discovered ligand for aGPCRs CD55 (decay-accelerating factor). CD55 interacts with ADGRE5 (CD97) (Hamann et al., 1996), but also chondroitin sulfate B (Stacey et al., 2003), $\alpha_5\beta_1$ and $\alpha_v\beta_3$ integrins (Wang et al., 2005), and CD90 (Wandel et al., 2012) can bind to CD97.

A

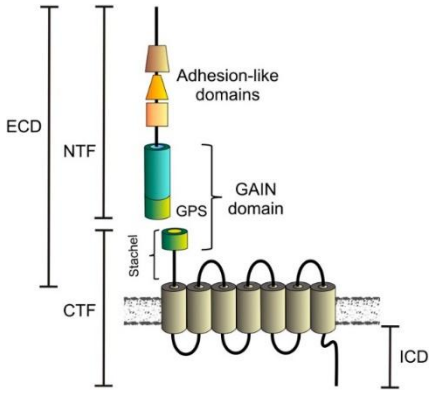

B

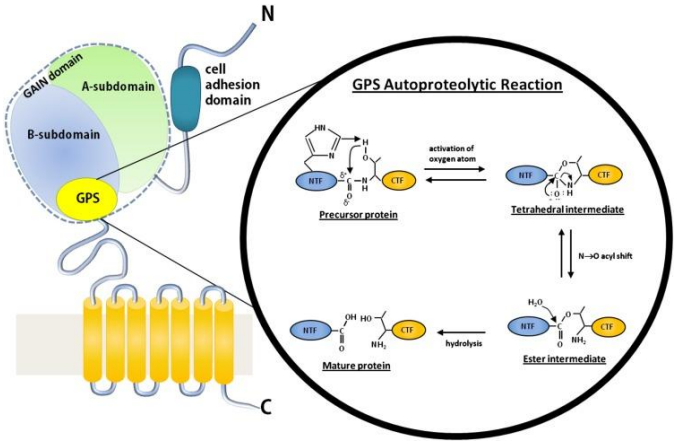

Figure 2: (A) Simplified structure of aGPCRs (Monk et al., 2015) and (B) mechanism of autoprotolysis (Hamann et al., 2015)

1.2.3. Activation and signaling of aGPCRs

aGPCRs, similarly like rhodopsin-like GPCRs, can be activated when high affinity agonist is binding to binding pockets of the receptor (Figure 3A). Only a few cases of agonist induced receptor activation were demonstrated (Monk et al., 2015). One of the examples is type III collagen, which activates RohA/ROCK signaling of GPR56 (Luo et al., 2014).

The second possible way of activating these receptors is via synthetic peptides derived from the *Stachel* sequence. This is a complex way of activating a receptor and usually requires different ECMs (Monk et al., 2015). Activation using *Stachel* sequence could cause a removal of NTF, which leads to independent CTF-mediated intracellular function and NTF function (Figure 3B).

In some cases, for example Gpr126, activation via *Stachel* may require an involvement of the ECM (i.e. laminin-211) (Petersen et al., 2015) (Figure 3C). Also, mechanical stimulation is one of the ways how to activate those receptors (Scholz et al., 2015a).

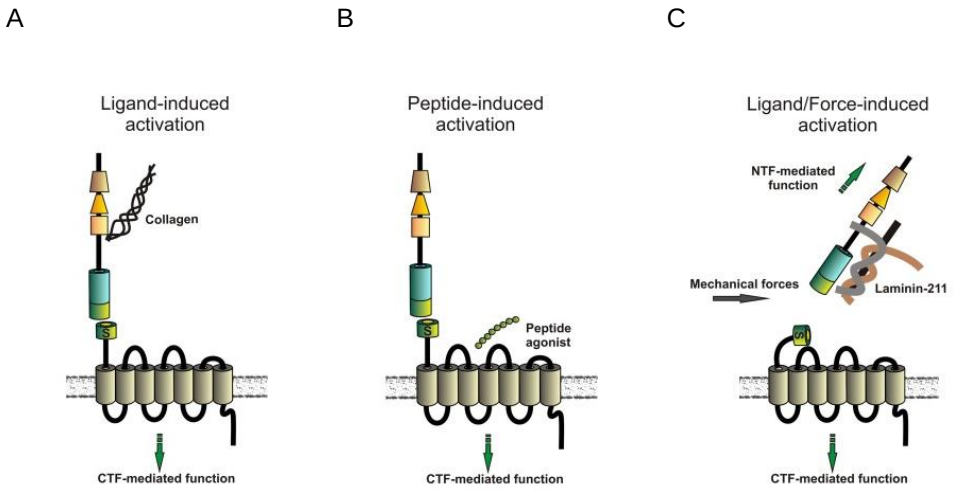

Figure 3: Three potential mechanisms of aGPCRs activation (Monk et al., 2015)

Even signaling of aGPCRs is much complicated in comparison to classical rhodopsin GPCRs. What these groups have in common is promiscuity for G proteins and a mechanism of desensitization (Monk et al., 2015).

1.2.4. The structure of Gpr111

Gpr111, as well as most of aGPCRs, has leucine and histidine next to N-terminus. Both of these amino acids are necessary for the cleavage of the receptor. The main difference between all members of aGPCRs and ADGRF2 (Gpr111) is that Gpr111 doesn't undergo autoproteolysis (Prömel et al., 2012). The structure of the receptor is very simple in comparison to other aGPCRs. It contains a large N terminus, a signal peptide, Cys-rich region, GPS motif and a 7TM domain, similarly like other aGPCRs. Interestingly, the GPS sequence in case of Gpr111 and Gpr115 is altered. Gpr115 lacks

leucine and instead of leucine it has an insertion of three amino acids. Gpr111 also lacks leucine, but it lacks a substitute of three amino acids. Additionally, Gpr111 also lacks histidine. This lack of two functioning significant amino acids makes the cleavage of Gpr111 impossible (Prömel et al., 2012).

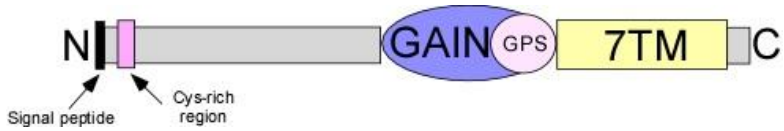

Figure 4: Simplified structure of Gpr111

1.2.5. Physiological role of aGPCRs

aGPCRs are found in all vertebrates (Fredriksson and Schiöth, 2005), close relatives of vertebrates (Kamesh et al., 2008), primitive animals (Putnam et al., 2007), in unicellular organisms and fungi (Krishnan et al., 2012). This indicates a very important role of these receptors in cell communication, which is reflected through cytoskeletal organization, migration, proliferation, apoptosis, differentiation etc. (Hamann et al., 2015). Many adhesion receptors such as members of ADGRB and ADGRC subfamily regulate cell shape, size and cytoskeletal organization (Antic et al., 2010), (Hashimoto et al., 2010). Those receptors are also involved in cell adhesion and migration of leucocytes (Hamann et al., 1996), neutrophils (Yona et al., 2008), and other immune cells as well as tumor cells (Galle et al., 2006). In addition aGPCRs are involved in cell proliferation (Mogha et al., 2013), differentiation (Monk et al., 2009), (Glenn and Talbot, 2013), (Mogha et al., 2013) and apoptosis (Koh et al., 2004).

aGPCRs are widely distributed and they play an important role in many organ systems. In the cardiovascular system, some members of aGPCRs are involved in formation of valves (Doyle et al., 2006) and angiogenesis (Wang et al., 2005). In the respiratory system, those receptors are important for formation of surfactant lipids, normal function and lung development (Yates et al., 2010). Several studies reported a pivotal role of aGPCRs in the musculoskeletal system. aGPCRs are associated with human height (Tönjes et al., 2009), (Kim et al., 2012), body weight and human skeletal frame size (Chan et al., 2012). Alteration in some aGPCRs is associated with adolescent idiopathic scoliosis (Kou et al., 2013), abnormal skeletal growth, osteoporosis etc. (Urano et al., 2012). aGPCRs are highly expressed in the nervous system and there they are involved in closure of the neural tube (Nishimura et al., 2012), neuronal cell adhesion (Chen and Clandinin, 2008), synapse formation and function (Duman et al., 2013), (Lanoue et al., 2013), (Stephenson et al., 2013), myelination (Monk et al., 2009), (Mogha et al., 2013) and axon growth (Chai et al., 2014), (Qu et al., 2014) etc. Due to high expression of aGPCRs in the brain and their involvement in many cellular processes in the brain, those receptors play a role in pathophysiology (Bonaglia et al., 2010) of behavioral disorders (Tobaben et al., 2002) and other neurological disease. A part from this aGPCRs are involved in a normal function of the endocrine system and in metabolic processes. For example, a lack of ADGRF5 (Gpr116) is linked to glucose intolerance and insulin resistance (Nie et al., 2012), deficiency of ADGRC2/3 (Celsr2/3), causes defects in pancreatic beta cell differentiation (Cortijo et al., 2012). A recent study shows

the role of aGPCRs in adipogenesis (Suchý et al., 2020). Beside of this, a few receptors (ADGRE1/EMR1, ADGRG3/GPR97, ADGRE5/CD97) are important for inflammation in the adipose tissue (Kolehmainen et al., 2015), (Shi et al., 2016).

1.2.6. Physiological role of Gpr111

Structural similarity between Gpr111 and Gpr115 is very high (65%) (Prömel et al., 2012) as well as their expression pattern (Demberg et al., 2017). It is considered that those receptors are developed during evolution of vertebrates and that they play function in skin specialization that is essential for life on land. Gpr111 as well as Gpr115 are expressed in squamous epithelium with an onset of expression very early during development of the epidermis in embryogenesis. Probably, due to the expression and role of these receptors they are present only in land living animals (Prömel et al., 2012).

1.3. Obesity

According to the definition of world health organization (WHO) overweight and obesity are defined as abnormal or excessive fat accumulation that presents a risk to health. The main cause of obesity and overweight is an energy imbalance between calories consumed and calories expended. Globally, there has been an increased intake of energy and a reduction of physical activity due to modern life style. Changes in dietary and physical activity have led to obesity becoming a pandemic problem (Meldrum et al., 2017) that has nearly tripled since 1975 https://www.who.int/topics/obesity/en/. Prediction of center for disease control and prevention (CDC) is that by 2030, about 49% of American adult citizens will be obese. On the other hand, WHO reported that 38 million children under the age of 5 were overweight or obese in 2019.

A simple index such as body mass index (BMI) can be used as an assessment of body weight or as a screen for weight categories that may lead to health problems. BMI is defined as a person's weight in kilograms divided by the square of height in meters (kg/m^2) https://www.who.int/news-room/fact-sheets/detail/obesity-and-overweight. BMI is inexpensive, easy method for defining overweight and it is calculated in the same way for adults and children. The interpretation of BMI is also same for men and women and for all body types and ages. In case of children and teenagers BMI should be age and gender specific due to changes in body fat. Also, percussion in interpretation should be taken in case of athletes, elderly and race https://www.cdc.gov/healthyweight/assessing/bmi/index.html.

Table 2: Body mass index https://www.cdc.gov/healthyweight/assessing/bmi/index.html

BMI	Weight Status
≤18.5	Underweight
18.5 – 24.9	Normal or Healthy Weight
25.0 – 29.9	Overweight
≥30.0	Obese

Overweight and obesity are major risk factors for a number of chronic diseases, including cardiovascular diseases such as heart disease and stroke, diabetes type 2 (T2D), osteoarthritis and some types of cancer (Meldrum et al., 2017). A part from these, obesity is also related to increases in arrhythmias, sudden cardiac death, asthma, obstructive sleep apnea syndrome, thrombophlebitis, gallstones, urinary incontinence, depression, sexual dysfunction (more for men), low quality of life etc. (Meldrum et al., 2017).

On the other hand, obesity in childhood is associated with a wide range of serious health complications such as breathing difficulties, fractures, onset of early markers of cardiovascular disease, insulin resistance and psychological disorders.

Overweight and obesity are very much preventable. By reducing food intake and increasing physical activity it is possible to deal with obesity. However, the problem of obesity is much complex due to life style, environmental factors and genes that also play very important roles in this worldwide pandemic and that is the reason why it is necessary to find adequate therapeutic approaches for this disease.

1.3.1. Adipose tissue (AT)

AT is a complex organ that plays the most important role in physiology and pathophysiology of metabolism (Rosen and Spiegelman, 2014). AT is composed of many different cell types: adipocytes, endothelia cells, immune cells, mesenchymal stem cells etc. (Martyniak and Masternak, 2017). Cell composition of AT makes this organ very important for regulation of different physiological processes. AT is involved in nutrition homeostasis, energy storage and acts as an endocrine organ (Rosen and Spiegelman, 2014).

AT is a metabolic organ that stores lipids in form of triglycerides (TG), but in period of starvation, AT can provide energy from TG in form of free fatty acids (FFA) through process of lipolysis (Coelho et al., 2013). Adipokines are molecules produced by AT and different depots of AT can produce variety of these molecules (Kershaw and Flier, 2004). Structure and function of adipokines are divers: some of them are hormones (leptin, adiponektin, etc), growth factors (IGF, VEGF, FGF etc.) or cytokines (IL-6,

TNFα) (Kershaw and Flier, 2004), (Alcalá et al., 2019). A part from these molecules, AT in enriched with a lot of enzymes (cytochrome P450-dependent aromatase, 3β-hydroxysteroid dehydrogenase (HSD), 3αHSD, 11βHSD1, 17βHSD, 7α-hydroxylase, 17α-hydroxylase, 5α-reductase, and UDP-glucuronosyltransferase) that are involved in (in)activation and conversion of steroid hormones (Meseguer et al., 2002) (Bélanger et al., 2002). It is also very important to emphasize that AT is contributing up to 100% of circulating estrogen in postmenstrual women and 50% of testosterone in premenopausal women (Meseguer et al., 2002), (Bélanger et al., 2002).

Beside above mentioned AT also provides important mechanical support for some organs such as eyes and kidneys and for parts of the body exposed to high level of mechanical stress i.e. feet (Rosen and Spiegelman, 2014).

Due to the presents of pluripotent cell as a part of stromal vascular fraction (SVF) in AT and production of variety of molecules, AT is considered an important organ for wound healing.

Adipocytes represent only about 30-40% of the cells present in AT (Lee et al., 2013). There are three different kinds of adipocytes in mammals: brown, white and beige/brite. These adipocytes have different morphological characteristics and diverse effects on lipid metabolism (Pfeifer and Hoffmann, 2015). According to dominant sort of adipocytes, there are two types of AT: brown and white.

In humans AT is located in two compartments of the body: below the skin (subcutaneous depots) and in the trunk (visceral depots) (Cinti, 2012) (Figure 5A).

In mice BAT is located interscapularly. On the other hand, WAT depots in mice are located within abdominal cavity and around ovaries in females and testes in males (Figure 5B).

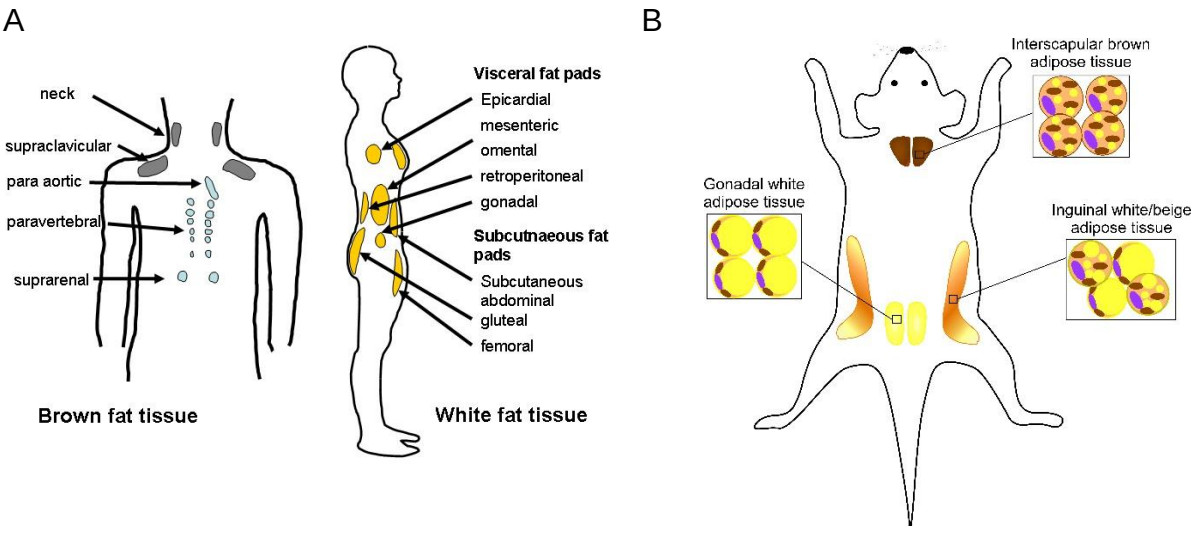

Figure 5: Localization of AT in humans (A) https://www.intechopen.com/books/neurodegenerative-diseases/influence-of-obesity-on-neurodegenerative-diseases **and in mice (B)**

Since AT plays such an important role in metabolism it is a proper target for treatment of obesity (Rosen and Spiegelman, 2014).

1.3.1.1. Brown adipose tissue (BAT)

BAT is a highly vascularized organ present only in mammals (Coelho et al., 2013) and it helps them to survive in cold environment (Cannon and Nedergaard, 2004). In mice, BAT occurs on embryonic day 15.5 (E15.5) and rapidly expands till birth (Schulz and Tseng, 2013). During embryonic development, BAs derive from precursor mesenchymal mesodermal stem cells (MSC) (Alcalá et al., 2019). These precursor cells are characterized by the expression of certain transcription factors such as myogenic factor 5 (Myf5), paired box protein 7 (Pax7), and engrailed-1 (En1) (Sanchez-Gurmaches and Guertin, 2014), (Wang and Scherer, 2014), (Ishibashi and Seale, 2015). Many transcription factors have been described as main regulators of BAT development and function, such as peroxisome proliferator-activated receptor γ (PPARγ), CCAAT/enhancer binding proteins (C/EBPα, C/EBPβ, C/EBPδ), PPARγ coactivator 1 alpha (PGC-1α), PRD1-BF1-RIZ1 homologous domain-containing 16 (PRDM16), and even microRNAs (Alcalá et al., 2019). BAs are enriched with mitochondria, uncoupling protein 1 (UCP1) and characterized with smaller lipid droplets (Figure 6). This makes them different from white adipocytes (WAs) (Pfeifer and Hoffmann, 2015).

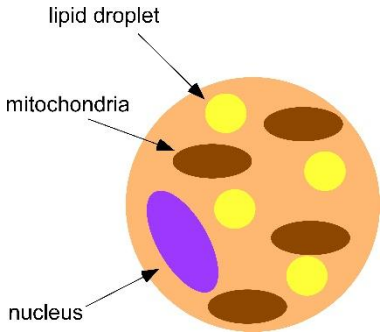

Figure 6: Schematic representation of brown adipocyte

The main function of BAT is transfer of energy into heat. BAT is essential for non-shivering thermogenesis (NST) and for cold induced thermogenesis. Both processes are under the control of norepinephrine (NE) that is released from sympathetic neurons. The most abundant adrenergic receptors through which NE induces thermogenesis in AT is G_s coupled β_3 receptors (Cannon and Nedergaard, 2004). After binding NE for β_3 receptors Gs protein activates adenylyl cyclase and increases cAMP levels. cAMP activates PKA, which activates hormone sensitive lipase (HSL). HSL hydrolyzes fatty acids from triglycerides (TG). Fatty acids are transported to mitochondria where β-oxidation occurs and tricarboxylic acid cycle (TCA). The result of these cycles is a generation of reduced electron carriers flavine adenine dinucleotide (FADH) and nicotinamide adenine dinucleotide (NADH). FADH and NADH are then oxidized by the electron transport chain through oxygen consumption. This results in a pumping out of protons from the inner mitochondrial membrane and the formation of a proton-motive force that drives the protons back into the mitochondrial matrix through the UCP1

(Cannon and Nedergaard, 2004). The energy generated in this way is released as heat (Figure 7).

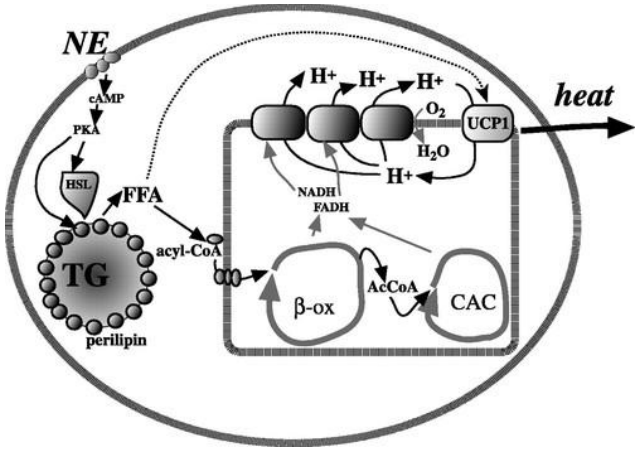

Figure 7: Schematic representation of thermogenesis in brown adipocytes (Cannon and Nedergaard, 2004); TG-triglcerydes, NE- norepinephrine, FFA- free fatty acid, β-ox- beta oxidation, HSL- hormone sensitive lipase, CAC- citric acid cycle, AcCoA- acetyl coenzyme A

BAT can also produce molecules called “batokines” and they act in autocrine or paracrine manner. Most of batokines are involved in vascularization, innervation and hypertrophy of BAT. Some important “batokines” are fibroblast growth factor 21 (FGF21), interleukin 6 (IL-6), neuregulin 4 (NRG4), endothelin 1 (ET1), adenosine and nitric oxide are among the first BAT-derived endocrine factors that were identified (Villarroya et al., 2017).

BAT is surrounded with WAT and that part of BAT is called BAT rim. On the other hand, pure BAT is named as BAT core.

1.3.1.2. White adipose tissue (WAT)

Similarly like BAs, WAs are also derived from mesodermal stem cells (MSCs) (Gesta et al., 2007b). Through developmental process MSCs will give rise to adipocyte lineage, which can further differentiate into white or brown adipocytes. The proteins and genes that represent potential molecular markers for white adpocytes (WAs) are: homeobox proteins (HoxA5, HoxA4, HoxC8), Glypican 4 (Gpc4), and Nr2f1 (nuclear receptor subfamily 2 group F member 1 or Coup-TF1), whereas subcutaneous adipocytes has higher levels of Hox A10, HoxC9, twist related proteins (Twist1 and Tbx15), short stature homeobox 2 (Shox2) and secreted frizzled-related protein 2 (Sfpr2) (Gesta et al., 2007b). Some studies characterize (Shan et al., 2013), (Sanchez-Gurmaches and Guertin, 2014) the linage from which white adipocytes will be generated as $Myf5^{-}$.

WAT begins to develop midgestation and reaches its maximal size relative to body weight at birth (Saely et al., 2012), (Alcalá et al., 2019). WAT depots in humans typically increase gradually throughout life (Gesta et al., 2007a).

The main characteristics of WAs are large lipid droplet and few mitochondria (Figure 8). Usually those cells have a low expression of UCP1 and metabolic processes such as

fatty acid oxidation and oxidative phosphorylation are not dominant in comparison to BAs (Lizcano, 2019).

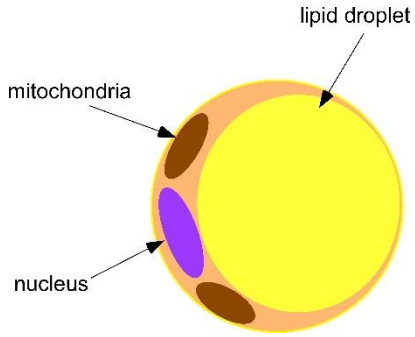

Figure 8: Schematic representation of white adipocyte

Due to extensive distribution all over the body, WAT is mainly involved in mechanical protection, thermal isolation and maintaining body temperature (Coelho et al., 2013). However, the main role of WAT is ability to store and provide energy when necessary (Coelho et al., 2013).

WAT has a very important secretory role. Some of the secreted molecules (adipokines) from WAT are hormones (leptin, acylation stimulating protein (ASP), adiponektin), cytokines and chemokines (TNFa, IL-1B, IL-6, IL8, CCL2. CXCL5 etc.), growth factors (transforming growth factor (TGFb) and vascular growth factor (VEGF) as well as regulatory molecules such as plasminogen activator inhibitor (PAI-1), visfatin, resistin, lipocalin, retinol binding protein etc. (Trayhurn and Beattie, 2001).

1.3.1.3. Beige/brite adipocytes

In addition to classical BAs, a second type of BAs that is present in WAT depots has been identified and named beige or brite cells (Pfeifer and Hoffmann, 2015), (Alcalá et al., 2019). Beige adipocytes are special because of their ability to dissipate energy, increase energy expenditure and to be differentiated from WAs. In humans, BAT is mainly composed of beige adipocytes and this makes these cells attractive therapeutic target for obesity and obesity related diseases (Lizcano, 2019).

Even though beige adipocytes arise from the same precursors as WAs, different endogenous and environmental stimuli play a very important role in development of beige cells (Ikeda et al., 2018). The beige adipocyte biogenesis or “beigeing” is induced with chronic exposure to cold, adrenergic stimulation, long term treatment with peroxisome proliferator–activated receptor γ (PPARγ) agonists (Lizcano, 2019), substances that increase cyclic guanosine monophosphate (cGMP) e.g. natriuretic peptides (NPs) and inhibitors of phosphodiesterase 5 (PDE5) (sildenafil) (Pfeifer and Hoffmann, 2015), interleukins (IL-4 and IL-6) and FGF21. All of these factors, which are capable of increasing energy expenditure by various mechanisms, have protective effects regarding obesity in animals fed a high-caloric diet and improve glucose homeostasis and insulin sensitivity (Phillips, 2019).

There is evidence that mature WAs can also be changed to beige adipocytes upon stimulation with specific factors e.g. (cold stimulation) (Rosenwald et al., 2013) and this phenomenon is known as trans-differentiation (Lizcano, 2019).

Common characteristics for beige and BAs are multilocular lipid droplets, high mitochondrial content and expression of brown specific genes such as *Ucp1*, *Ppargc1α*, *Prdm16* (Pfeifer and Hoffmann, 2015) (Figure 9).

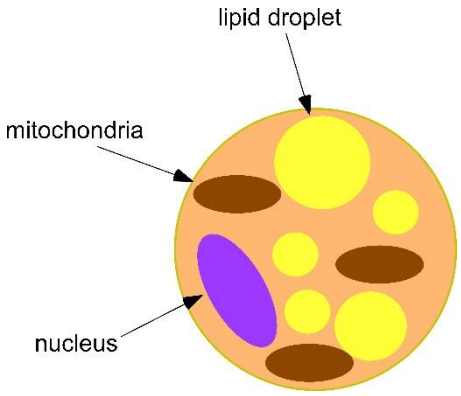

Figure 9: Schematic representation of beige adipocyte

1.4. Cilia and ciliopathies

Ciliopathies are a group of diseases caused by genetic mutations which leads to defects in structure and function of primary cilium https://www.ciliopathyalliance.org/ciliopathies. Cilia are microscopic hair like structures or organelles that extend from the surface of nearly all mammalian cells https://www.ciliopathyalliance.org/cilia. Primary cilia are like small antennas that receive signals from extracellular environment and usually one cell has one cilium.

To date mutations in over 40 genes are considered to be related to different ciliopathies. Cilia dysfunction can manifest as a constellation of features such as retinal degeneration, renal disease, cerebral anomalies and are usually followed by congenital fibrocystic diseases of the liver, diabetes, obesity and skeletal dysplasia (Alcalá et al., 2019), (Waters and Beales, 2011).

The most frequent and the most described ciliopathies are: Alström Syndrome, Bardet-Biedl Syndrome, Joubert Syndrome (JBTS), Jeune Asphyxiating Thoracic Dysplasia (JATD), Nephronophatis, policistic kidney disease, primary ciliary dyskinesia, rethinitis pigmentosa and Usher syndrome https://www.ciliopathyalliance.org/ciliopathies. Interestingly, only Alström Syndrome and Bardet-Biedl Syndrome (BBS) cause obesity (Vaisse et al., 2017).

The physiological role of primary cilia in regulation of metabolism and energy homeostasis has to be elucidated.

In many studies (Lee et al., 2015), (Marion et al., 2012), (Vaisse et al., 2017) the role of primary cilium is linked to leptin and insulin signaling as well as to hypothalamic neurons that control appetite.

1.4.1. Structure of primary cilium

The main physiological role of primary cilia is sensation and transduction of different extracellular signals inside the cell. Cilia are enriched with ion channels, different types of receptors that mediate transduction of Hedgehog (HH), Wnt, Notch, Hippo signaling, GPCRs, receptor tyrosine kinases, mTOR, and TGFβ signals (Wang and Dynlacht, 2018).

The cilium comprises a microtubule (MT)-based axoneme containing a ring of nine outer microtubule doublets (Louka et al., 2018). Axoneme is growing from the basal body toward outside of cells and it is encapsulated by cell membrane (Lee et al., 2015). The cellular membrane that is covering the axoneme is different from the cell membrane and this membrane is enriched with phosphoinositides $PI_{(4,5)}P_2$, which are important for ciliary function (Lee et al., 2015). Between the basal body and the cilium is the ciliary transition zone (TZ), which contains specialized gating structures such as Y-links that along with the basal body transition fibers control the entrance and exit of ciliary proteins. The intraflagellar transport (IFT) system zips up (anterograde) and down (retrograde) axonemal microtubules to mediate the transport of specific ciliary cargo, such as receptors, into or out of the organelle, whereupon they are degraded or recycled. Cilia can also release ectosomes by shedding off membrane-enclosed material from the surface of the organelle. The function of these extracellular vesicles has been linked to maintenance of ciliary integrity, balancing of intraciliary signaling events and/or in transmission of signals across cells (Anvarian et al., 2019).

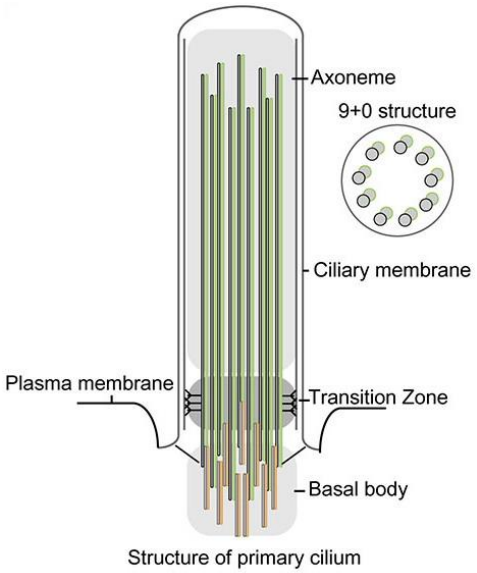

Figure 10: Schematic representation of primary cilium (Park et al., 2019)

1.4.2. Canonical and non-canonical Hedgehog signaling (HH)

Hedgehog signaling is described as the curtail signaling pathways involved in cell differentiation processes such as adipogensis (Fontaine et al., 2008a), angiogenesis (Moran et al., 2012) and tumor development (Sari et al., 2018).

Hedgehog signaling could be activated by three ligands: Sonic Hedgehog (Shh), Indian Hedgehog (Ihh), or Desert Hedgehog (Dhh). Shh and Ihh have similar functions in many tissues and they signal into the primary cilium. Shh has roles in cell types in the nervous system and in patterning of the limbs, whereas Ihh has critical roles in skeletal development (Bangs and Anderson, 2017). On the other hand Dhh appears to be restricted to the gonads and may also depend on primary cilia for its activity (Nygaard et al., 2015).

Hedgehog signaling is initiated by the binding one of the ligands to the 12-transmembrane protein Patched (Ptch1), relieving suppression of the 7-transmembrane protein Smoothened (Smo). In turn, Smo translocates into the cilia membrane and activates an intracellular cascade that results in activation of the glioblastoma transcriptional factors Gli2 and Gli3. Gli1 is one of their target genes and has been characterized as a reliable marker of Hedgehog signaling activity (Riobo and Manning, 2007). In the absence of the ligand HH receptor Ptch1 represses Smo and the pathway is off (Lee et al., 2015). When Smo is suppressed, transcriptional factors are proteolytically converted into transcriptional repressor full-length Gli (Gli-FL). Once the pathway is active Gli-FL are converted into the active forms (GliA) (Figure 11).

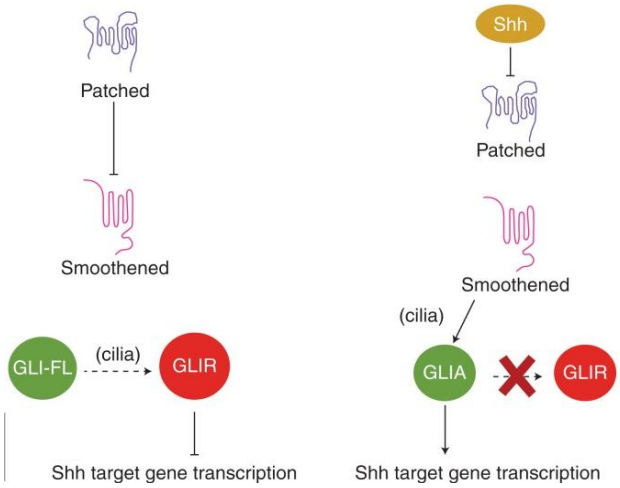

Figure 11: Schematic representation of Hedgehog signalling (Bangs and Anderson, 2017)

Non-canonical HH signaling is mainly described in malignant diseases. In case of non-canonical HH signaling, transcriptional factors Gli can be activated by other molecules or signal pathways independently of SMO (Gu and Xie, 2015b). The identified downstream effect of this non-canonical HH signaling activation is cytoskeleton remodeling and cell migration via involvement of the small Rho GTPases Rac1 and

RhoA (Razumilava et al., 2014). This signal pathway is usually present in cells with impaired cilia expression.

Beside RhoA signaling, non-canonical HH signaling pathway is associated with TGFβ, PI3K, PKC Akt signaling (Gu and Xie, 2015a).

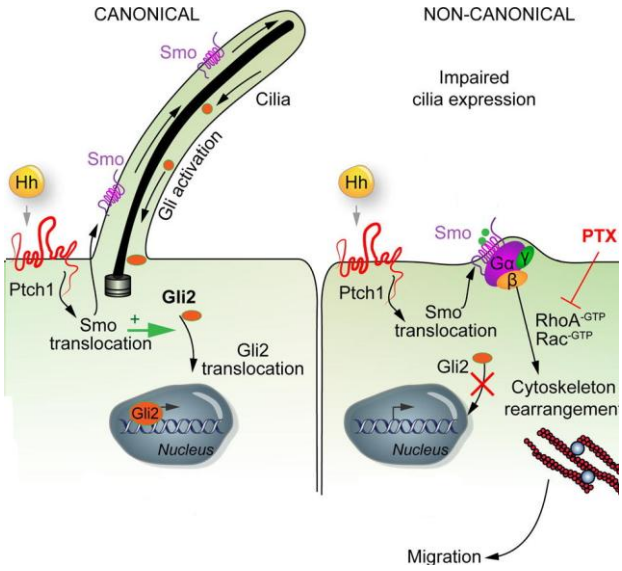

Figure 12: Canonical and non-canonical HH signaling (Razumilava et al., 2014)

1.5. Aim of the PhD thesis

Previous study from our group profiled the transcript levels of GPCRs and data show that aGPCRs was one of the largest class of receptors represented in pre- and mature BAs (Klepac et al., 2016). Additionally, publicly available RNA-Seq data (Vernia et al., 2016) showed that 37% of all aGPCR are significantly expressed in adipose tissue, highlighting the importance of this class. One of the four aGPCRs that was significantly upregulated in adipocytes was Gpr111 (Suchý et al., 2020). However, the role of aGPCR as well as Gpr111 in adipose tissue is largely unknown.
The overall goal of this thesis was to investigate the role of Gpr111 in AT. Therefore, the major questions that occurred were:

1. Does the lack of GPR111 have an impact on differentiation of BAs and WAs?
2. What is the role of GPR111 in AT under lean and obese conditions?
3. What are the effects of cold exposure on murine AT lacking GPR111?
4. What is the major signal pathway linked to GPR111?

To address the mechanism involved in signaling of Gpr111 as well as effects of Gpr111 depletion on *in vitro* differentiation, brown and white adipocytes were isolated from Gpr111$^{-/-}$ (KO) mice. To further investigate the role of Gpr111 *in vivo*, KO mice were analyzed under HFD conditions and after one week of cold exposure.

2. Material and methods

2.1. Chemicals and compounds

If it is not depicted otherwise, all common chemicals were purchased from: Merck KGaA (Darmstadt), AppliChem GmbH (Darmstadt), VWR International GmbH (Darmstadt), Sigma-Aldrich Chemie GmbH (Munich) and Carl Roth GmbH (Karlsruhe). Chemicals, compounds and equipment used for particular experiment are listed in a separate section. Water for experiments was purified and distilled with PURELAB® water purification system, Elga Veolia.

2.2. In vivo experiments

2.2.1. Animals

GPR111$^{-/-}$ (KO) mice were received as a gift from Takeda Cambridge Limited ("Takeda") company. All mouse strains were maintained and bred in the animal facilities – Haus für Experimentalle Therapie (HET), University Hospital Bonn and at the Institute of Pharmacology and Toxicology. The mice had free access to standard rodent diets (Ssniff® R/M-H) and water. Animals were housed in a 12:12 light-dark (LD) cycle, at 23 ± 1°C. Mice at age of 8 weeks were used for breeding. At an age of 3 weeks after birth, mice were separated by sex, marked with ear punches and housed in separate cages.
All animal studies were performed according to German animal welfare laws. Animal experiments were permitted by the Landesamt für Natur, Umwelt und Verbraucherschutz (LANUV) Nordrhein-Westfalen, Germany, number of permition 81-02.04.2018.A332.

2.2.2. Diet induced obesity (DIO) experiments

For diet induce obesity experiments, six week old mice were fed with a high fat diet (HFD; 60% of calories from fat, D12492) or a normal diet (ND; D12450B), purchased from Ssniff GmbH, Germany, for 12 weeks.
In 17 week old mice, glucose tolerance test (GTT) was performed. Mice were starved for 5 hours. Glucose solution (0.25g/ml) was prepared in sterile saline (NaCl) and injected intraperitoneal (i.p) into mice according to their body weight (8µl of glucose solution/g of body weight). Glucose was measured before injection, 15, 30, 60, 90 and 150 minutes after injection using Accu-Check® Aviva Nano, Roche.
In the end of HFD period, mice were metabolically characterized. Oxygen consumption and motility were measure with Phenomaster (TSE Systems) at 23^0 C every 2 minutes for 24h and at 4^0 C for 1h. During the study, the mice were maintained in single cage, on a daily cycle of 12 h light (06:00–18:00 hours) and 12 h darkness (18:00–06:00 hours), and were allowed free access to food and water. Body composition was determined using Bruker minispec.

2.2.3. Long term cold exposure

Eight week old mice were acclimatized for 3 days at 16ºC. After acclimatization period, mice were exposed to 4ºC for 7 days. Oxygen consumption was measured with Phenomaster (TSE Systems) at 4ºC every 2 minutes for 24h. During the study, the mice were maintained in single cage, on a daily cycle of 12 h light (06:00–18:00 hours) and 12 h darkness (18:00–06:00 hours), and were allowed free access to food and water. Body composition was determined using Brucker® minispec.

2.3. Cell culture methods

2.3.1. Materials in cell culture

5ml, 10ml, 25ml serological pipette, Sarstedt, 86.1253.001/86.1253.001/86.1254.001

6,1 2, 24, 96 well plates, Sarstedt, 86.1836.001/ 83.3921.005/ 83.3922/83.3925.500

TPP® 6, 12-plates, Techno Plastic Products, 92006/92012

175cm^2 cell culture flask, Sarstedt, 83.3912.002

0.5ml, 1.5ml, 2ml micro centrifuge tube-(Eppendorf tube), Sarstedt, 72.704.004/

72.690.001/72.691

100mm cell culture dish, Sarstedt, 83.1802.001

15ml and 50ml centrifuge tube (falcon tube), Sarstedt, 62.554.001/ 62.548.004

0.22µm filter, VWR, 514-0061

100µm Nylon mesh Merc Milipore, NY1H00010

Cryogenic vials, Sarstedt, 72.379.992

Cell Counting chamber, Invitrogen, C10283

Folded filters 240nm, Whatman, ThermoFisher Scientific, 10311651

Cell scraper, Croning Falcon™, 353085

Microscope cover glasses 14mm, Glaswarenfabrik Karl Hecht GmbH & Co. Sondheim,

Germany, 41001114

Trypan Blue Solution, 0.4%, ThermoFischer Scientific, 15250-061

Trypsin inhibitor, Sigma-Aldrich, T9128

Dimethylsulfoxide (DMSO), Carl Roth, A994.2

Dexamethasone Sigma-Aldrich, D4902

Fetal bovine serum, Sigma-Aldrich, F7524

3,3‘5- Triiodo-a-tyronine sodium, Sigma-Aldrich, T6397

Sodium-L-ascorbate, Sigma-Aldrich, A4034

L-(-) Norepinephrine (+) bitartarate salt monohydrate, Sigma-Aldrich, A9512

HEPES, Lonza, BE17-737E

DMEM (1x) +Glutamax™-I+4.5g/L D-glucose, -pyruvate, ThermoFisher Scientific, 61965-026

DMEM (1x) +Glutamax™-I+4.5g/L D-glucose, +pyruvate, ThermoFisher Scientific, 31966-021

DMEM (1x) +Glutamax™-I+4.5g/L D-glucose, 25mM HEPES-pyruvate, ThermoFisher Scientific,21063-029

Penicillin, Streptomycin (P/S), Biochrom AG, Berlin, A2213

Collagenase Type II, Worthington-UK, LS004177

Bovine Serum Albumin (BSA), Fatty acid free, Sigma-Aldrich, A7030

D (+)-Biotin, Sigma-Aldrich,8.51209

3 isobutyl-1methylxantine (IBMX), Sigma Aldrich, I5879

Panthotenate, Sigma Aldrich, P5155

Insulin, Sigma Aldrich, I6634

Rosiglitazone, Sigma Aldrich, R2408

Oil red O, Sigma Aldrich, O9755

Free glycerol reagent, Sigma Aldrich, F6428

Glycerol standard solution, Sigma Aldrich, G7793

Ethylene glycol-bis(β-aminoethyl ether)-*N*,*N*,*N*′,*N*′-tetraacetic acid (EGTA), Sigma Aldrich, E4378

$MgCl_2x6H_2O$, Scharlau, MA 0036

Lactobionic acid, Sigma Aldrich, 153516

Taurine, Sigma Aldrich, T 0625

KH_2PO_4, Merck, 104873

HEPES, Sigma Aldrich, H7523

D-sucrose, Roth, 4621.1

KOH, Sigma Aldrich, P1767

Digitonin, Sigma Aldrich, D5628-1G

Sodium pyruvate, Sigma Aldrich, P2256-25G

Malonic acid, Sigma Aldrich, M1296-100G

L-glutamic acid monosodium salt hydrate, Sigma Aldrich, G1626-100G

Sodium succinate dibasic hexahydrate, Sigma Aldrich, S2378-100G

Guanosine5'-diphosphate disodium salt, Abcam, ab146529

Carbonyl cyanide p-trifluoro-methoxyphenyl hydrazine (FCCP), Tocris, 0453

Sodium azide (NaN_3), Alfa Aesar, L13716

Octanoyl-DL- carnitine (chloride), Cayman, 15048

Paraformaldehyd (PFA), Roth, 0335.3

SAG, MedChemExpress, HY-12848

2.3.2. Equipment in cell culture

Cell counter, ThermoFisher Scientific, Countess

Centrifuge, ThermoFisher Scientific, Heraeus™ Biofuge™ Stratos™, Eppendorf

Incubator, HeraCell 150, Heraeus, Hanau

Laminar air flow, HeraSafe, Heraeus, Hanau

Laica Mycroscope, Mycrosystem CMS Germany

Autoclave, VX-150, Systec

EnSpire™ multimode plate reader, PerkinElmer, USA

Plate shaker MS 3 basic, IKA®

O2k FluoroRespirometer, Oroboros Istruments, Austria

2.3.3. Isolation and culture of stromal vascular fraction (SVF) from BAT

BAT was taken from newborn mice (Néchad et al., 1983). Adipose tissue was dissected and chopped into small pieces and placed into the falcon with digestion buffer. Falcons were placed into a water bath at 37^0 C and shaken every 5 minutes. After approximately 30 min all tissue debris was removed by filtration through a 100µm nylon mesh and placed on ice for 30 min. The middle phase, which contains SVF was filtered through a 30µm nylon mesh and centrifuged at 700 x g for 10 min. The pellet was re-suspended in culture medium. Cells were seeded on 6-well plates and grown at 37° C, 5% CO2 and 95% H2O (Figure 14).

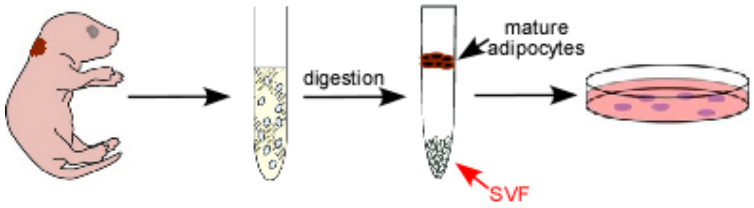

Figure 13: Schematic representation of BAs isolation for newborn BAT

Digestion buffer:
NaCl.....0.72 g
KCl.....37.3 mg
Ca2Cl .....19.1 mg
Glucose.....99.1 mg
HEPES.....2.38 g
dissolved in 100 ml H2O, pH was adjusted with 5M NaOH, sterile filtered and stored at 4° C.

the following substances were added before use:
BSA.....1.5%
Collagenase II .....2 mg/ml
sterile filtered.

Culture medium:
prepared in 396.2ml of DMEM (1x) +Glutamax™-I+4.5g/L D-glucose, -pyruvate and store at 4°C
FBS.....10%
P/S.....1%
Insulin.....4nM
Triiodothyronine-Na.....4nM
HEPES.....10mM
Sodium ascorbate.....25µg/ml

Stock solution (40µg/ml) of Trijodothyronin-Na (T3):
T3-Na.....2mg
dissolved in 1 ml 1N NaOH and added to 49ml of DMEM –pyruvate. Store at 4ºC up to 4 weeks.

Stock solution (10mg/ml) of sodium ascorbate:
Na-ascorbate.....10mg
dissolved in 10ml of PBS, sterile filtered and store in aliquots at -20ºC.

Phosphate-buffered saline (PBS):
NaCl.....137mM
Na_2HPO_4……..8mM
KH_2PO_4…….....1,4mM
KCl……2,7mM
dissolved in distillated H2O (dH_2O) and adjusted to pH 7.4, then autoclaved.

Growth medium
prepared usingDMEM (1x) +Glutamax™-I+4.5g/L D-glucose, - pyruvate
FBS.....10%
P/S.....1%

2.3.3.1. Immortalization procedure

One day after isolation (day 1) cells had to be immortalized. Lentivirus containing the SV40 large T antigen was used for immortalization. Cells were washed once with PBS and 800µl growth medium containing 200ng/well of the virus was added to the cells. The next day, the medium was filled up to 2 ml. Medium was changed every second day till cells reached confluence. When cells have reached confluence, they were trypsinized and seeded again on 10 cm dishes.

2.3.3.2. Trypsinization and cryo preservation of BAs

Cells were maintained in growth medium till they reached confluence. Cells were washed once with PBS, after that 1ml of 10x Trypsin was added and cells were placed in an incubator for 5min at 37^0 C. Detached cells were re-suspended in growth medium, centrifuged at 1000rpm for 10 min. Further on, cells could be frozen and stored for longer time period or re-seeded for passaging. For cryo preservation, the pellet was re-suspended in growth medium and 10% of DMSO. Cell cryos were placed for 20 min on ice, 20 min at -20^0 C, 1 day at -80^0 C and afterwards cells were transferred to liquid nitrogen (-196° C).

2.3.3.3. Differentiation of immortalized brown adipocytes

To differentiate the immortalized cells into brown adipocytes, 1.0 x 10^6 cells were seeded per plate (day -4). After 48h the medium was exchanged with differentiation medium (day -2). When cells reached confluence (day 0), adipogenic program was induced by treating cells with induction medium. 48h after induction (day 2), medium was exchanged to differentiation medium (diff.), which was replaced every second day till day 7.

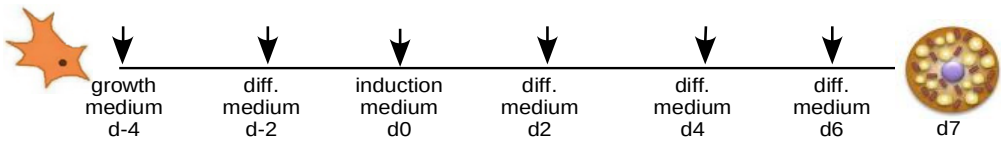

Figure 14: Schematic representation of BAs differentiation

Differentiation medium:
prepared inDMEM (1x) +Glutamax™-I+4.5g/L D-glucose, - pyruvate
FBS.....10%
P/S.....1%
Insulin.....20nM

Triiodothyronine-Na.....1nM

Induction medium:
prepared in DMEM (1x) +Glutamax™-I+4.5g/L D-glucose, - pyruvate
FBS.....10%
P/S.....1%
Insulin.....20nM
Triiodothyronine-Na.....1nM
Dexamethason.....1µM
Isobutylmethylxanthine.....0,5mM

2.3.4. Isolation and culture of stromal vascular fraction (SVF) from WATi

WATi was taken from 8-12-week old wild type mice C57Bl/6J. Tissue was chopped and placed in 50 ml falcon tubes containing digestion medium. Falcons were placed into a water bath at 37^0 C and shaken/vortexed every 5 minutes. After digestion, all tissue debris were removed through 100µM nylon mesh. Falcons were centrifuged at 1000 rpm for 10 min. Floating fraction of adipocytes is carefully removed and the pellet was re-suspended in growth medium. Cells were seeded on 175cm^2 cell culture flasks. Flasks were kept in the incubator at 37°C and 5% CO_2 for 24h. On the next day, flasks were washed with PBS and fresh growth medium was added. Cells were grown till confluence. Once when cells reached confluence, they were detached from the flasks using trypsin similarly like it was explained in paragraph 2.3.3.2. Cells were counted and cryopreserved in cryo-medium and stored at -150.

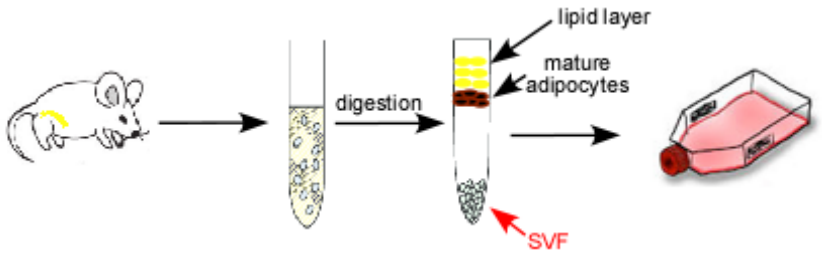

Figure 15: Schematic representation of WAs isolation

Digestion buffer:
prepared in DMEM Glutamax™ I + 4.5 g/l Glucose - pyruvate
BSA.....0.5%
Collagenase II .....1.5 mg/ml
sterile filtered with 0.22µm filter prior to use

Growth medium:
prepared using DMEM Glutamax™ I + 4.5 g/l Glucose - pyruvate
FBS.....10%
P/S.....1%

Medium for cryo conservation:
prepared in FBS
Dimethyl-sulfoxide (DMSO)…….....10%

2.3.4.1. Differentiation of white adipocytes

Thawed cryopreserved cells were plated on 6 or 12-well TPP plates (70,000 or 150,000 cells/well respectively), containing growth medium. Growth medium is replaced every second day till cells reached confluence. Once when cells are confluent (day 0), they were induced by replacing growth medium with induction medium, for two further days (day 2). Thereafter, the cells were differentiated in maintenance medium till day 12, with medium changes every second day.

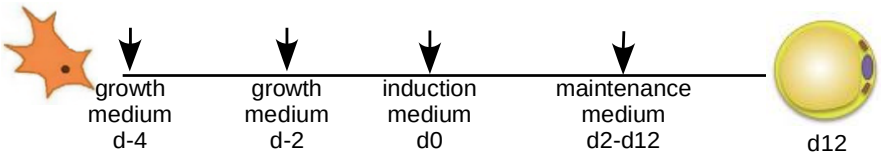

Figure 16: Schematic representation of differentiation of WAs

Induction medium:
prepared in DMEM (1x) +Glutamax™-I+4.5g/L D-glucose, + pyruvate
FBS.....10%
P/S.....1%
Insulin.....172nM
Triiodothyronine-Na.....1nM
Dexamethason.....1µM
Isobutylmethylxanthine.....0.5Mm
ABP……1:1000
Rosiglitazone……1Mm

Stock solution of ABP
prepared in water, aliquated and stored at 20 ^{0} C
L-ascorbate……....50mg/ml
D-biotin……1Mm
Pantotenate……17mM

Maintenance medium:
prepared ininDMEM (1x) +Glutamax™-I+4.5g/L D-glucose, + pyruvate
FBS.....5%
P/S.....1%
Insulin.....172nM
Triiodothyronine-Na.....1nM
ABP……1:1000

2.3.5. Oil Red O staining of differentiated adipocytes

Oil Red O is a diazo dye which is used for visualization of lipids in tissues or cells. After accumulation in fat droplets the lipids appear red.
Differentiated adipocytes (BAs or WAs) were washed once with PBS and fixed with 4% PFA for 15 min at RT. After two washes with PBS cells were then stained with Oil Red O working solution for 4h at RT and were washed three times with water.

Paraformaldehyde solution
Paraformaldehyde (PFA).....40 g
dissolved in 960ml of PBS pH 7.4, stirred at 55ºC until it's resolved and stored at 4ºC.

Oil Red O stock solution (5 mg/ml)
Oil Red O.....0.5 g
Isopropyl alcohol 99% .....100 ml
dissolved with a magnetic stir bar o/n, stored at RT

Oil Red O working solution (3 mg/ml)
Oil Red O stock solution.....6 ml
H2O.....4 ml
Working solution should be prepared on day of experiment and filtered through a paper filter.

2.3.6. Glycerol assay (lipolysis)

Fatty acids in our organism don't circulate freely, they are bound to glycerol, those esters are called triglycerides (TG). Lipolysis is a reaction that involves enzymatic hydrolysis by lipase of the triglycerides to glycerol and free fatty acids. Glycerol released during lipolysis will be converted through several enzymatic reactions to quinoneimine which absorbance can be measured at 540nm. An increase in absorbance directly correlates with production of glycerol. In the first reaction step glycerol will be phosphorylated by adenosine-5`-triphosphate (ATP) forming glycerol-1-phosphate (G-1-P) and this reaction is catalyzed by glycerol kinase (GK). In the next step, glycerol-1-phosphate will be oxidized by glycerol phosphate oxidase (GPO) to dihydroxyacetone phosphate (DAP) and hydrogen peroxide (H_2O_2). Peroxidase (POD) catalyzes the final reaction in which H_2O_2 couples with 4-aminoantipyrine (4-AAP) and with sodium N-ethyl-N-(3-sulfopropyl) m-anisidine (ESPA) and generates quinoneimine https://www.sigmaaldrich.com/content/dam/sigma-aldrich/docs/Sigma/Bulletin/f6428bul.pdf.

$$\text{Glycerol + ATP} \xrightarrow{\text{GK}} \text{G-1-P + ADP}$$
$$\text{G-1-P + } O_2 \xrightarrow{\text{GPO}} \text{DAP + } H_2O_2$$
$$H_2O_2 \text{ + 4-AAP + ESPA} \xrightarrow{\text{POD}} \text{Quinoneimine dye + } H_2O$$

Cells were washed tree times with DMEM (-phenol red; -pyruvate) and 400µl of lipolysis medium for 12 well plate was added (+/- NE). Cells were incubated for 2h at 37°C and 5% CO_2. In the meantime, free glycerol reagent and glycerol standard were pre-warmed to RT. After 2h of incubation, supernatant mixed with glycerol reagent (40µl of supernatant and 60µl free glycerol reagent) was measured in duplicates in 96 well plate using EnSpire™ plate reader (λ540nm). Blank (40µl of lipolysis medium and 60µl free

glycerol reagent) and standard (5µl standard reagent and 95µl free glycerol reagent) were measured in triplicates.
Glycerol content was calculated using the formula:

$$\frac{(A_{sample}-A_{blank})}{(A_{standard}-A_{blank})} \text{ x concentration of standard}$$

Results were additionally normalized to protein content. Amount of protein was measured using Bradford assay (2.5.3.3)

Lipolysis medium (always freshly prepared)**:**
BSA (free fatty acid) 2%
dissolved in DMEM (1x) +Glutamax™-I+4.5g/L D-glucose, 25mM HEPES-pyruvate*, keep at 37ºC.*

2.3.6.1. *Ex vivo* lipolysis

AT was extracted from mice and placed in ice cold lipolysis medium without BSA. Required amount of BAT is 2-3mg and 10-15mg of WATg/WATi. Tissue was placed into a new 24 well plate with 400µl of lipolysis medium per well. After that tissue was cut into small pieces and incubated for 2h at 37°C and 5% CO_2. After 2h of incubation, glycerol content was measured in the same way as it is being explained in 2.3.6.
Glycerol release was normalized to amount of tissue that was used in the assay.

2.3.7. Measurement of mitochondrial respiration

Oxygraph 2k® is a device for measuring oxygen consumption as an readout of mitochondrial function in real time https://www.ncbi.nlm.nih.gov/pmc/articles/PMC5408571/pdf/jove-120-54985.pdf.
Oxygraph is an instrument characterized with very high resolution and sensitivity in biological samples (cells, tissues and isolated mitochondria). It is equipped with two chambers with a stopper, which contain injection ports. Through these ports detergents are injected, substrates/un-coupler inhibitors etc. Inside the chambers there are polarographic oxygen sensors (golden cathode and silver anode) for measurement of oxygen concentration, a membrane and a certain amount of buffer. Samples prepared in the buffer are constantly stirring inside the chamber at 37^0 C. Stirring is very important for oxygen diffusion. Constant changes in oxygen consumption, injections and other parameters are shown in real time on the monitor of the computer. Oxygen consumption rates are calculated using Oroboros® software and expressed as nmol/µg*min.

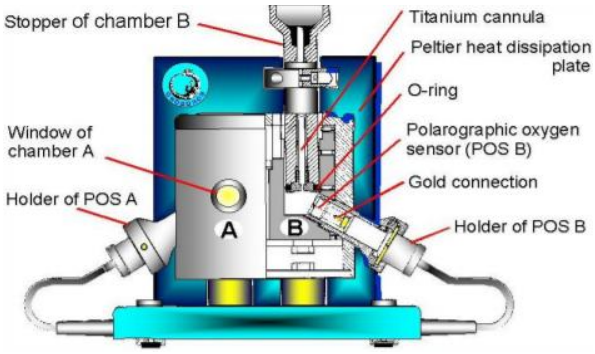

Figure 17:Important parts of the OROBOROS®oxygraph
In the picture, A marks a glass window, through which it is possible to observe stirring of the sample. B marks the glass chamber which is filled with buffer and samples are placed inside the bufferI; both chambers are housed in a copper block (temperature-regulated and insulated). Peltier thermopiles are in thermal contact between copper block and Peltier heat dissipation plate. Polarographic oxygen sensor (POS) with butyl india rubber sleeve for sealing the POS against the glass chamber https://www.oroboros.at/.

2.3.7.1. Preparation and calibration of oxygraph

When it is not in use, chambers of oxygraph are filled with 70% ethanol. On the day of the measurement it is necessary to wash chambers and stoppers 3-5 times with 70% ethanol and 3-5 times with water and finally 2 times with MIR05 buffer. For the measurement of cells, in chambers 1.6ml (2ml for tissue) of MIR05 was added and oxygraph sensors were calibrated. Calibration takes minimum 20 minutes. This process must be repeated before any new measurement.

2.3.7.2. Cell preparation for oxygraph measurements

Brown or white adipocytes were cultured as it was described in (2.3.3.3. and 2.3.4.1). Oxygraph measurement was performed on mature cells on d7 of BAs and d12 of WAs. First, cells were washed 2 times with PBS and 2 times with MIR05 buffer, gently scraped and re-suspended in 450µl of MIR05 buffer avoiding big clusters. Homogenous cell suspension (400ml) was added into the chamber and chamber was closed with the stoppers carefully to remove air bubbles. After achieving a stable and constant state of respiration the following substances were added:

1) detergent for permeabilization - digitonin (25µg/ml)
2) substrate for fatty acid oxidation - Octanoylcarnitine (1mM)
3) tricarboxylic acid cycle (TCA) substrates – pyruvate (2mM), malate and glutamate (10mM) (PMG)
4) substrate for Complex II of respiratory chain – succinate (10mM)
5) inhibitor of UCP1 mediated proton flux – guanylyl diphosphate, GDP (2mM)
6) uncoupler – Carbonyl cyanide p-trifluoro-methoxyphenyl hydrazine, FCCP (1mM)
7) inhibitor of cytochrome C oxidase – sodium azide, NaN3 (50mM)

2.3.7.3. Adipose tissue preparation for oxygraph measurement

Oxygraph measurement of tissue samples is best performed on freshly isolated samples. After extracting the tissue from the mice, samples were kept prior to use in serum free DMEM medium at 37^0 C. Due to high respiratory capacity 2-3mg of BAT was sufficient. On the other hand, 10-15mg of WAT is required for this measurement. Tissue was cut in small pieces and placed into the chamber, with 2ml of MIR05 buffer. Further on, procedure is the same like it is explained in 2.3.7.2.

Mitochondrial respiration buffer (MIR05):
EGTA……0.90g
MgCl2x6H2O……....0.610g
Taurine……..2.502g
KH2PO4…….....1.361g
HEPES……..4.77g
D-sucrose……....37.65g
Lactobionic acid ……....120ml (0.5M)
BSA……..1g
Dissolved in 800ml H2O, stir at 30ºC; adjust pH to 7.1 with KOH, add lactobionic acid and BSA in the end, add H_2O to a final volume 1l and store frozen at -20ºC.

Table 3: Substances used in measurement of oxygen consumption

	Substance	Stock concentration	Diluent	Remarks and storage
1	Digitonin	525 µg/ml	H_2O	always freshly prepared and kept at 37ºC. Powder at RT
2	Octanoylcarnitine	50mM	H2O	-20ºC
3	Pyruvate	2M	H_2O	always freshly prepared. RT as a powder, aliquots at-20ºC
4	Malate	400mM	H_2O	Powder at RT, aliquots at-20ºC
5	Glutamate	2M	H_2O	Powder at RT, aliquots at-20ºC
6	Succinate	1M	H_2O	-20ºC
7	GDP	1M	H_2O	-20ºC
8	FCCP	1mM	99% ethanol	-20ºC and protected from light
9	NaN3	4M	H_2O	-20ºC

2.4. Immunological methods

2.4.1. Materials

Mouse Leptin DuoSet ELISA kit, R&D systems, DY498-05

Click-IT™ EdU cell proliferation kit, thermoFisher Scientific, C10337

Immu-Mount™ ThermoFisher Scientific, 9990402

Normal goat serum (NGS), Cell Signaling, 54250

Triton®X-100, BDH Prolabo Chemicals,28817.295

Direct cAMP ELISA kit, Enzo, ADI-900-066

2.4.2. Equipment

Leica DMI4000 B microscope Leica Mikrosysteme Vertrieb GmbH

Leica DFC425 C camera Leica Mikrosysteme Vertrieb GmbH

Confocal microscope, Zeiss 5

Spectrophotometer, Eppendorf, Bio Photometer

ImageJ software

Plate reader EnSpire™

2.4.3. EdU Proliferaton assay and microscopy

To measure proliferation of BAs and WAs isolated form WT and GPR111 KO mice, the Click-iT® EdU Assay was used. EdU (5-ethynyl-2´-deoxyuridine) is a nucleoside analog of thymidine and it is incorporated into DNA during active DNA synthesis. Detection is based on a click reaction, a copper-catalyzed covalent reaction between an azide and an alkyne https://www.thermofisher.com/order/catalog/product/C10337#/C10337. Cells were seeded on cover slips 12h before adding EdU (10µM). Proliferation frame was 48h. After 48h, cells were fixed with 1ml of 4% PFA for 15min, washed with 3%BSA in PBS, permeabilized with 0.5% Triton® X-100 in PBS for 20 min. Click-iT® EdU Assay cocktail and Hoechst were prepared following manufacturer's instructions. Cells were incubated protected from light at RT, first in EdU cocktail for 30 min, washed two times with PBS and incubated for the next 30 min in 1ml Hoechst solution (1:2000) in PBS. After 30 min, cells were washed with PBS and mount with Immu-Mount™ under a coverslip. Fluorescence microscopy was performed with a Leica DMI4000 B microscope with a Leica DFC425 C camera. Pictures were quantified using ImageJ software and results are represented as a percent of EdU+ cells.

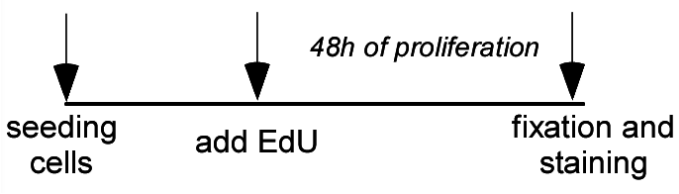

Scheme 1: Schematic representation of EdU staining.

Triton 0.5%
prepared in 10ml PBS
Triton® X-100…….....50µl

Blocking solution 50ml (3% BSA)
prepared in PBS
BSA……..1.5g

2.4.4. Immunofluorescence (IF) staining of cilia

Brown adipocytes (50.000 cells) were seeded on coverslips. Next day, when cells were attached, medium was changed to induction medium. Day after induction cells were washed with PBS, fixed with 4% PFA for 1 hour at 4ºC. Further on, cells were washed with PBT, two times and blocked in blocking solution for 1 hour at 4ºC.
Dilution of primary antibody was prepared in blocking solution without normal goat serum (NGS). Cells were incubated in primary antibody overnight at 4^0 C. Next day, cells were washed 2x5 minutes with PBT and secondary antibodies were added. Cells were incubated in secondary antibody for 2h at RT, protected from light, with gentle agitation. After incubation, cells were washed with PBT 2x5 minutes and mount with Immu-Mount™ under a coverslip. For visualization of cilia, confocal microscope was used. Pictures were quantified using ImageJ® software and results are represented as a number of cilia per total cell number.
Antibodies used for detection are listed below (Table 4).

PBT
prepared in 100ml PBS
Triton® X-100…….....200µl

Blocking solution (2%BSA+1%NGS)
Prepared in 50ml PBT
BSA……...1g
NGS……..500µl

Table 4: List of antibodies for immunofluorescence staining of cilia

Target/ Antibody name	Source	Dilution
Arl13b	Proteintech	1:500
Anti-acetyl-tubulin	Merck KGaA	1:500
Alexa Fluoro 488 Phalloidin	ThermoFisher Scienific	1:1000
Donkey anti-Rabbit IgG, Alexa Fluor 647	ThermoFisher Scienific	1:500
Goat anti-Mouse IgG, Alexa Fluor 555	ThermoFisher Scienific	1:500

2.4.5. Phalloidin staining of stress fibers

Phalloidin is a bicyclic peptide that belongs to a family of toxins isolated from the deadly Amanita phalloides mushroom. Fluorescent and biotinylated phalloidins bind F-actin with strong affinity https://www.thermofisher.com.
Cells were seeded on 6 well plate and grown for 48h. After 48h, cells were starved and shaken on orbital plate shaker for 1h. Later on, cells were fixed with 4% PFA, permeabilized with 0.1% Triton™X-100 for 15 min. Phalloidin staining was performed according to the manufacturer's instructions. Microscopic pictures were taken using Leica DMI4000 B microscope.

2.4.6. Serum leptin level measurement (Leptin ELISA)

Serum leptin levels were measured using a Mouse Leptin DuoSet ELISA kit according to the manufacturer's instructions. Serum samples from mice that were fed with HFD/ND were diluted in regent diluent in ratio 1:4. All samples were analyzed in duplicates. Absorbance was recorded using an EnSpire™ plate reader at 450nm.

2.4.7. cAMP concentration (cAMP ELISA)

The concentration of cAMP in brown preadipocytes was determined using cAMP ELISA kit according to manufacturer's instructions and each sample was analyzed in duplicate. Absorbance was recorded using an EnSpire™ plate reader at 405nm. Results were normalized to protein content.

2.5. Biochemical methods

2.5.1. Materials

Electrophoresis/western blotting system: Mini Trans-Blot® Cell system (BioRad)

Nitrocellulose blotting membranes (GE Lifesciences), A29434120

Acrylamide, Rotiphorese® Gel 30 (37.5:1), Carl Roth GmbH, 3029.1

SuperSignal™ West Pico PLUS Chemiluminescent Substrate, ThermoFisher Scientific, 34579

SuperSignal™ West Femto Maximum Sensitivity Substrate, ThermoFisher Scientific, 34096

Bovine Serum Albumin (BSA), Carl Roth GmbH, 8076.3

Coomassie dye, Coomassie brilliant blue, Merck, 1.15444.0025

Color protein Broad Range, Bio Labs, 0021405

Protease inhibitor cocktail, Complete® EDTA-free Roche, Mannheim, 11873580

Tris, Roth, AE15.3

Glycin, Roth, 3908.3

Natriumchlorid (NaCl), Roth, 3957.1

Sodium-dodecyl sulphate (SDS), Roth, 2326.2

Tri-NAtriummonovanadat (NaF), Roth, 0735.2

Tris HcL6.8

Bromphenol blue, Roth, T116.1

2.5.2. Equipment

Bench-top Vortex, Laboratory shaker / orbital / vortex / bench-top 444-1378 (VWR)

Centrifuges, Thermo Fischer Scientific, Heraeus™ Biofuge™ Stratos™, Eppendorf

Chemiluminescence reader, GE Healthcare Europe, Freiburg, ImageQuant LAS 4000

Homogenizer workcenter, T10 basic, IKA®

Ultrasonic homogenizers, Sonoplus, Bandelin

Photometer, Eppendorf, Hamburg, Biophotometer D30

Power supply, Consort bvba, Turnhout, Belgium, Electrophoresis power supply, EV202

Thermomixer, Eppendorf, Hamburg, 5350

Glas plates mini Protean®, Bio Rad, 1653312

2.5.3. Western blotting

2.5.3.1. Protein extraction from fat tissues

Two hundred µl of ice cold lysis buffer was added into tissue samples and the tissues were homogenized using a tissue homogenizer (Ultra-Turrax). Further homogenization was done using ultrasonic homogenizers. The homogenized tissue lysates were centrifuged (13000rpm, 4°C) for 25 minutes. The clear supernatant was carefully

collected in a fresh Eppendorf tube (1.5ml), not disturbing the pellet or the floating lipid layer. In case of samples isolated from HFD fed mice, centrifugation step was repeated one time more.

2.5.3.2. Protein extraction from cells

For protein isolation from pradipocytes (70 µl) and from mature adipocytes (120 µl) of ice ice-cold lysis buffer was added into the wells. Cells were scraped with cell scraper and collected into a new Eppendorf (1.5ml) tube. Cell suspension was homogenized using ultrasonic homogenizer and centrifuged (13000rpm, 4°C) for 25 minutes. Clear supernatant was transferred into a new 1.5ml tube.

Lysis buffer:
Tris-HCl (pH=7.5)……..50mM
NaCl…….....150mM
NP-40……..1%
Sodium-deoxycholate……..0.5%
Sodium-dodecyl sulphate (SDS)……..0.1%
EDTA……....0.1mM
EGTA …….....0.1mM
Dissolved in H2O, filtrated and store at 4 ^{0} C.
Before use, the following aditives were added:

Complete®EDTA free (25x) ……..40µl/ml
NaF……..10mM
Na_3VO_4……..1mM

2.5.3.3. Quantification of proteins with the Bradford protein assay

The Bradford assay is quick and accurate spectroscopic analytical procedure used to measure the concentration of protein in a solution. This assay is based on an absorbance shift of the dye Coomassie Brilliant Blue G-250. The Coomassie Brilliant Blue G-250 dye exists in three forms: anionic (blue), neutral (green), and cationic (red). This dye specifically interacts with arginine, tryptophan, tyrosine, histidine and phenylalanine residues. Under acidic conditions, the red form of the dye is converted into its blue form, binding to the protein being assayed. If there's no protein to bind, then the solution will remain brown. While the free dye displays an absorbance maximum at 470 nm the bound dye has an absorbance maximum at 595 nm https://bio-protocol.org/bio101/e45. The protein content is determined using a BSA standard ranging from 1 to 30µg as a reference. 2µl of protein lysates were diluted to 100µl with 0.15 M NaCl solution, 1 ml Coomassie solution was added and incubated for 2 min. The samples were collected in cuvettes and absorbance measured at 595nm, followed by determination of protein concentration (µg/ml).

Coomassie solution:
Coomassie brilliant blue G-250.....50 mg
EtOH 95%.....25 ml
Phosphoric acid 85% .....50 ml
filled up to 500 ml with H_2O, stored at 4° C protected from light

2.5.3.4. Sample preparation for Western blot

Equal amounts of protein (50µg) from lysates were prepared for WB experiments. Volumes were equalized by addition of water. Three times concentrated loading buffer (3X Laemmli) was then added to achieve an end volume with 1X concentration. To reduce disulfide bonds, β-mercaptoethanol was added in ratio 1:20. The samples were heated to 95°C for 10 minutes. After a short spin-down, the samples are ready for loading.

3X Laemmli buffer:
Tris-HCl (pH=6.8) 125mM
Glycerol..... 20%
SDS……..17%l
Bromphenol blue……..0.015%
dissolved in H2O and stored at -20 ^{0} C.

2.5.3.5. Sodium dodecyl-sulphate polyacrylamide gel electrophoresis (SDS-PAGE)

SDS-PAGE (sodium dodecyl sulfate-polyacrylamide gel electrophoresis) is a discontinuous electrophoretic system developed by Ulrich K. Laemmli which is commonly used as an analytical method to separate proteins with molecular masses between 5 and 250 kDa. To perform discontinuous gel electrophoresis differentially buffered separating and stacking gels are poured on top of each other between glass plates. The proteins that pass first through a stacking gel get concentrated at the stacking/separating gel interface. In the separating gel the proteins are separated according to molecular size in denaturing gel (containing SDS). Polyacrylamide gels were prepared as the below provided chart (10ml/ gel) (Table 5). Prepared proteins were loaded into pockets of stacking gel. Gels were run in 1X electrophoresis buffer at 100V for 90-120 minutes at room temperature using the Mini Trans-Blot® Cell system.

Table 5: Ingredients needed for separation and stacking gel

Separation gel:

	8%	**10%**	**12%**	**15%**
H_2O	4.6ml	4ml	3.3ml	2.3ml
30% Acrylamide	2.7ml	3.3ml	4ml	5ml
1.5M Tris (pH=8.8)	2.5ml	2.5ml	2.5ml	2.5ml
20% ammonium persulfate	0.05ml	0.05ml	0.05ml	0.05ml
N-N-N'-N'-Tetramethyl ethylene diamnine (TEMED)	6µl	4µl	4µl	4µl

Stacking gel (6ml)

H_2O	3.4ml
30% Acrylamide	0.83ml
1M Tris (pH=8.8)	0.63ml
20% ammonium persulfate	0.05ml
N-N-N'-N'-Tetramethyl ethylene diamnine (TEMED)	6µl

10x Electrophoresis buffer:
Tris.....250mM
Glycine.....2M
SDS……..0.1%l
dissolved in H2O and pH adjusted to 8.3.

2.5.3.6. Western blotting

Upon completion of SDS-PAGE, the gels were carefully removed from the gel run cassette, placed in the Mini Trans-Blot® Cell system transfer assembly. A nitrocellulose membrane was placed on top of the gel and air bubbles at the gel-membrane interface were carefully removed. Proteins from the gel were transferred onto the membrane by application of a 300mA transverse electric field, for 90 minutes. Thereafter, the

membranes were removed from the cassette, labeled, briefly washed with TBS-T and blocked in blocking buffer minimum 1h at RT. The membranes were incubated in primary antibody solutions that were prepared in filtrated blocking buffer overnight at 4°C with gentle agitation. On the next day, the membranes were washed three times (5 min) in TBS-T and incubated in appropriate HRP-conjugated secondary antibody solutions (in 1% BSA TBS-T) for an hour at room temperature. Upon completion of secondary antibody incubation, the membranes were washed again 3x5 minutes in TBS-T. The washed membranes were covered in enhanced Super Signal ™West Pico Plus chemiluminescence substrate or with Super Signal ™West Femto Maximum Sensitivity chemiluminescence substrate solution for 1-3 minutes, and luminescence was immediately measured in an ImageQuant LAS 4000 chemiluminescence reader. The bands were quantified with ImageJ software. Thereafter, the membranes were stripped with stripping buffer for up to 15 minutes, washed 3 times for 5 minutes with TBS-T, blocked and incubated with primary antibody solution for the next protein of interest.

Antibodies used for immune-detection of proteins on a nitrocellulose membrane are listed below (Table 6).

Transfer buffer (1X):
10X electrophoresis buffer.....10%
Methanol.....20%
H_2O……70%

10 x TBS:
Tris .....24.3 g
NaCl.....80 g
dissolved in 1000 ml H2O, adjusted to pH 8.0 with HCl

TBS-T (0.1%):
Tween-20 .....1 ml
10 x TBS .....100 ml
H2O.....900 ml

Blocking buffer (5%):
BSA.....5 g
TBS-T.....100 ml

Stripping buffer:
Glycine.....2.M
SDS.....1%

Dissolved in H2O and pH adjusted to 2 with HCl.

Table 6: List of antibodies for Western blot

Target/ Antibody name	Source	Dilution
UCP1	Cell Signaling Technologies	1:1000
Calnexin	Cell Signaling Technologies	1:2000
HRP-conjugated anti-rabbit IgG	Cell Signaling Technologies	1:5000

2.6. Molecuar biology methods

2.6.1. Materials

Transcriptor First Strand Synthesis Kit, Roche, 04379012001

Diethyl pyrocarbonate (DEPC), Carl Roth, K028.1

innuSOLV RNA Reagent, Analytik Jena, 845-SB-2090100

SYBR® Green PCR Master Mix, Thermo Fischer Scientific, 4309155

Phire Tissue Direct PCR Master Mic, ThermoFisher Scientific, F170L

Ethanol, Roth, 9065.4

2-Propanol, Roth, 6752.4

Trichlormethan/Chloroform, Roth, 6340.1

2.6.2. Equipment

Autoclave, VX-150, Systec GmbH, Linden

Electrophoresis chamber: RunOne™ Electrophoresis System, Embi Tec San Diego, CA, USA

Gel casting chambers: RunOne™ Agarose Gel Casting Systeme, Embi Tec San Diego, CA, USA

Incubator, AL01-07-100, Advantage Lab bvba, Schilde, Belgium

Microwave, Severin, Sundern

Spectrophotometer, NanoDrop 2000, ThermoFisher Scientfic

Real-time PCR machine, Applied Biosystems® StepOnePlus™ System, ThermoFisher Scientific

Thermocycler, T1 Thermocycler, Biometra GmbH, Göttingen

Thermomixer,5350, Eppendorf, Hamburg

UV light transilluminator, GelDoc®XR, BioRad, München

QuantityOne® Software, BioRad, München

2.6.3. Preparation of genomic DNA and genotyping

For genotyping mice, small pieces of earlobe or tail biopsies were used. DNA was extracted and amplified using Phire™ Tissue Direct PCR Master Mix according to manufacturer's instructions. After digestion, samples were mixed with 2X Phire tissue master Mix, primers and water. PCR was done using the program listed in table 7.

Genotyping PCR:

gDNA……1µl
2xPhire tissue direct PCR master Mix ……..10µl
Forward primer GPR111+/+ (10pmol/µl) ……1µl
Forward primer GPR111-/- (10pmol/µl) ……..…1µl
Reverse primer GPR111+/- (10pmol/µl) ……1µl
H_2O add to 20µl

Primers used for genotyping:

GPR111-/- For: 5'-ACCCATGGCGATGCCTGCTT-3'

GPR111+/+ For: 5'-TTGCCATCCTCACACCACTGC-3'

GPR111+/- Rev: 5'-CATGGACTCCTACCCACAAAACCGATG-3'

Table 7: PCR cycling program used for genotyping

Step	Time	Temperature
Initial denaturation	5 min	98^0 C
Denaturation	5s	98^0 C
Annealing	5s	72^0 C
Extension	30s (35-40x)	72^0 C
Final extension	1 min	72^0 C

2.6.4. Agarose gel electrophoresis

Agarose gel electrophoresis is a simple method for separating, identifying, or purifying DNA fragments. Agarose was diluted in 1x TBE buffer to create a 2% solution which was heated in the microwave. For 100 ml agarose solution, 8µl ethidium bromide (800 ng/ml final) was added. The melted agarose was poured into casting chambers, allowed to harden at RT and placed into an electrophoresis chamber containing 1 x TAE buffer. Samples were loaded on the agarose gel and electrophoresis was performed at 100 V at RT. DNA bands were visualized under an UV light transilluminator (GelDoc®XR, BioRad) using QuantityOne® software(BioRad).

50 x TBE:
Tris.....2 M
Acetic acid 5.71%
Na_2-EDTA 50mM
Dissolved in H2O and store at RT.

2.7. RNA isolation and reverse transcription

2.7.1. RNA extraction from the tissue with high lipid content

To tissue explants 1ml of InnuSOLV reagent was added, followed by homogenization. Samples were incubated at RT 5min, centrifuged at 12000rpm for 10 minutes. Lipid monolayer was formed on the top of the samples. The lower part was carefully, avoiding lipid layer, transferred into a new 2 ml Eppendorf tube. 300µl of chloroform was added and samples were vortexed and incubated at RT for 3 min. Further on, samples were centrifuged at 12000rpm for 30min at 4^0 C. The upper aqueous phase (≈1ml) was transferred to a fresh 2ml Eppendorf tube, avoiding the DNA containing interphase. Again, 200µl of chloroform was added, samples were vortexed, incubated at RT for 3min, centrifuged at 12000rpm for 15min at 4^0 C. The upper aqueous phase (≈700µl) was moved to 1.5ml Eppendorf tube. 500µl of isopropanol was added, shaken by hand and incubated 5min at RT and centrifuged at 14000rpm for 10min at 4^0 C. After centrifugation, supernatant was carefully discarded and the pellet was washed with 1ml of 70% ethanol. Samples were centrifuged at 14000rpm for 7min at 4^0 C. Washing with ethanol was repeated 3 times. The pellet was dried under the fume hood for 30 min. Samples were resolved in DEPC water and incubated for 10min at 55^0 C. Concentration of RNA was measured using Nanodrop and stored at -80^0 C.

2.7.1.2. RNA extraction from cells

InnuSOLV reagent (1ml) was added on each well of 6 or 12 well plate. Cell suspension was collected into 1.5ml Eppendorf tube. 200µl of ice-cold chloroform ($CHCl_3$) was added. The tubes were then thoroughly shaken (but not vortexed) and left standing at room temperature for five minutes. The samples were then centrifuged (13000rpm, 4°C) for 15 minutes. After centrifugation, up to 500µl of the clear upper phase was carefully collected (not disturbing the DNA containing interphase) in new labeled Eppendorf (1.5ml) tubes. Into these 500µl of ice-cold isopropanol was added, and the tubes were shaken vigorously. The samples were then centrifuged (13000rpm, 4°C) for 15 minutes. The supernatant was discarded and the pellet was washed with 75% ethanol (diluted in DEPC treated water). The samples were shortly vortexed to re-suspend the pellet, followed by centrifugation (13000rpm, 4°C) for 10 minutes. Washing step with 75% ethanol was repeated two more times. After the last centrifuge, the supernatant was discarded and the tubes were left to dry for 15-20 minutes under the flow of chemical hood. The dried RNA pellet was resolved in DEPC-treated water (up to 50µl, depending on pellet size), at 55°C for five minutes. RNA content was determined using the Nanodrop and samples were stored at -80^0 C.

2.7.1.3. cDNA synthesis

One microgram of total RNA was used for reverse transcription into complementary DNA (cDNA). Reverse transcription was performed using the Transcriptor first strand synthesis kit (Roche), per manufacturer's instructions. The resulting cDNA was diluted 1:10 in water.

2.7.1.4. Quantitative real-time polymerase chain reaction (qRT-PCR)

qPCR is a method for monitoring the accumulation of DNA product from a PCR reaction in real time. qPCR instrument contains a thermal cycler (PCR machine) and an optical module that detects fluorescence during the measurement. To track DNA amplification in real time, oligonucleotides and a fluorescent reporter were added to all samples. Increase of fluorescence is correlating with amplification of DNA. In the end of the measurement results were shown as an amplification plot. Steps of qPCR program have been listed in table 8 and the list of oligonucleotides used for qRT-PCR analyses in table 9.

qPCR reaction mix:
cDNA (1:10) 4µl
Forward primer (10pmol/µl) 0.5µl
Reverse primer (10pmol/ml) 0.5µl
2xSYBR Green master mix 5µl

Table 8: qPCR program

Step	Time (s)	Temperature (ºC)
1	**600**	95^0 C
2	**10**	95^0 C
3	**15**	72^0 C
4	**90**	72^0 C
5	**1**	82^0 C
Melting curve		
6	**1**	95^0 C
7	15	65^0 C
8	-	95^0 C

Table 9: qRT-PCR primer list

Gene name	Organism		Primer sequence (5' – 3')
Hprt	Mouse	*Forward*	GTCCCAGCGTCGTGATTAGC
		Reverse	TCATGACATCTCGAGCAAGTCTTT
Pparγ	Mouse	*Forward*	ACTGCAGCCCCCTATAGT
		Reverse	GGATCAGTTGGGTCAGTGGG
Ucp1	Mouse	*Forward*	TAAGCCGGCTGAGATCTTGT
		Reverse	GGCCTCTACGACTCAGTCCA
Ppargc1a	Mouse	*Forward*	GCACACACCGCAATTCTCCCTTGTA
		Reverse	ACGCTGTCCCATGAGGTATTGACCA
Gapdh	Mouse	*Forward*	GGCTGCCCAGAACATCAT
		Reverse	CGGACACATTGGGGGTAG
Lep	Mouse	*Forward*	TGGCTGGTGTCAGATTGCTC
		Reverse	TAGTGCAAGGTTCTCTGAGCG
Gpr111	Mouse	*Forward*	CGCCATTATCACACTTGCCG
		Reverse	GCATCCGGACTTACCTGGAG
Tnfa	Mouse	*Forward*	CCCTCACACTCAGATCATCTTCT
		Reverse	GCTACGACGTGGGCTACAG
Ccl2	Mouse	*Forward*	TGGAGCATCCACGTGTTG
		Reverse	GCTGGTGAATGAGTAGCAGCA
Gli1	Mouse	*Forward*	CACCGTGGGAGTAAACAGGCCTTCC
		Reverse	CCAGAGCGTTACACACCTGCCCTTC
Ptch1	Mouse	*Forward*	CTCAGGCAATACGAAGCACA
		Reverse	GAGAAGGAGCCAGAGTCCAG
Smo	Mouse	*Forward*	CTCTTCCTGGTTAGCACCTTAAAAC
		Reverse	GTGTGTGAGAGTGTATGTGTGTGTG
LepR	Mouse	*Forward*	TCTCATGACCACTACAGATGAACC
		Reverse	TCTGCAACCGTCACACCATT

2.8. Immunohistochemistry

2.8.1. Materials

Simport™ Scientific unisette™ Tissue Processing/Embedding Cassette, ThermoFisher Scientific, 11655610

Paraplast®, Carl Roth, 39602004

Tissue embedding station: Embedding Center/ Dispenser + Hot plate EG1160, Leica

DAB peroxidase substrate kit, Biozol Diagnostica Vertrieb GmbH, SK-4100

Roti®histokitt, Carl Roth, T1602

Hematoxylin solution according to Mayer, Sigma Aldrich, 51275

Eozyn Y solution, Sigma Aldrich, HT110216

Menzel™, Microscope Coverslips, ThermoFisher Scientific, 11778691

Signal Stain Boost IHC Det. (HRP. Rab), Cell Signaling, 8114S

2.8.2. Equipment

Embedding tray Leica)

EVOS® FL Color Imaging System (Thermo-Fischer Scientific)

Microtome: HM335E Rotary microtome (Microm)

2.8.3. Sample preparation

Freshly isolated tissue explants from WT and KO mice were fixed in 4% PFA (no longer then 16h). Fixed tissue samples were washed twice (5 minutes each) with ice-cold PBS. Next, the samples were placed in 50% ethanol for 3x20 minutes with gently agitation at 4°C. Thereafter, the samples were moved into 70% ethanol for 3x20 minutes at 4°C. Dehydration was completed with 3x20 minutes incubation of the samples in 95% ethanol (at room temperature), followed by 3x20 minutes incubation in 100% ethanol. This was followed by a 3x10 minute incubation in xylol at room temperature. Xylol was replaced with liquid paraplast at 60°C, for 2x1 hour incubations. The samples were moved to a fresh beaker containing liquid paraplast and stored at 60°C overnight. The next day, the dehydrated samples were embedded in paraplast and stored at room temperature or at 4°C. Embedded sections of tissue were cut into 4µm thick sections using a microtome and placed on a slide. Slides were dried in the incubator at 42^0 C, overnight.

2.8.4. Hematoxylin/Eosin staining (H&E)

It is a quick, widespread histological stain, which can visualize a large number of different tissue structures. Hematoxylin stains nucleic acids and thereby cell nuclei blue, while eosin stains the cytoplasm and extracellular matrix pink.
In order to perform a hematoxylin/eosin staining, paraffin sections were deparaffinized twice for 2 min in xylol. Tissue sections were rehydrated by incubation in 100%, 90%, 80%, 70%, 50% ethanol and PBS for 2 min. Slides were then treated for 10 seconds min with hematoxylin and washed for 15 minutes under tap water. Further on, slides were dipped into a bicker with eosin for 1 minute. Samples were washed in tap water 4 times for 1 minute. After this step, samples were dehydrated by submerging the slides for 2 minutes in gradually higher percent solution of ethanol each (50%,75%,95%,100%) and mounted with Roti® histokit. Slides were dried under the flow and pictures were taken using the microscope EVOS® FL Color Imaging System at 20x and 40x magnification.

2.8.5. UCP1 staining

Similarly, as it was described in 2.8.4, slides were washed 3 times for 5 minutes in xylol, then dehydrated 3 times for 5 minutes in ethanol (100%, 96%,75%) and in the end 2 times for 5 minutes in water. After this, slides were first dipped in 20mM sodium citrate (pH 6) for 20 minutes at 75-80^0 C to be unmasked and the procedure was repeated once again in 10mM sodium citrate. Slides were washed 3 times for 5 minutes in distillated water (dH_2O). To saturate endogens peroxidase, slides were incubated for 10 minutes in 3% hydrogen peroxide (H_2O_2). In the end, slides were washed once again for 5 minutes in (dH_2O). To prevent unspecific binding, slides were blocked in blocking solution for 1hour in a humid chamber. UCP1 antibody was diluted (1:500) and added to the slides. Slides were incubated over night at 4^0 C in a humid chamber. The next day, primary antibody was removed and slides were washed 3 times for 5 minutes with PBS-T. Secondary HRP anti rabbit antibody was added directly on slides. Slides were incubated for 1 hour at RT. After incubation, slides were washed 3 times for 5 minutes with PBS-T and developed using DAB kit following manufacturer's instructions. The stained sections were mounted with Roti® histokit. Slides were dried under the flow and pictures were taken using the microscope EVOS® FL Color Imaging System at 20x and 40x magnification.

20mM Natriumcitrat-dihydrat pH6:
$C_6H_5O_7Na_3x2H_2O$.....5.882g
filled up to 1000 ml with milipore H2O, stored at RT

Peroxidase solution
30% H2O2 .....20ml
add dH_2O up to 200 ml

PBS-T:
prepared in PBS
Tween ® 20……..….0.1%
stored at RT, light protected

Blocking Puffer
prepared in PBS
Tween ® 20……0.1%
Normal goat serum (NGS)……2.5%

Solution for primary and secondary antibody:
prepared in PBS
Tween ® 20……0.1%
Normal goat serum (NGS)……...0.25%

2.9. Statistical analysis

If it's not stated differently all results have been represented as mean ± SEM. Comparison between two data sets was done using *Student t test (two tailed)*. On the other hand, comparison between more than two sets was done using *one-way ANOVA* followed by a *Bonferroni multiple comparison post-test.* P-values <0.05 were considered as significant (*p<0.05., **p<0.01, ***p<0.001).
qPCR data are represented as the geometric mean of $2^{-\Delta\Delta Ct}$ values, with error bars calculated as $2^{-(\Delta\Delta Ct \pm SEM(\Delta Ct))}$, according to (Yuan et al., 2006). Statistical analysis of qPCR data was performed on ΔCt values only.
Statistical analysis was performed using Graph Pad Prism 6.0.

3. Results

3.1. Expression pattern of Gpr111

Unbiased screening results of 347 GPCRs show presence of 182 GPCRs in pre-adipocytes and 230 in mature BAs. Class A and aGPCRs represented the two largest classes in both pre- and mature BAs (Klepac et al., 2016). One of the identified aGPCRs was Gpr111.
To validate the screening results, mRNA levels of Gpr111 were analyzed in pre- and mature BAs and WAs (Figure 18B). Also, mRNA levels of Gpr111 were analyzed in murine ATs as well as in the brain, the skin, the lungs and the liver (Figure 18C). Additionally, mRNA levels of Gpr111 were investigated in AT of newborn mice, 8 week (8w) and 20 week (20w) old mice (Figure 18D). The expression pattern of Gpr111 was investigated in AT of mice after they were exposed to cold (4ºC) for one week (Figure 18E) and when mice were fed with HFD (Figure 18F).

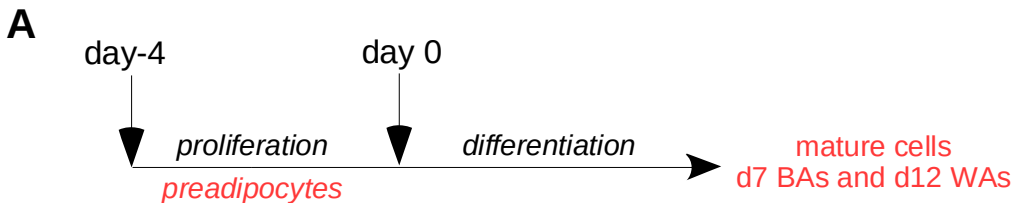

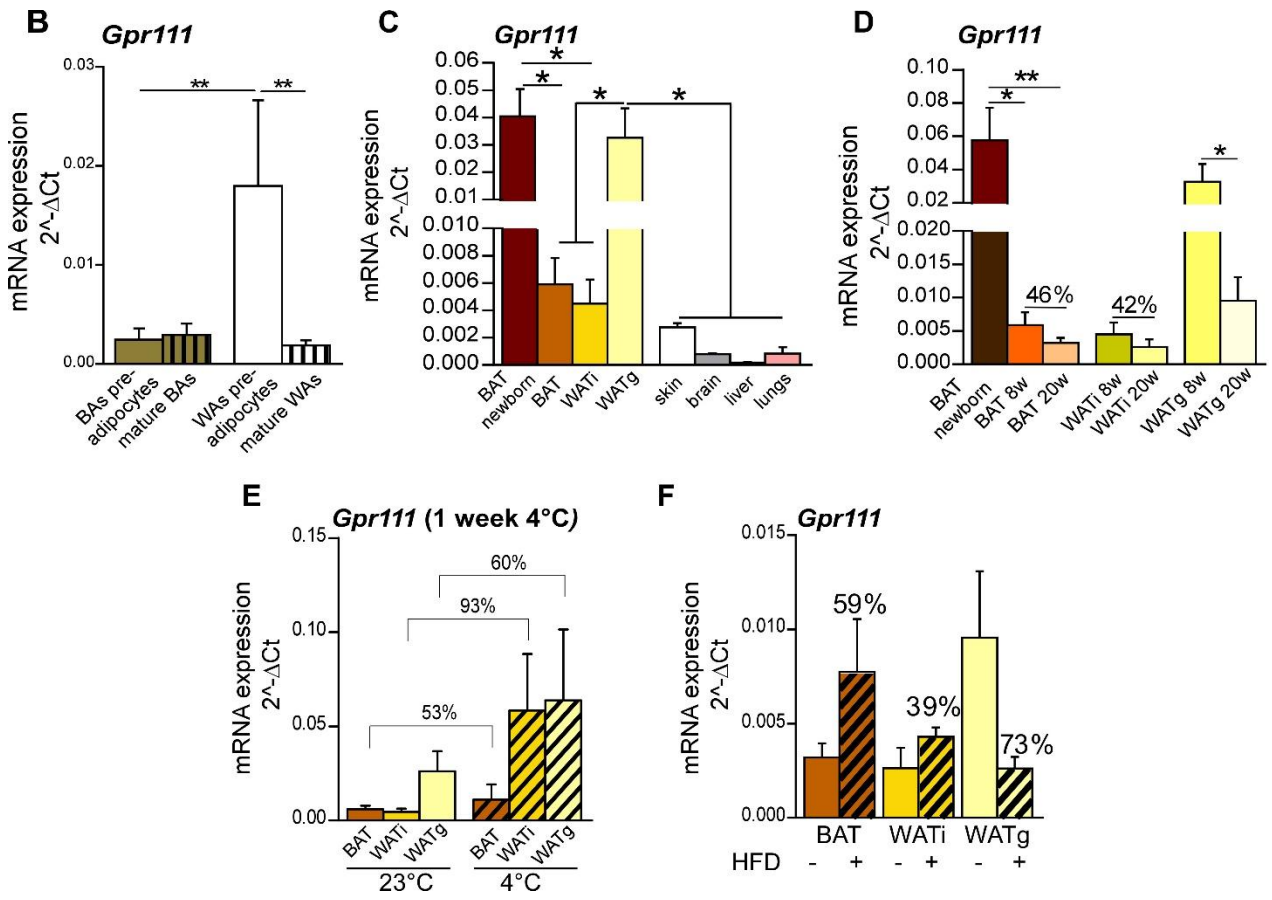

Figure 18: Expression pattern of Gpr111
(A) Simplified, schematic representation of differentiation of adipocytes (B) mRNA expression levels of Gpr111 in pre- and mature BAs and WAs. (C) mRNA expression levels of Gpr111 in different tissues of 8 week old mice. (D) mRNA expression of Gpr111 levels in AT of newborn, 8 and 20 week old mice. (E) Expression of Gpr111 in AT after 1 week of cold exposure (4ºC) (F) Expression of Gpr111 in AT after HFD. Expression data are normalized to *Hprt* and represented on a bar graph as mean ± SEM, ANOVA, n= 3-16, *<0.05, **p<0.01; *** p<0.001

qPCR analysis of *Gpr111* in adipocytes correlates with screening results. *Gpr111* is expressed in pre- and mature adipocytes. However, expression of *Gpr111* was significantly higher in WAs preadipocytes (0,018 ± 0,009) in comparison to BAs preadipocytes. Interestingly, *Gpr111* expression was significantly lower in mature WAs in comparison to WAs preadipocytes (Figure 18B).

Gpr111 is also expressed in murine fat tissues. However, expression of *Gpr111* is significantly higher in WATg (0,032 ± 0,011) in comparison to BAT and WATi. These data indicate a potential role of *Gpr111* in WATg (Figure 18C).

The expression pattern of *Gpr111* in other organs such as skin, brain, lungs and liver was used for comparison. Interestingly, expression of *Gpr111* is significantly higher

(0,026 ± 0,011) in WATg in comparison to all other organs which were analyzed (Figure 18C).

It is very important to emphasize changes in *Gpr111* expression during ageing. Namely, expression of *Gpr111* is the highest in BAT of newborn mice, furthermore, expression is significantly lower in BAT (0,006 ± 0,002) of 8 week old mice and the lowest in BAT of 20 week old mice (0,003 ± 0,001). Although statistically not significant, the expression of *Gpr111* in BAT of 20 week old mice, was 46% lower than in 8 week old mice. Similar trend in *Gpr111* reduction was observed in case of WATi, where the expression of Gpr111 was 42% lower in case of 20 week old mice. Equivalently, WATg of 20 week old mice was significantly reduced (0,009 ± 0,003) in comparison to WATg from 8 week old mice (Figure 18D).

In AT of mice that were exposed to cold (4^0 C) for 1 week, expression of GPR111 was increased in comparison with AT of mice that were housed at 23^0 C. Namely, mRNA levels of Gpr111 were 53% increased in BAT, 93% in WATi and 60% in WATg in the group of mice that were exposed to cold in comparison to control group (23^0 C) (Figure 18E).

An interesting phenomenon in the expression pattern of *Gpr111* was observed in a case where mice were fed with HFD or ND (Figure 18F). Expression of *Gpr111* is increased in BAT (59%) and WATi (39%) of mice fed with HFD. However, the expression was 73% reduced in WATg.

In summary, Gpr111 seems to play a very important role in AT, especially in WATg. Expression of Gpr111 undergoes changes during ageing and HFD.

3.2. Role of Gpr111 in BAs

3.2.1. Loss of Gpr111 promotes differentiation of BAs

To explore the role of Gpr111 in BAs, cells were isolated from BAT of Gpr111$^{+/+}$ (WT) and GPR111$^{-/-}$ (KO) newborn mice. Isolation, immortalization and cultivation were performed according to the protocol that is explained in 2.3.3, 2.3.3.1, 2.3.3.3 and differentiated, mature BAs were then analyzed.
To investigate the effect of Gpr111 depletion on lipid accumulation in BAs, Oil Red O staining was performed on day 7 (d7) of differentiation of BAs (Figure 19A). Additionally, mRNA expression of adipogenic (*Pparγ*) and thermogenic (*Ucp1*) markers was analyzed using qPCR (Figure 19B). Furthermore, UCP1 protein expression was evaluated using Western blot (Figure 19C).

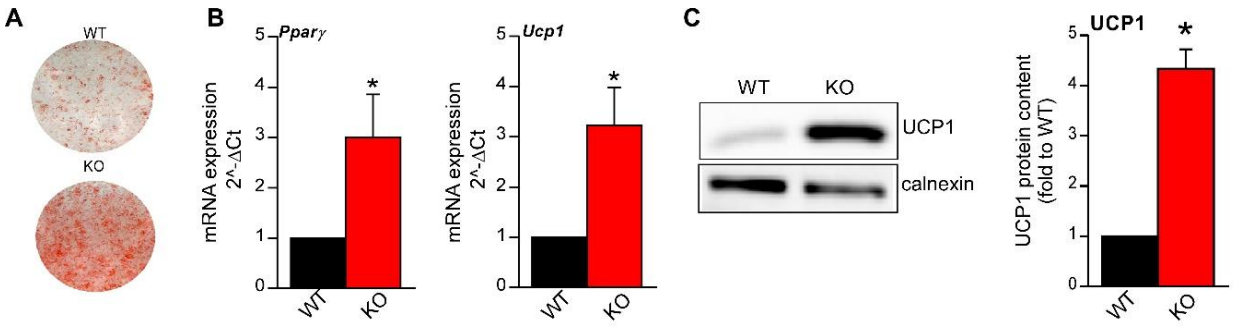

Figure 19: Effects of Gpr111 ablation on differentiation of BAs
(A) Representative Oil Red O staining of differentiated BAs. (B) mRNA expression of adipogenic (*Pparγ*) and thermogenic (*Ucp1*) markers. (C) Representative immunoblot of UCP1 in WT and KO BAs. Calnexin was used as a loading control. Expression data are normalized to *Hprt* and represented on a bar graph as mean ± SEM, *Student* t-test, n= 4, *<0.05.

Oil Red O staining shows a massive increase in accumulation of lipid droplets in KO cells. mRNA expression of *Pparγ* (2,996 ± 0,861) and *Ucp1* (3,230 ± 0,753) are significantly increased in KO cells. Similarly, protein levels of UCP1 were significantly higher in KO BAs.

Taken together, these results indicate an important role of *Gpr111* in differentiation of BAs.

3.2.2. Effects of Gpr111 ablation on BAs function

The most characteristic metabolic processes in BAs are lipolysis and oxygen consumption. To investigate the effects of Gpr111 deletion on metabolism in BAs *in vitro*, lipolysis assay and measurement of oxygen consumption were performed. Assays were performed with mature cells on d7.
NE was used as a positive control in lipolysis assay, because it is reported that NE stimulates glycerol release (Nedergaard and Lindberg, 1979). Basal as well as NE stimulated glycerol release was significantly increased in KO BAs (3,613 ± 0,667) in

comparison to WT (Figure 20A). Correspondingly, KO BAs show a higher oxygen consumption rate (Figure 20C). Namely, basal (1,356 ± 0,175) as well as UCP1 mediated respiration (1,035 ± 0,110) were significantly higher in KO BAs in comparison to WT.

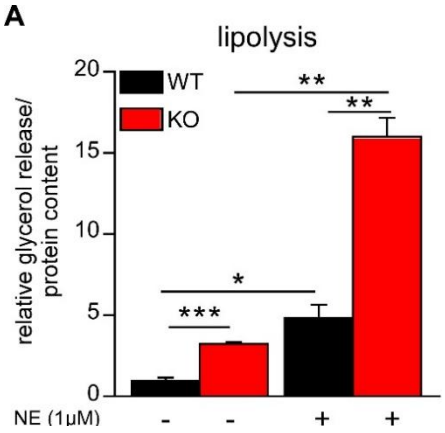

B

WT

KO

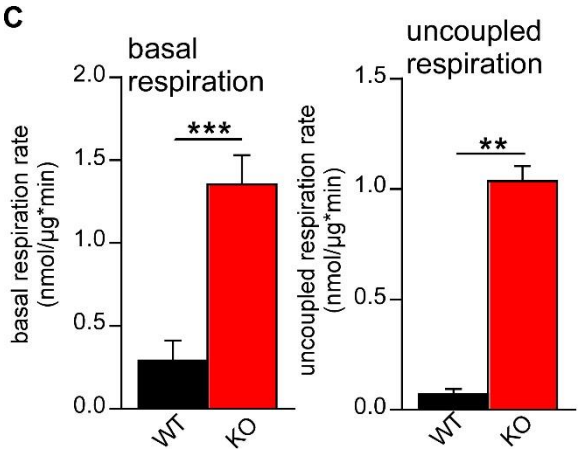

Figure 20: Effects of Gpr111 ablation on BAs function
(A) Relative glycerol release of differentiated BAs with and without presence of 1µM NE. (B) Representative oxygen consumption curves (WT-upper panel, KO-lower panel) (C) Basal and UCP1 mediated respiration. Results are represented on a bar graph as mean ± SEM. ANOVA was used for analysis of lipolysis data and *Student* t-test for oxygen consumption results. 4 different pools of cells were used for lipolysis and 3 for oxygen consumption measurement. *p<0.05, **<0.01, ***<0.001

These results lead to the conclusion that lack of Gpr111 improves metabolic function of BAs.

3.2.3. Lack of Gpr111 has no effect on proliferation of BAs

The huge effect of Gpr111 ablation on BAs differentiation and function could be a consequence of higher proliferation rate of cells. For a group of aGPCRs an impact on proliferation and mechanosensation was reported (Hamann et al., 2015).

To investigate the impact of Gpr111 depletion on BAs proliferation primary brown adipocytes were isolated from $Gpr111^{+/+}$ and $Gpr111^{-/-}$ eight week old mice. Cell isolation and cultivation was performed as it was described in 2.3.3, 2.3.3.3. Primary cells were seeded on glass cover slips and stained with EdU as it is explained in 2.4.3.

Surprisingly, primary $Gpr111^{-/-}$ BAs didn't proliferate more in comparison to WT (Figure 21).

This result confirmed that previously described effects of Gpr111 ablation on differentiation and function of BAs are not due to proliferation of these cells.

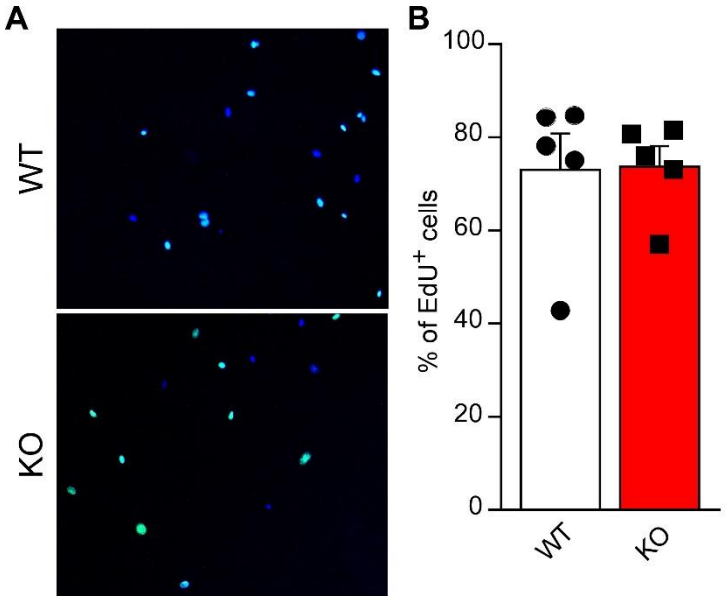

Figure 21: Lack of Gpr111 has no effect on proliferation of BAs
(A) Representative pictures of cellular proliferation measured via EdU assay (merge EdU and DAPI). (B) Quantification of EdU assay. Results are represented on a scatter plot bar graph as mean ± SEM, *Student* t-test, n=5 independent cell culture experiments.

3.3. Role of Gpr111 in WAs

3.3.1. Loss of Gpr111 promotes differentiation and browning of WAs

To investigate the role of Gpr111 in WAs, cells were isolated from 8-12 week old WT and KO mice. Isolation and cultivation was performed as it is explained in 2.3.4, 2.3.4.1. Cells were differentiated till day 12 (d12) and afterwards Oil Red O staining, qPCR and Western blot analysis were performed (Figure 22).

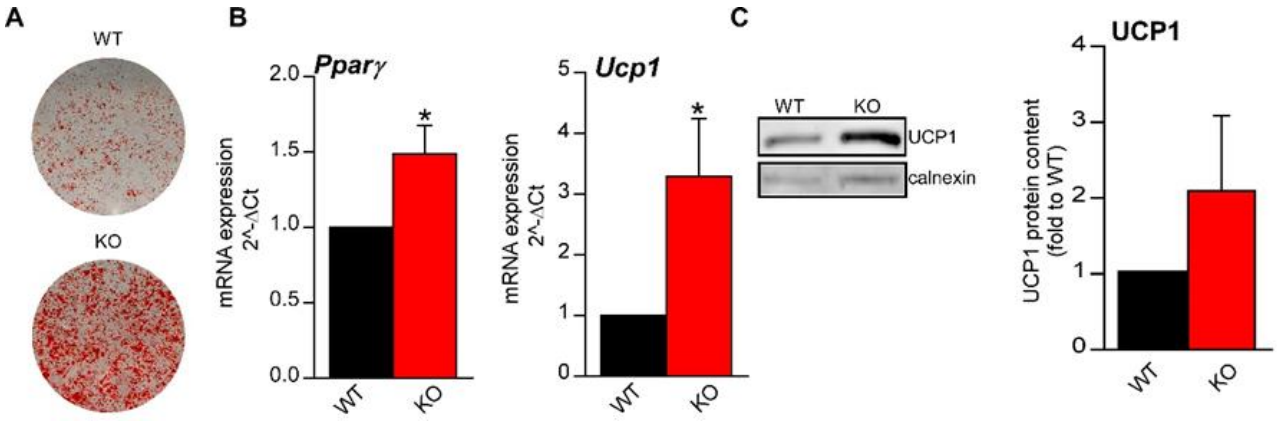

Figure 22: Loss of Gpr111 promotes differentiation of WAs
(A) Representative Oil Red O staining of differentiated WAs. (B) mRNA expression of adipogenic (*Pparγ*) and thermogenic (*Ucp1*) markers. (C) Representative immunoblot of UCP1 in WT and KO WAs. Calnexin was used as a loading control. Expression data are normalized to *Hprt* and represented on a bar graph as mean ± SEM, *Student* t-test, n= 7 independent cell culture experiments, *<0.05.

Oil Red O staining shows a higher accumulation of lipid droplets in KO WAs (Figure 22A). mRNA expression of *Pparγ* (1,489 ± 0,187) is significantly increased in KO cells, as well as mRNA expression of *Ucp1* (3,287 ± 0,945) (Figure 22B). Additionally, Western blot analysis shows a higher abundance of UCP1 protein in KO WAs (Figure 22C).

Browning or beigeing of WAs is a phenomenon when WAs express characteristics of BAs and this was explained in detail in 1.3.1.3. High expression of UCP1 on mRNA as well as on protein level in KO WAs is a clear indication of browning of KO WAs. To prove this phenomenon, mature WT and KO WAs were additionally stimulated with NE (1µM) for 16h and mRNA expression of *Ucp1* was analyzed (Figure 23).

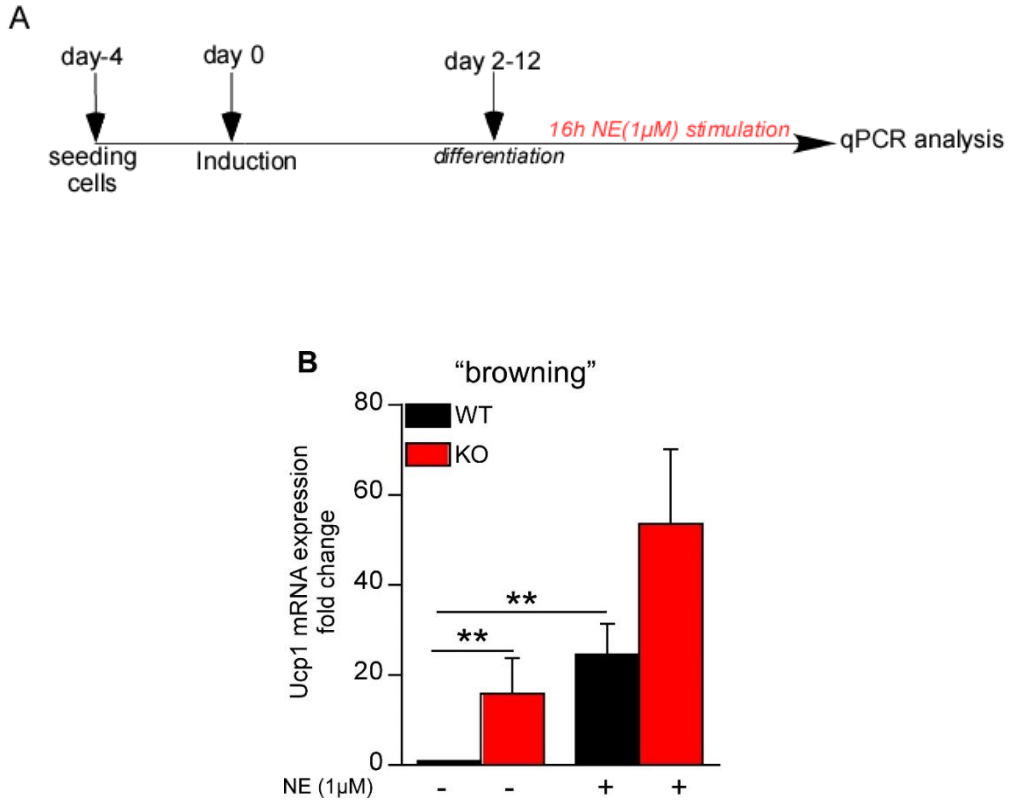

Figure 23: Lack of Gpr111 promotes browning of WAs
(A) Schematic representation of treatment. (B) mRNA expression of Ucp1. Expression data are normalized to *Hprt* and represented on a bar graph as mean ± SEM, ANOVA, n= 20 different pools of cells, *<0.05.

NE stimulated browning of WT cells through increase of *Ucp1* expression of 77,7%. However, NE couldn't increase browning of KO cells, probably because of a high basal expression of *Ucp1*. Once more, *Ucp1* expression is significantly higher in KO WAs in comparison to WT cells (Figure 23B).

In summary, these results show a strong effect of Gpr111 deficiency on differentiation and browning of primary WAs.

3.3.2. Effects of Gpr111 deletion on function of WAs

As it was described before, WAs and WAT in the body serve as lipid depots and it can provide energy in the form of FFA through lipolysis. Even though, UCP1 mediated respiration and oxygen consumption in general are not highly represented processes in WAs and WAT. However, strong *in vitro* evidence (3.3.1) of browning of KO WAs indicates that KO WAs show a feature of beige adipocytes.
To measure the effects of Gpr111 deletion on WA function lipolysis assay and oxygen consumption measurement were performed on d12 of WAs.

As a positive control of lipolysis, NE was used.

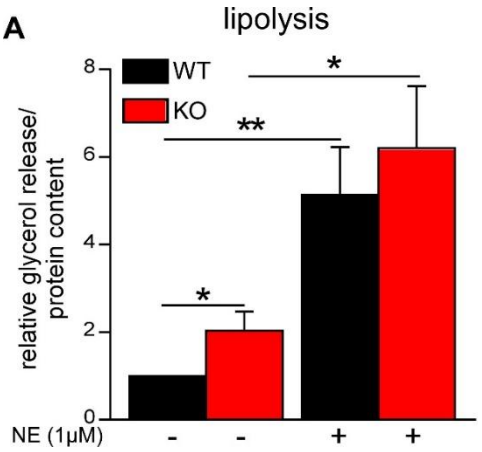

B

WT

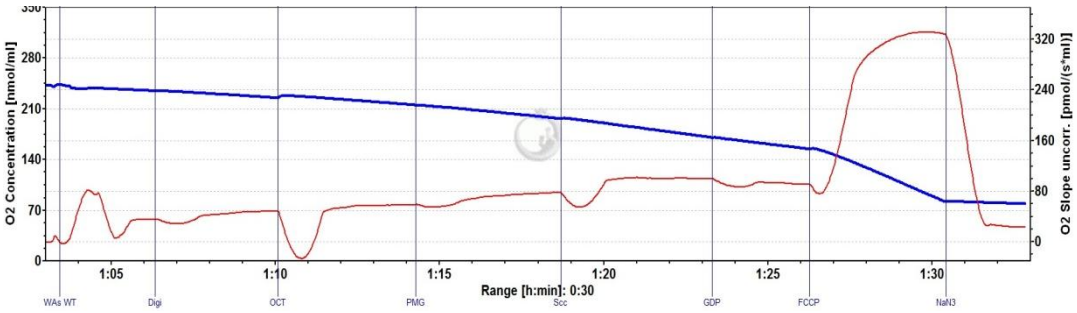

KO

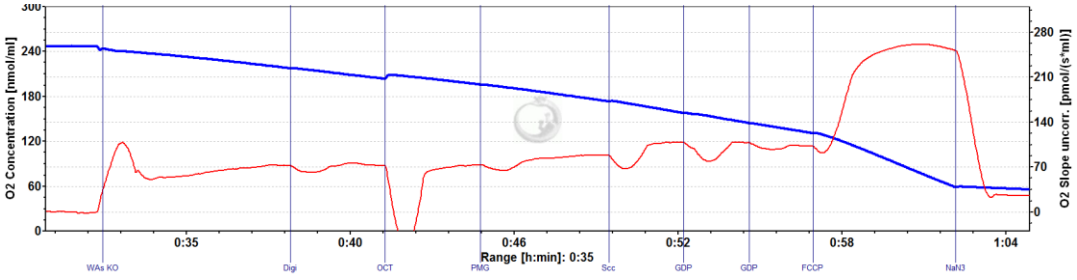

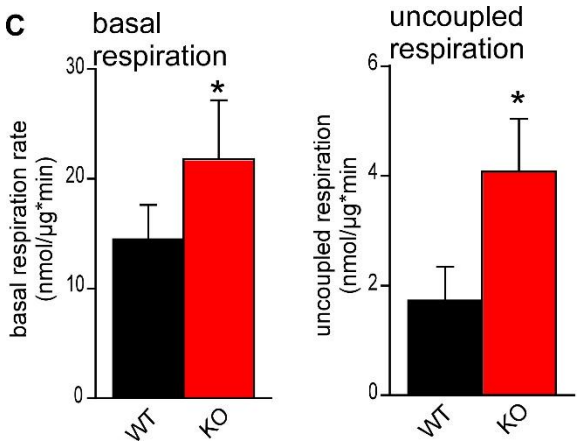

Figure 24: Effects of Gpr111 deletion on function of WAs
(A) Relative glycerol release of differentiated WAs with and without presence of 1µM NE. (B) Representative oxygen consumption curves (WT-upper panel, KO-lower panel) (C) Basal and UCP1 mediated respiration. Results are represented on a bar graph as mean ± SEM. ANOVA was used for analysis of lipolysis data and *Student* t-test for oxygen consumption results. 8 different pools of cells were used for lipolysis and 12 for oxygen consumption measurement. *p<0.05.

According to previous results, it was expected that KO WAs have a significantly higher lipolytic rate (2,035 ± 0,432) in comparison to WT cells (Figure 24A). Similarly, basal (21,80 ± 5,367), as well as UCP1 mediated respiration (4,078 ± 0,958) were significantly higher in KO WAs (Figure 24C).
Taken together, these results clearly indicate that a lack of Gpr111 improves metabolic function of WAs.

3.3.3. Lack of Gpr111 increases proliferation of WAs

Likewise, in BAs the loss of Gpr111 improves differentiation and function of WAs and it was necessary to examine the proliferation rate. EdU proliferation assay was performed in the same way as it is explained in 2.4.3.

Unexpectedly, cells that lack Gpr111 proliferate more in comparison to WT cells (Figure 25).

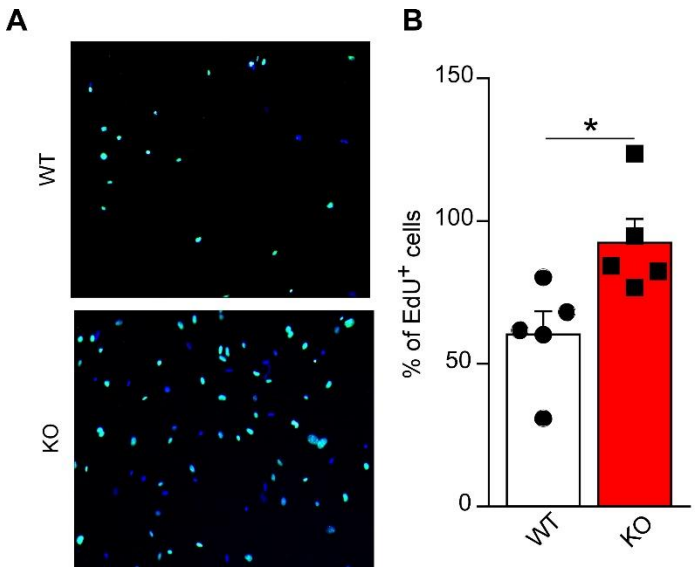

Figure 25: Lack of Gpr111 increases proliferation of WAs
(A) Representative pictures of cellular proliferation measured via EdU assay (merge EdU and DAPI). (B) Quantification of EdU assay. Results are represented on a scatter plot bar graph as mean ± SEM, *Student* t-test, n=5 independent cell culture experiments, *p<0.05.

Contrary to the results that were obtained using primary BAs, lack of Gpr111 in WAs increased proliferation of these cells. This could be a reason for better differentiation and function of primary KO WAs.

3.4. Lack of Gpr111 in adult mice increases energy expenditure (EE)

Eight week old mice were housed at 23ºC for 10 days in metabolic cages in which whole body EE and motility were measured (Figure 26A, B, E and F). Same animals were exposed to cold (4ºC) for 1 hour and EE was determined (Figure 26C and D). Cold exposure was used to stimulate BAT activity. In the end of the experiment body composition was evaluated using nuclear magnetic resonance (NMR) Bruker minispec (Figure 26G). Next, animals were sacrificed, AT and other organs were extracted and weighed (Figure 26H and I).

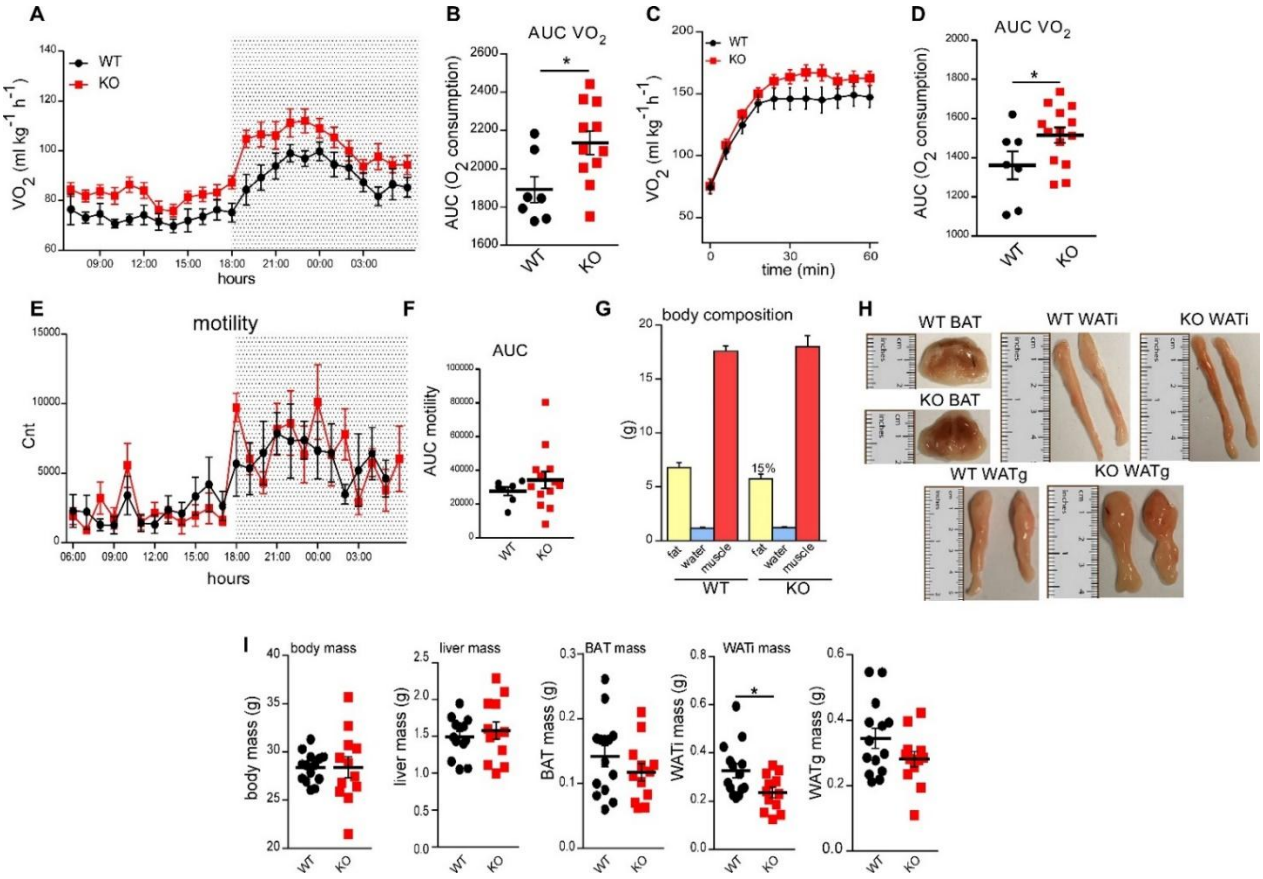

Figure 26: Adult Gpr111 KO mice housed at 23ºC have higher oxygen consumption
(A) Energy expenditure at 23ºC is represented as points and connecting line with error bars, n(WT)=7; n(KO)=11(B) Area under the curve (AUC) of energy expenditure at 23ºC is represented as scatter plot(C) Energy expenditure at 4ºC is represented as points and connecting line with error bars, n(WT)=7; n(KO)=14 (D) AUC of energy expenditure at 4ºC is represented as scatter plot (E) Motility of mice housed at 23ºC is represented as points and connecting line with error bars (F) AUC of motility at 23ºC is represented as scatter plot, n(WT)=6; n(KO)=8 (G) Body composition is represented as a bar graph n(WT)=6; n(KO)=5 (H) Representative pictures of AT (I) Body mass and organ weights of mice after 10 days housing at 23ºC are represented as scatter plot n(WT)=14; n(KO)=12. All data were assessed using *Student* t-test and they are represented as mean ± SEM, *<0.05.

EE of GPR111 KO mice was significantly higher (2135 ± 62,69) than EE of WT mice (Figure 26A and B). Similar pattern was observed when mice were exposed to cold for 1h (1515 ± 39,51) (Figure 26C and D). There was no change in motility between WT

and KO mice (Figure 26E and F). However, NMR results show that KO mice have 15% less fat in comparison with WT. BAT and WATi of KO mice are more brown than BAT and WATi of WT mice (Figure 26H). GPR111 KO mice have significantly less WATi mass (0,236 ± 0,022). Besides, KO mice have 18% less BAT and 19% less WATg mass (Figure 26I). Nevertheless, there were no changes in total body mass and liver mass between these two groups.

All *in vivo* observed results are in the line with *in vitro* observations and additionally indicate that the lack of *Gpr111* induces browning of WAT.

3.4.1. Lack of Gpr111 in adult mice promotes browning of WAT

After measurement in metabolic cages at 23ºC, mice were sacrificed, fat and other organs were extracted. To prove *in vivo* findings, immunohistochemistry, qPCR and Western blot analysis of fat tissues were performed (Figure 27A-D).

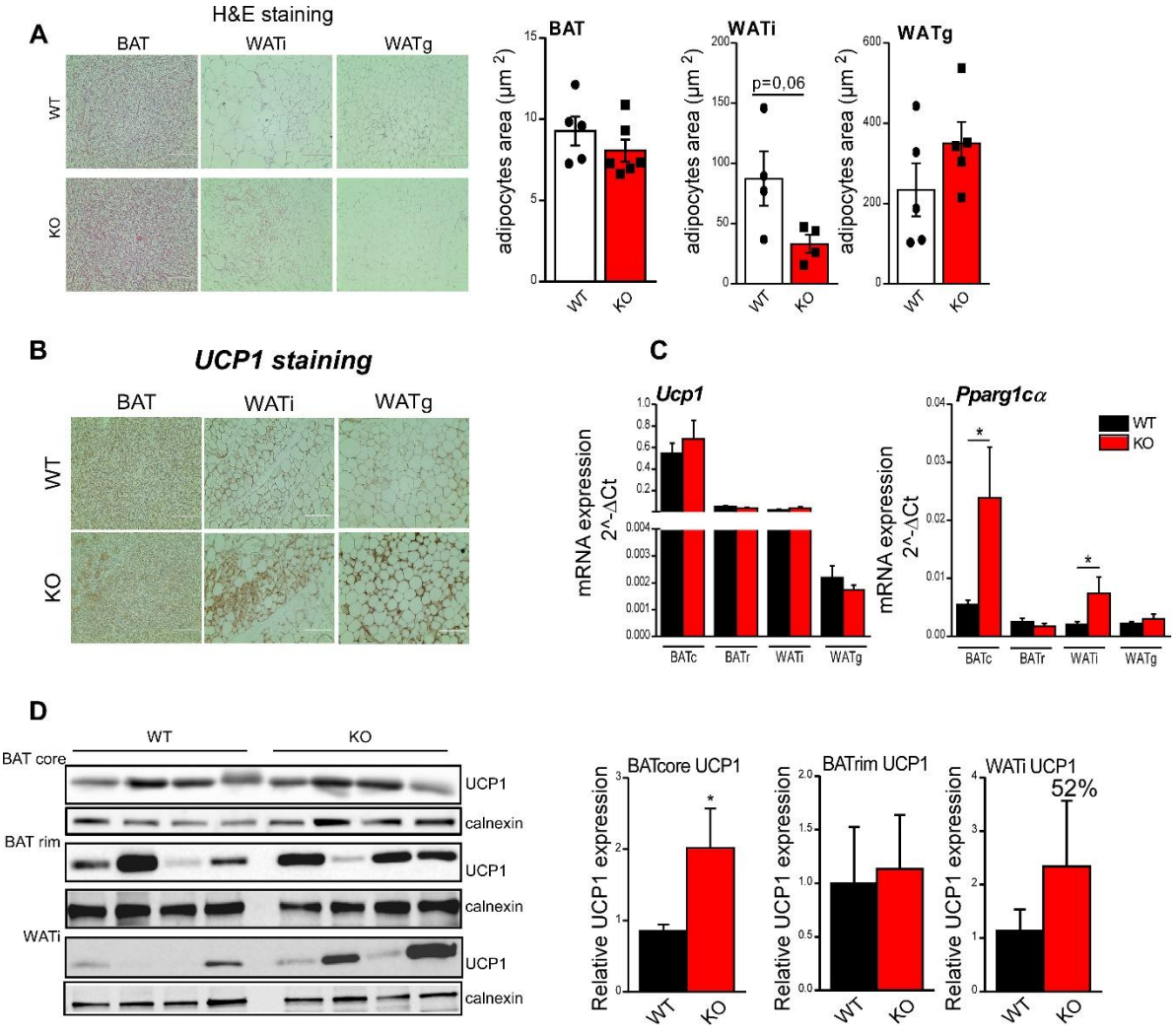

Figure 27: Lack of Gpr111 in adult mice promotes browning of WAT
(A) Representative pictures and quantification of H&E staining. Data are represented on scatter plot bar graph as a mean ± SEM (B) Immunohistological staining of UCP1 in fat tissues (C) mRNA expression of *Ucp1* and *Pparg1cα.* (D) Representative immunoblot and densitometric quantification of immunoblot normalized to loading control-calnexin. Western blot quantification data are represented on a bar graph as mean ± SEM, *Student* t-test, n= 8, *<0.05. Expression data are normalized to *Gapdh* and represented on a bar graph as mean ± SEM, *Student* t-test, n= 10-13, *<0.05.

H&E as well as UCP1 staining of BAT did not show a big difference between WT and KO. However, UCP1 staining shows a higher abundance of UCP1 in WAT of KO mice. On the other hand, H&E staining shows a reduction in cell size of WATi (33,31 ± 7,479)

in KO samples (Figure 27A). Smaller size of cells and detection of UCP1 in WAT tissue is a clear indicator of browning.

mRNA expression of *Ucp1* was unchanged in all tissue samples. However, mRNA expression of *Pparg1cα* was significantly increased in BAT core (0,024 ± 0,008) of KO mice as well as in WATi (0,007 ± 0,003) (Figure 27C). Western blot analysis shows a significant increase in UCP1 protein in BAT core (2,016 ± 0,553) of KO mice. An increase of 52% in UCP1 protein was observed in cases of KO WATi (Figure 29D).

To finally confirm the browning phenotype, oxygraph measurements of explanted fat tissues were performed according to the protocol that was in detail explained in 2.3.7.

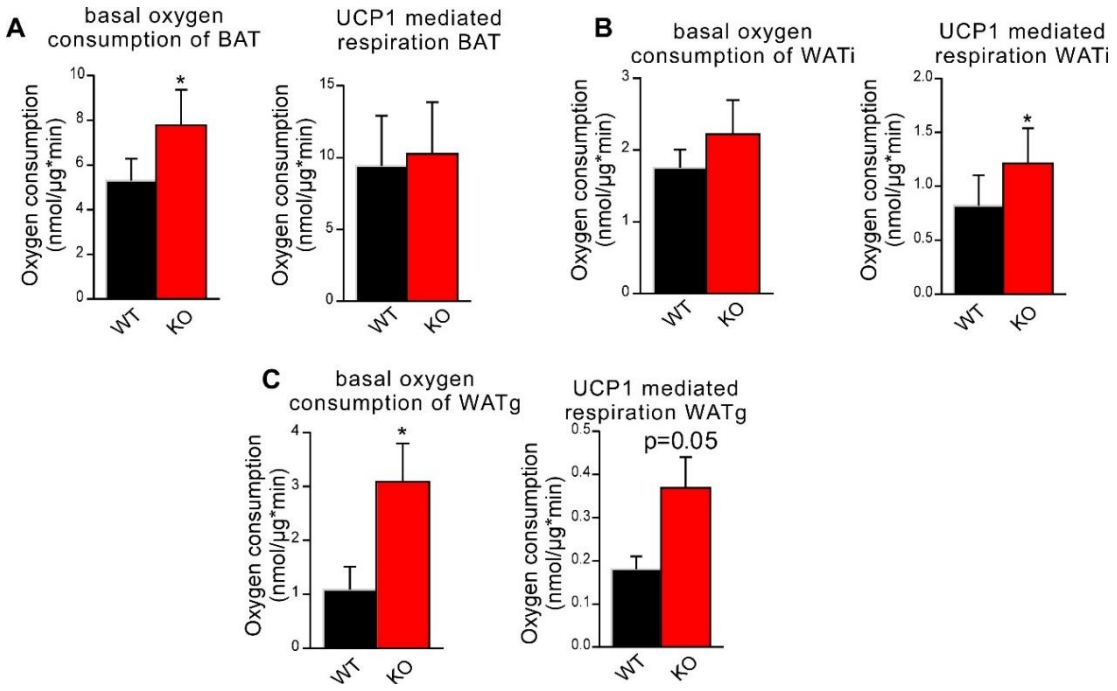

Figure 28: Gpr111 deletion promotes *ex vivo* oxygen consumption of AT
(A) Basal and UCP1 mediated respiration of BAT n=7. (B) Basal and UCP1 mediated respiration of WATi n=6 (C) Basal and UCP1 mediated respiration of WATg n=5-6. Results are represented on a bar graph as mean ± SEM. *Student* t-test, *p<0.05.

In correlation with our previous *in vitro* results oxygen consumption was increased in fat tissues of KO mice. Basal oxygen consumption of Gpr111 KO in BAT (Figure 28A) was significantly increased (7,777 ± 1,594) in comparison to WT, but there was no difference between genotypes in case of UCP1 mediated respiration. Basal oxygen consumption of Gpr111 KO WATi was 22% higher than in WT. UCP1 mediated respiration was significantly higher in Gpr111 KO WATi (1,214 ± 0,324) (Figure 28B). Surprisingly, basal (3,093 ± 0,706) as well as UCP1 mediated respiration (0,369 ± 0,071) of Gpr111 KO WATg were significantly increased in comparison with WT (Figure 28C).

Taken together, these results prove an important role of Gpr111 in adipose tissue *in vivo*.

3.5. Cold exposure of Gpr111$^{-/-}$ mice cause metabolic changes

Exposing mice to cold (4ºC) is the simplest way to increase sympathetic outflow and activity of BAT. Mice were first acclimatized at 16ºC and then exposed to 4ºC for one week 2.2.3. EE, motility, body composition and food intake were followed (Figure 29A-F).

After the *in vivo* measurements in metabolic cages, animals were sacrificed, AT and other organs were extracted and weighed (Figure 29G and H).

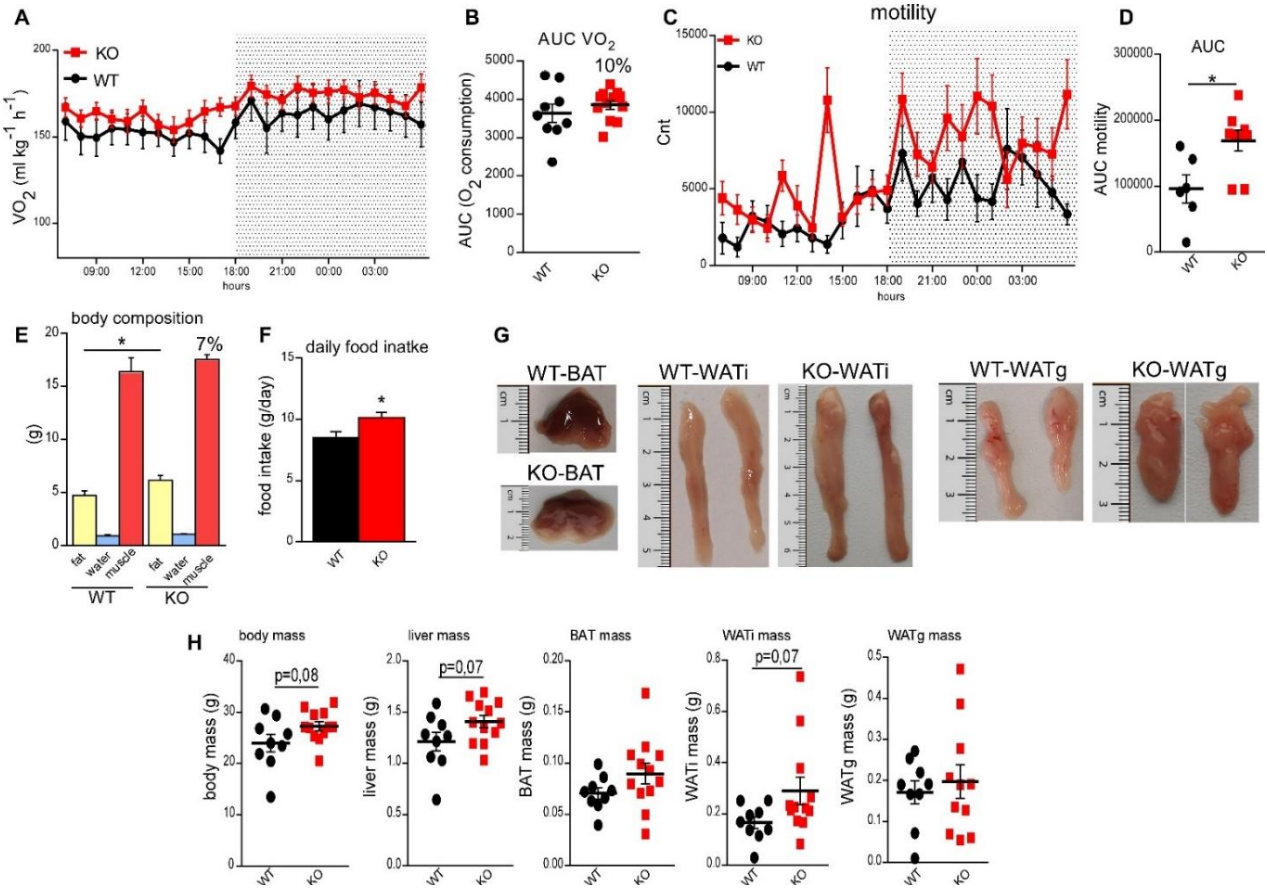

Figure 29: Cold exposure of Gpr111-/- mice cause metabolic changes
(A) Energy expenditure at 4ºC is represented as points and connecting line with error bars, n(WT)=9; n(KO)=12 (B) Area under the curve (AUC) of energy expenditure at 4ºC is represented as scatter plot (C) Motility of mice housed at 4ºC is represented as points and connecting line with error bars n(WT)=6; n(KO)=9 (D) AUC of motility is represented as scatter plot (E) Body composition is represented as a bar graph, n(WT)=9; n(KO)=12 (F) Daily food intake is represented as a bar graph, n(WT)=5; n(KO)=7 (G) Representative pictures of AT (H) Body mass and organ weights of mice after 7 days housing at 4ºC are represented as scatter plot, n(WT)=9; n(KO)=12. All data were assessed using *Student* t-test and they are represented as mean ± SEM, *<0.05.

EE of KO mice was 10% higher in comparison to WT (Figure 29A and B). Unusually, KO mice moved significantly more (169226 ± 15434) than WT mice (Figure 29C and D). NMR shows a significant increase in fat mass (6,142 ± 0,457) and muscle mass (7%) in KO mice (Figure 29E) that could be explained through the fact that KO mice eat much

more (10,15 ± 0,411) than WT (Figure 29F). Body weight as well as fat tissue masses were slightly increased in KO mice in comparison to WT (Figure 29H). However, pictures of AT show strong browning phenotype in WAT of KO mice (Figure 29G).

In summary, cold exposure has a strong effect on EE and body composition of KO mice. Nevertheless, low temperature has huge impact of feeding behavior and motility of KO mice.

3.5.1. Cold exposure of Gpr111$^{-/-}$ mice induces massive browning of WAT

To investigate further effects of cold stimulus on AT of Gpr111 KO mice, immunohistochemistry, qPCR and Western blot analysis of fat tissues were performed (Figure 30A-D).

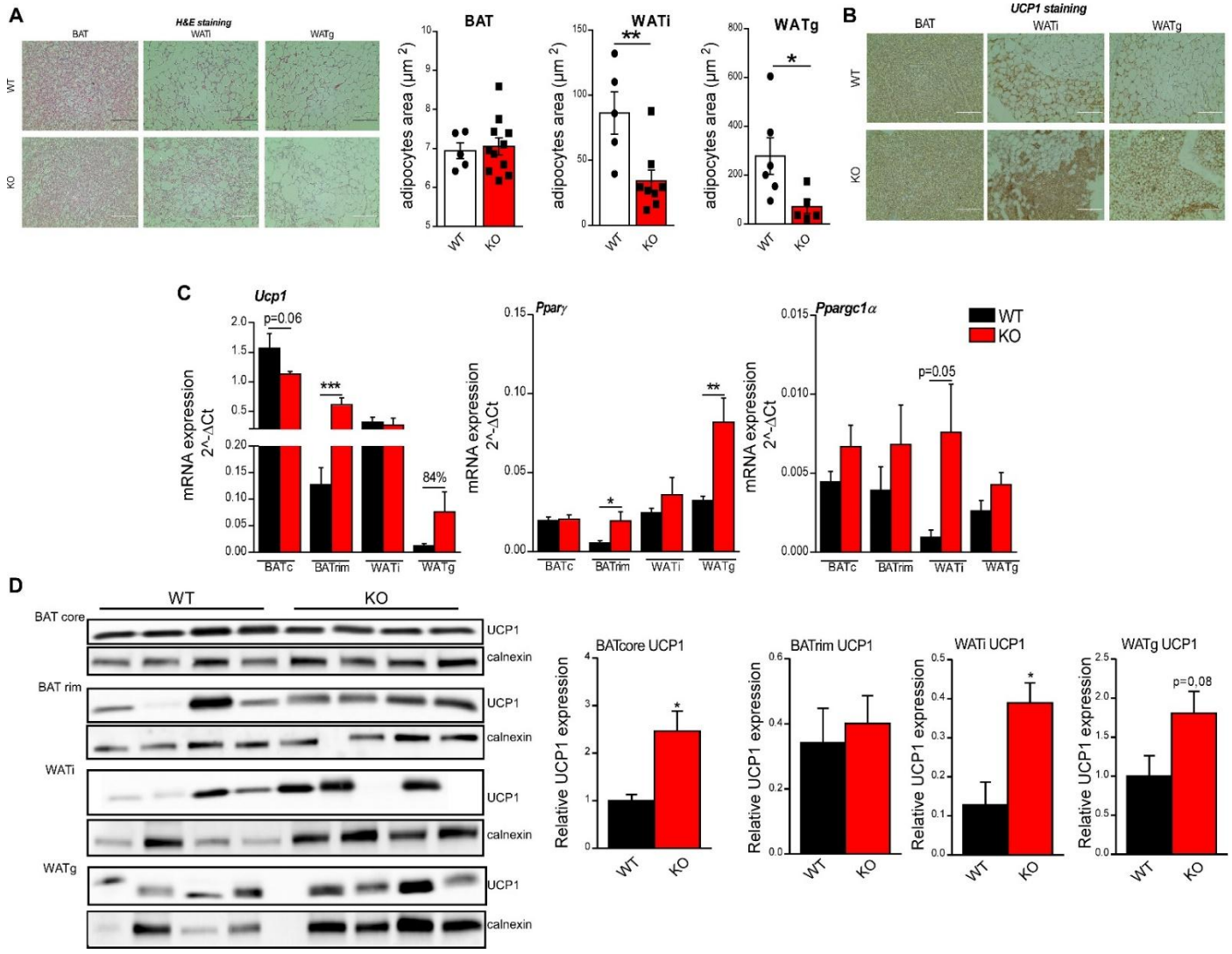

Figure 30: Cold exposure of Gpr111-/- mice induces massive browning of WAT
(A) Representative pictures and quantification of H&E staining of fat tissues. Data are represented as a scatter plot bar graph as a mean ± SEM (B) Immunochistological staining of UCP1 in fat tissues (C) mRNA expression of *Ucp1*, *Pparγ* and *Pparg1cα.* Expression data are normalized to *Gapdh* and represented on a bar graph, n= 10-13 (D) Representative immunoblot and densitometric quantification of immunoblot normalized to loading control-calnexin, n=4. Quantification is represented on a bar graph as mean ± SEM, *Student* t-test, *<0.05.

Histological analysis shows huge browning of WAT of KO mice. Smaller cells that are clearly visible in WAT indicate a transition from white to beige cells (Figure 30A and B).

On mRNA level *Ucp1* was significantly increased in BAT rim of KO mice (0,610 ± 0,114) that again demonstrates browning of WAT that surrounds BAT. Similarly, expression of *Pparg* is significantly increased in BAT rim of KO mice (0,019 ± 0,006) and an increase of *Pparg1cα* is 43% in comparison to BAT rim of WT mice. mRNA expression of *Pparg1cα* was increased in KO WATi (0.007 ± 0.003) in comparison to WT. On the other hand, expression of Ucp1 was 84% higher in WATg of KO mice in comparison to WT. *Pparγ* was significantly (0.082 ± 0.0151) and *Ppargc1α* was slightly (40%) increased in WATg of KO mice (Figure 30C).

Although, there was a reduction in *Ucp1* expression in KO BAT, Western blot shows a significant increase (2.465 ± 0.420). Significant increase of UCP1 on protein level was observed in case of KO WATi (0.389 ± 0.051) and an increase of 55% in KO WATg (Figure 30D).

Once again these data confirmed the browning phenotype of KO mice.

3.6. Analysis of the effect of DIO in GPR111 KO mice

Gpr111 WT and KO mice were fed with HFD or ND for 12 weeks. Body mass was measured every week and after 11 weeks of HFD, GTT was performed. mice were metabolically characterized in metabolic cages at 23ºC and acutely, for 1h at 4ºC (Figure 31 and Figure 32), furthermore body composition was examined using Brucker minispec (Figure 31D). Afterwards, mice were sacrificed, AT and other organs were isolated and weighed (Figure 31E and F).

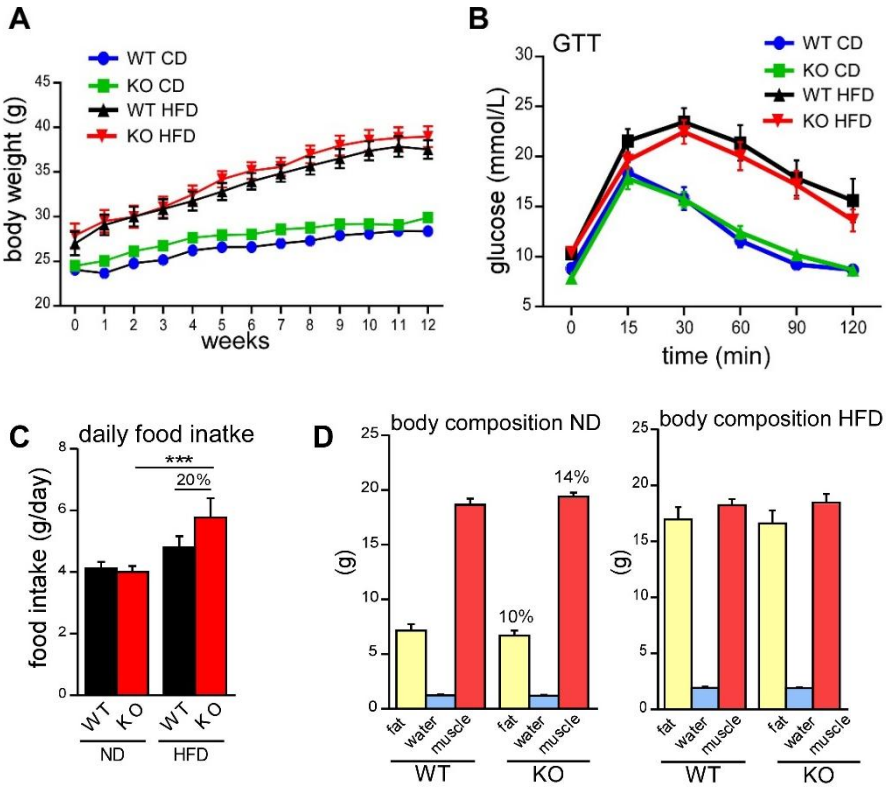

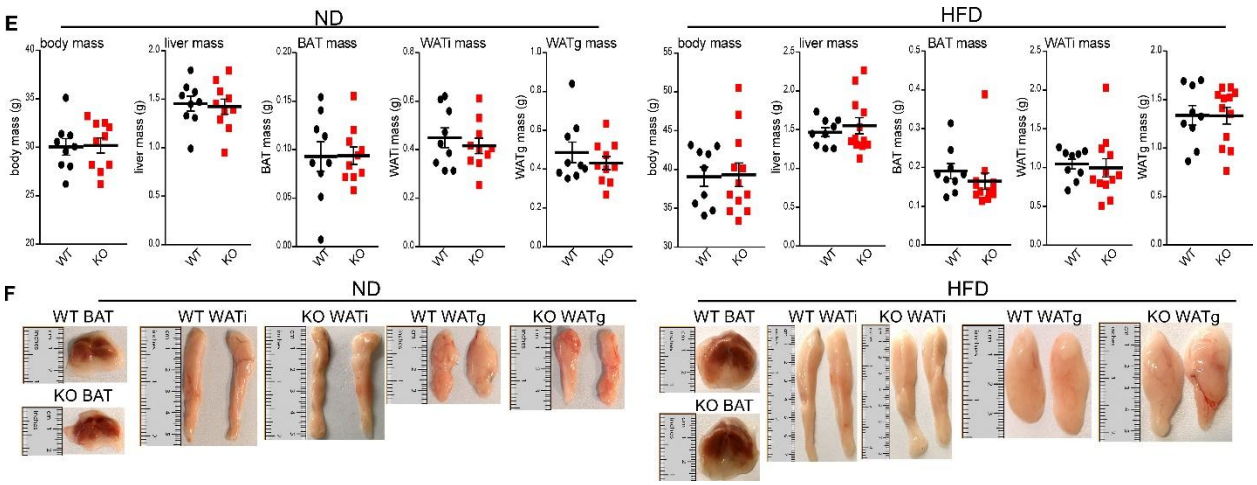

Figure 31: Effect of HFD on body weight, body composition and glucose tolerance of Gpr111 mice. (A) Changes in body weight of Gpr111 WT and KO mice during 12 weeks of HFD, represented as points and connecting line with error bars n(WT-ND)=10; n(KO-ND)=9, n(WT-HFD)=9; n(KO-HFD)=12 (B) Glucose tolerance test, represented as points and connecting line with error bars n(WT-ND)=10; n(KO-ND)=9, n(WT-HFD)=9; n(KO-HFD)=12 (C) Daily food intake is represented as a bar graph, n=10 (D) Body composition is represented as a bar graph n(WT-ND)=10; n(KO-ND)=9, n(WT-HFD)=9; n(KO-HFD)=12
(E) Body mass and organ weights of mice after 12 weeks of ND/HFD are represented as scatter plot, n(WT-ND)=10; n(KO-ND)=9, n(WT-HFD)=9; n(KO-HFD)=12. (F) Representative pictures of AT after ND/HFD. All data were assessed using *Student* t-test and they are represented as mean ± SEM, ***<0.001.

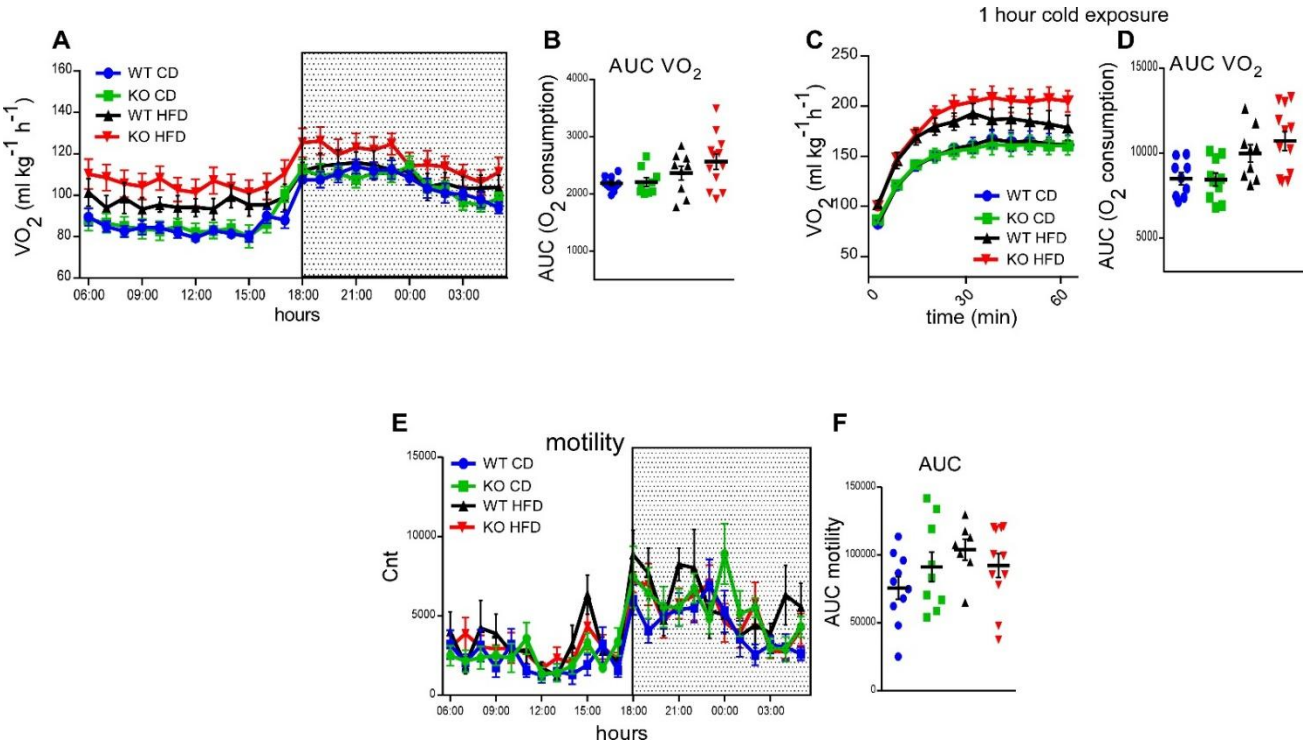

Figure 32: Effect of HFD on energy expenditure and motility of GPR111 WT and KO mice
(A) Energy expenditure at 23ºC is represented as points and connecting line with error bars, n(WT-ND)=10; n(KO-ND)=9, n(WT-HFD)=9; n(KO-HFD)=12 (B) Area under the curve (AUC) of energy expenditure at 23ºC is represented as scatter plot. (C) Energy expenditure at 4ºC is represented as points and connecting line with error bars, n(WT-ND)=10; n(KO-ND)=9, n(WT-HFD)=9; n(KO-HFD)=12 (D) AUC of energy expenditure at 4ºC is represented as scatter plot (E) Motility of mice housed at 23ºC is represented as points and connecting line with error bars n(WT-ND)=9; n(KO-ND)=12, n(WT-HFD)=7; n(KO-HFD)=11 (F) AUC of motility is represented as scatter plot. All data were assessed using *Student* t-test and they are represented as mean ± SEM.

During HFD feeding, WT and KO mice similarly gained weight, and there was no significant difference between genotypes (Figure 31A). Surprisingly, there was no difference in GTT (Figure 31B). However, EE of KO mice fed with HFD was 8% higher in comparison to WT group (Figure 32A and B). Similarly, after 1h of cold exposure, EE of KO mice fed with HFD was 7% increased in comparison to WT mice on the same diet (Figure 32C and D). Significant difference in motility could not be observed between genotypes (Figure 32E and F).

Body composition did not change in the group of mice fed with HFD, but KO mice fed with ND had 10% less fat mass and 14% more muscle mass (Figure 31D).

KO mice on HFD eat 20% more than WT mice, but there was no difference in food intake in the group of mice fed with ND (Figure 31C).

Represented pictures as well as body and muscle mass did not show any significant difference between WT and KO mice (Figure 31D, E and F).

Taken together, there was no significant differences in EE between Gpr111 KO and WT mice during diet induced obesity (DIO). Also, no major differences were found in body and fat mass.

3.6.1. Analysis of UCP1 in AT of Gpr111 KO mice on HFD

To investigate further effects of HFD on AT of Gpr111 KO mice, immunohistochemistry, qPCR and Western blot analysis of fat tissues were performed. Also, serum leptin levels as well as expression of leptin receptor in the brain were examined.

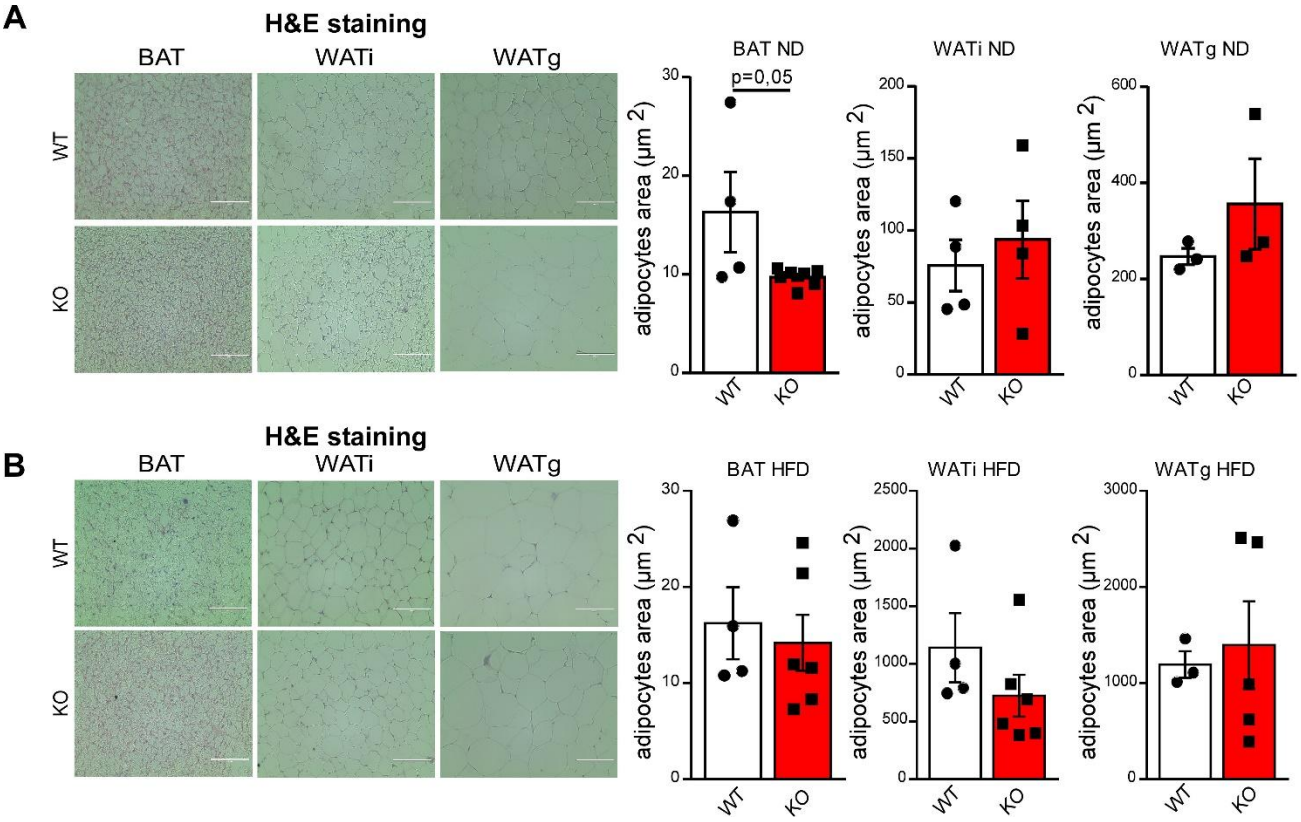

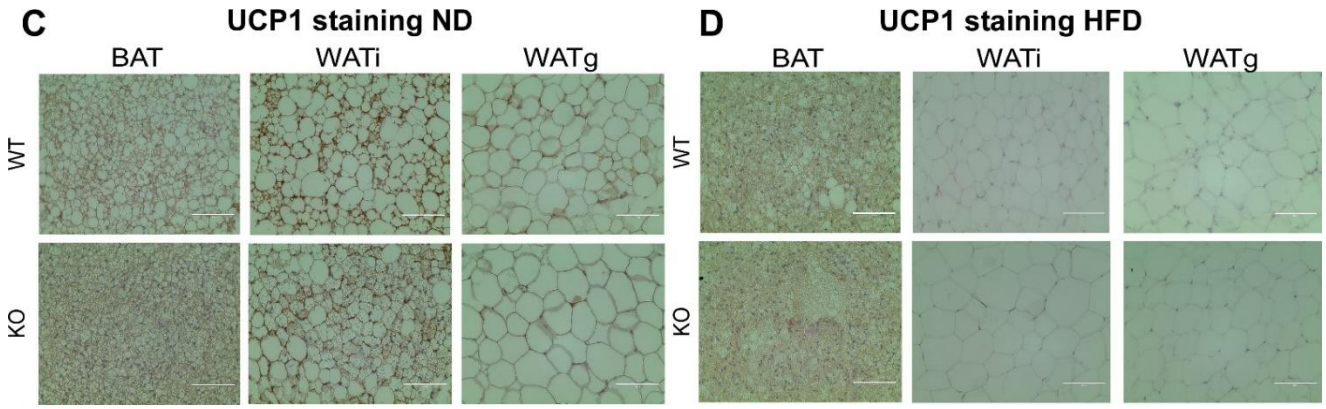

Figure 33: Histological analysis of ATs of Gpr111 mice after 12 weeks of HFD
(A) H&E staining and quantification of AT of Gpr111 mice fed with ND or (B) HFD. (C) UCP1 staining of AT of Gpr111 mice fed with ND or (D) HFD. Quantification results are represented on a scatter bar plot as a mean ± SEM, n=4-6, *Student* t-test. HFD induces reduction of UCP1 in AT of Gpr111 KO mice

Histological analysis did not show any significant difference between WT and KO mice after ND as well as after HFD.

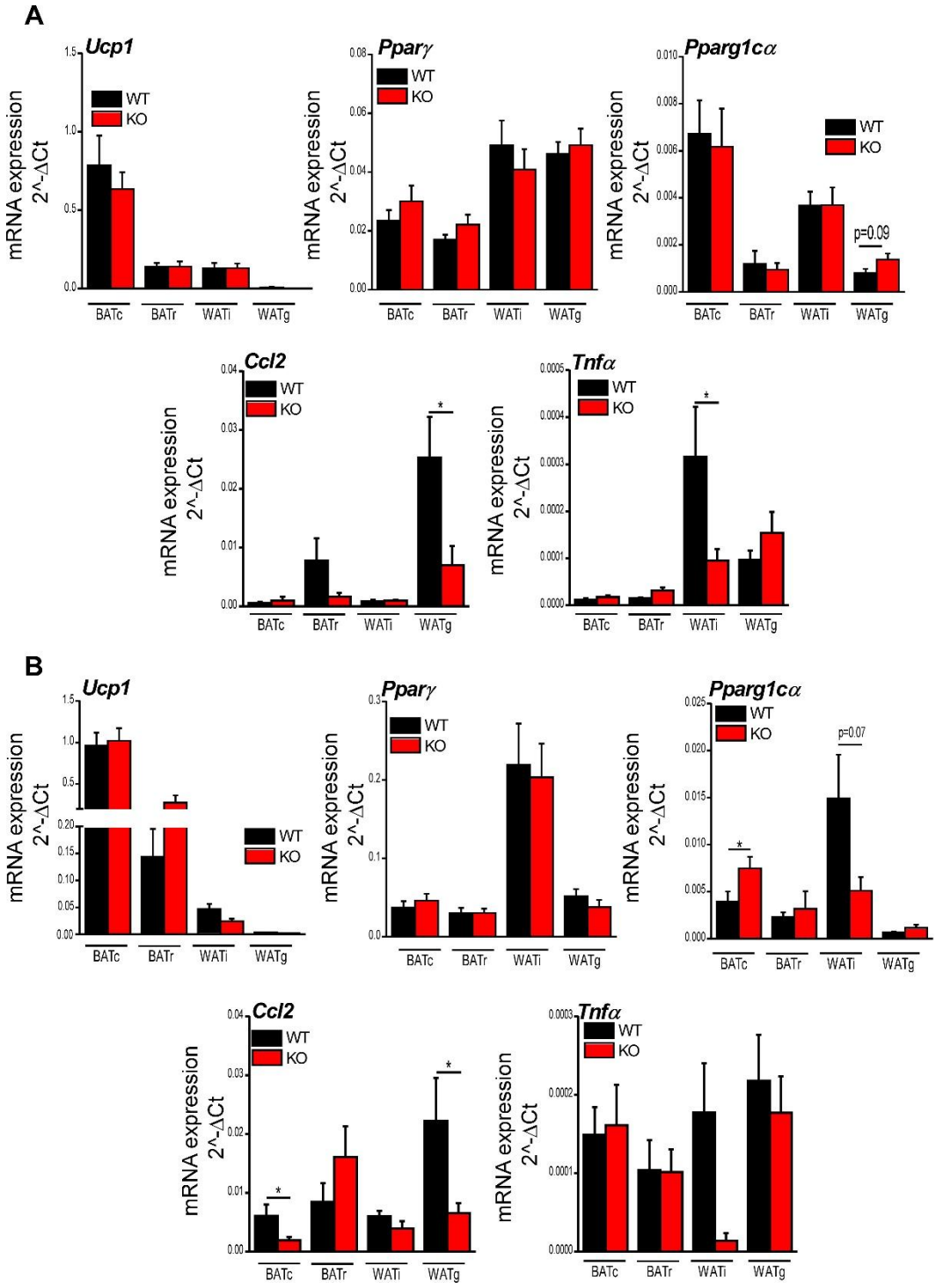

Figure 34: qPCR analysis of ATs of Gpr111 mice after 12 weeks of ND or HFD
(A) mRNA expression of *Ucp1*, *Pparγ*, *Pparg1cα, Ccl2, Tnfα* in fat tissues after feeding animals with ND or HFD (B). Expression data are normalized to *Gapdh* and represented on a bar graph, n= 9-11
All expression data are represented on a bar graph as mean ± SEM, *Student* t-test, *<0.05.

On mRNA level *Ucp1* was increased by 48% only in BAT rim of KO mice after HFD. However, in all other tissues and groups *Ucp1* and *Pparγ* were not significantly

changed. Surprisingly, expression of *Pparg1cα* was highly upregulated (43%) in WATg of KO mice fed with ND and significantly increased in BAT core of KO mice fed with HFD. In contrast, *Pparg1cα* was strongly reduced (66%) in WATi of KO mice fed with HFD (Figure 34A and B).

To investigate the effects of HFD on inflammation in ATs of Gpr111 KO mice, pro-inflammatory markers (*Ccl2 and Tnfα*) were analyzed. *Ccl2* was significantly reduced in WATg of KO mice (ND 0.007 ± 0.003), (HFD 0,007 ± 0,002) in both kinds of diet. Additionally, *Ccl2* was significantly downregulated in BAT core of KO mice (0,002 ± 0,0006) after HFD. Similarly, *Tnfα* was significantly reduced in WATi of KO mice fed with HFD (1,403e-005 ± 9,350e-006) and ND (9,494e-005 ± 2,425e-005) (Figure 34A and B).

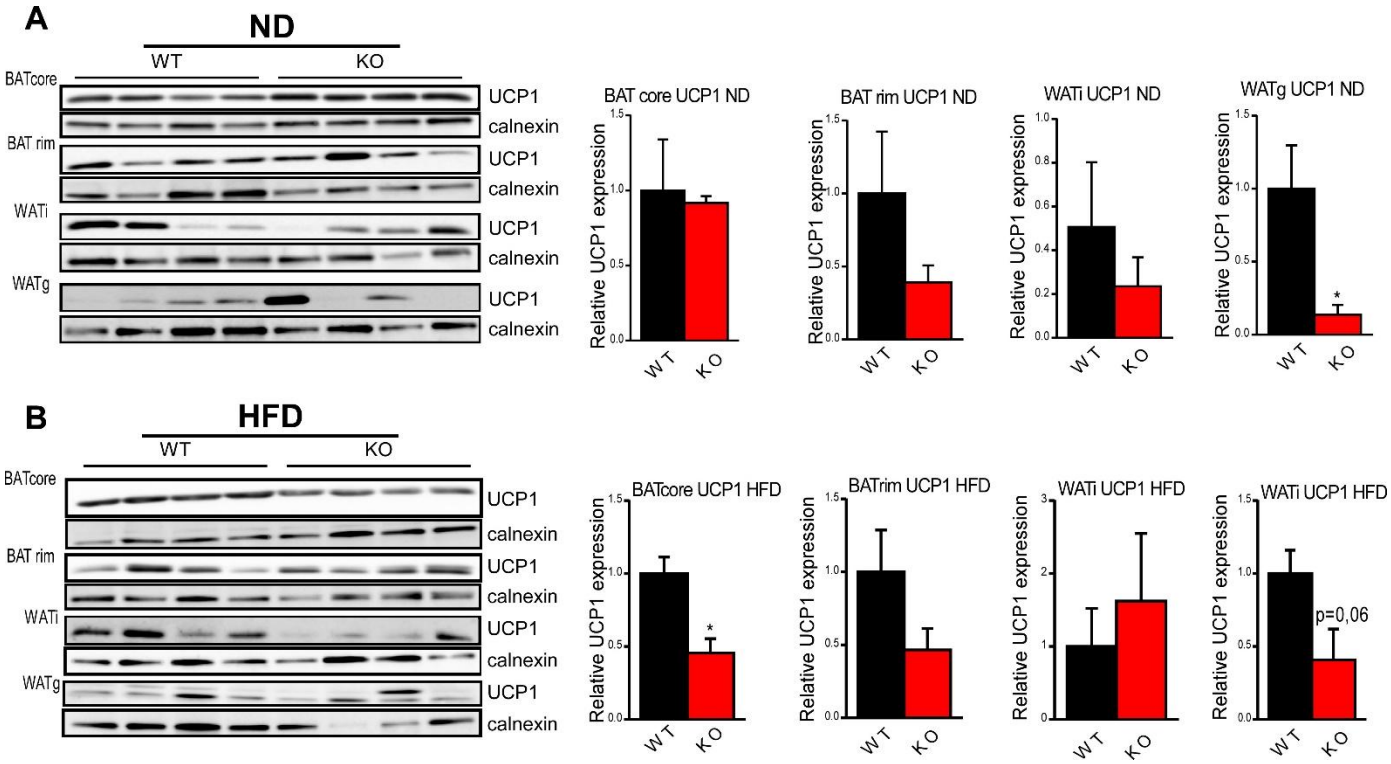

Figure 35: Western blot analysis of ATs of Gpr111 mice after 12 weeks of ND or HFD
(A) Representative immunoblot of UCP1 expression in fat tissues after feeding animals with ND or HFD (B) and densitometric quantification of immune blot normalized to loading control (calnexin), n=4. mRNA Quantification is represented on a bar graph as mean ± SEM, *Student* t-test, *<0.05.

To determine whether protein levels of UCP1 in AT are changed after HFD/ND, Western blot was performed. Western blot analysis show that UCP1 was not changed only in BAT core of mice fed with ND and in WATi of HFD group. In all other fat tissues, independent of diet, UCP1 was reduced in KO mice: BAT rim ND (0,391 ± 0,117), WATi ND (0,235 ± 0,132), WATg ND (0,137 ± 0,067), BATc HFD (0,455 ± 0,097), BAT rim HFD (0,465 ± 0,145), WATg HFD (0,407 ± 0,213) (Figure 35A and B).

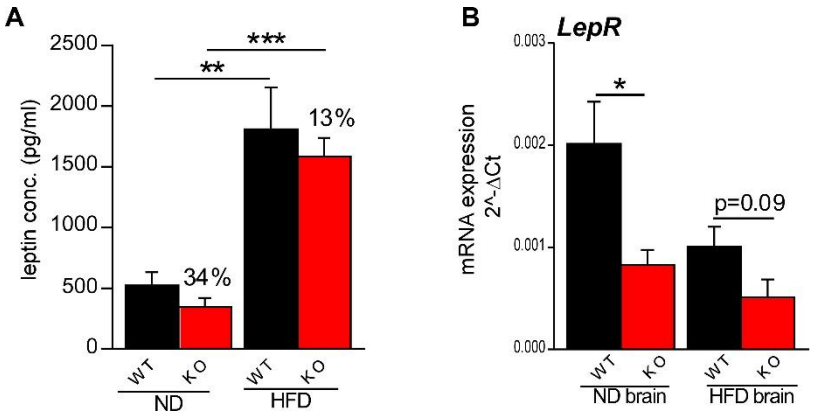

Figure 36: Serum leptin levels and expression of leptin receptor in GPR111 WT and KO mice after HFD

(A) Serum leptin levels in group of WT and KO mice after HFD/ND, n=8-12, results are represented on a bar graph (B) mRNA expression of leptin receptor in a brain of mice after HFD/ND, data are represented on a bar graph n=5, *ANOVA,* **<0.01, ***<0.001

To explain why KO mice under HFD eat much more, levels of leptin were examined in serum of WT and KO mice after ND or HFD. Serum leptin levels were slightly (34%) downregulated in KO mice fed with ND. However, difference in serum leptin was minor (13%) after HFD (Figure 36A). Next, mRNA expression of leptin receptor (*LepR*) was analyzed in the brain of WT and KO mice. Leptin receptor was significantly downregulated in KO mice (0,0008 ± 0,0002) fed with ND and strongly decreased (50%) in a group of KO mice under HFD (Figure 36B).

Even though previous *in vivo* data (Figure 31 and 33) indicated that KO mice fed with HFD show similar phenotype as WT mice, reduction of pro-inflammatory markers in WAT is still a sign of partially healthy obesity. On the other hand, serum leptin levels and expression of LepR could indicate development of leptin resistance in KO mice under HFD.

3.7. Molecular mechanism of Gpr111 signaling

3.7.1. Gpr111 signaling is related to HH signaling in cilia

Relying on previously acquired *in vivo* and *in vitro* data and taking into account the role of aGPCRs in mechanosensation I tried to find a link between Gpr111 and organelles important for mechanosignal transduction (Scholz et al., 2015b). Cilia are organelles that can sense mechanical signals and transfer the information into the cell (Nguyen et al., 2015). Mechanical stress is a very important factor which has a huge influence on adipocytes during obesity (Gregor and Hotamisligil, 2007).

The most important signaling pathway that takes place in cilia is HH signaling. HH signaling pathway genes have a strong influence on BA differentiation and they are the most abundant and visible in preadipocytes after induction. Later on, during maturation of BAs, cilia and HH related genes are less detectable (Nosavanh et al., 2015b). mRNA expression of the most important elements of HH signaling (*Ptch1, Smo and Gli1*) were examined in BAs (Gpr111 WT and KO) as well as in AT of Gpr111 WT and KO mice (Figure 37A and B).

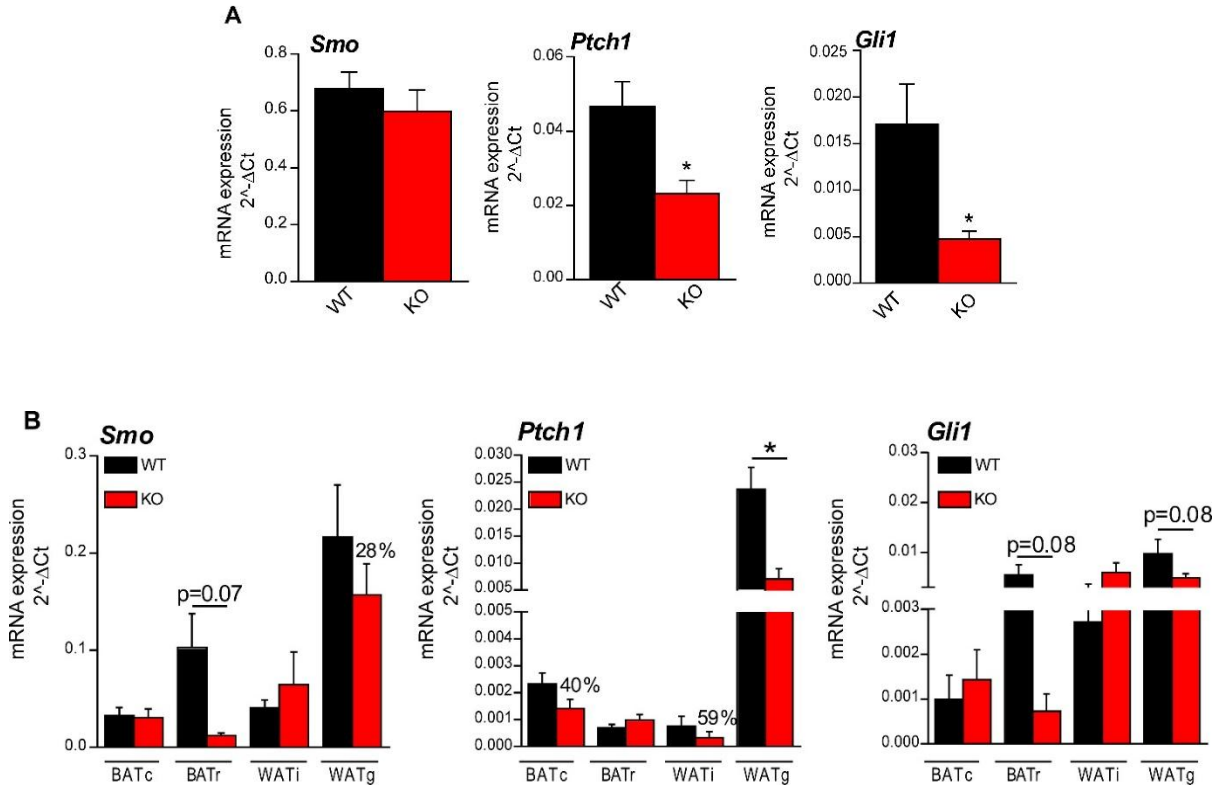

Figure 37: Expression of important genes of HH signaling
(A) mRNA expression of Smo, Ptch1 and Gli1 in BAs, n=4-7 of independent cell culture experiments (B) mRNA expression of *Smo*, *Ptch1* and *Gli1* in AT of Gpr111 WT and KO mice, n=7-11. Expression data in cells are normalized to Hprt (Gapdh in tissues) and represented on a bar graph, mean ± SEM, *Student* t-test, *<0.05.

All genes involved in HH signaling are downregulated in Gpr111 KO cells. Even though, *Smo* is only 12% reduced, expression of *Ptch1* (0,023 ± 0,004) and *Gli1* (0,005 ± 0,0008) is significantly decreased in KO cells. This means that HH signaling is impaired in KO cells (Figure 37A). Similarly, in tissue samples *Smo* was downregulated in BAT rim (0,012 ± 0,002) and slightly (28%) in WATg in KO samples. Expression of *Ptch1* was significantly downregulated in KO WATg (0,007 ± 0,002), but a strong reduction in expression of *Ptch1* was also observed in KO BATc (40%) and KO WATi (59%). Moreover, slight reduction in *Gli1* expression was observed in KO BAT rim (0,0007 ± 0,0004) and KO WATg (0,005 ± 0,0008) (Figure 37B). Genes were analyzed from fat tissues in whole, not from adipocytes and that could be a reason why reduction of HH genes is not remarkably strong as in case when WT and KO BAs were used.

To investigate further HH signaling in BAs, cells were treated with smoothend agonist (SAG) which acts on SMO and it should stimulate HH signaling and increase expression of *Gli1*. BAs were grown in growth media to reach confluence, next day cells were induced and 24h after induction, cells were treated with 1µM SAG (Figure 38A).

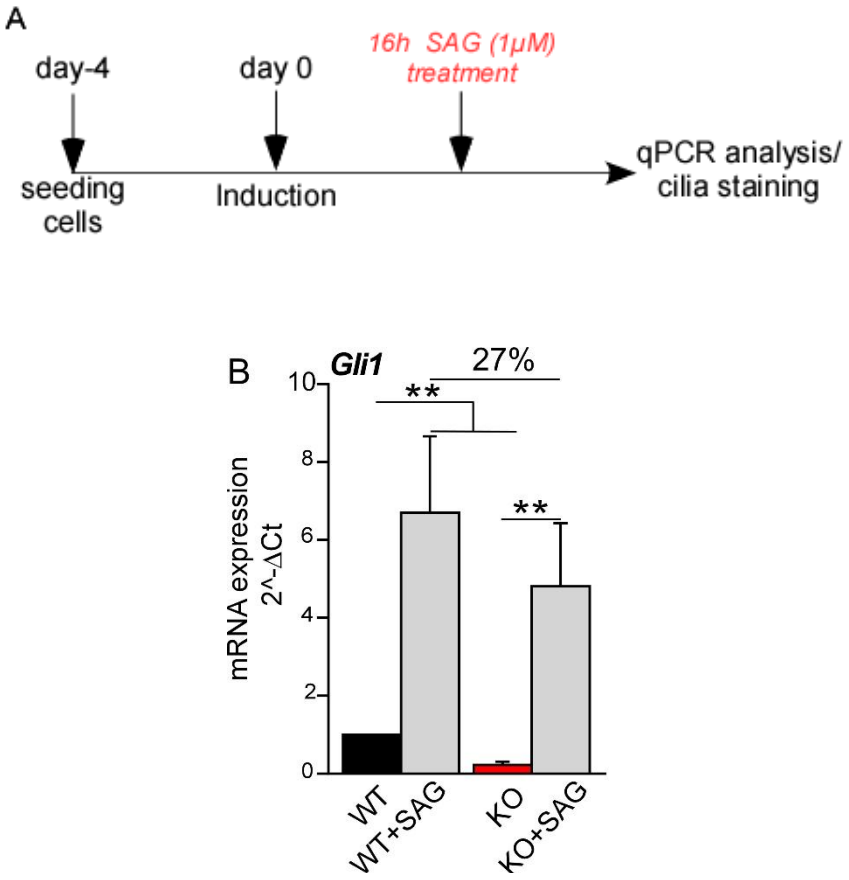

Figure 38: Treatment of BAs with SAG
(A) Schematic representation of SAG treatment after induction of BA (B) mRNA expression of Gli1 in BAs after 16h treatment with SAG. Expression data are normalized to *Hprt* and represented on a bar graph, n=4 of independent cell culture experiments, mean ± SEM, ANOVA, **<0.01.

Treatment with SAG significantly increases expression of *Gli1* in WT (8,068 ± 1,996) as well as in KO (5,970 ± 1,600) cells (Figure 38B). However, SAG couldn't increase *Gli1* expression to maximum as in WT cells. Expression of *Gli1* in KO cells after treatment with SAG was 27% less than in WT treated with SAG.

To further prove that *Gpr111* signals through the cilium, immunofluorescence staining of cilia in BAs was performed (Figure 39A).

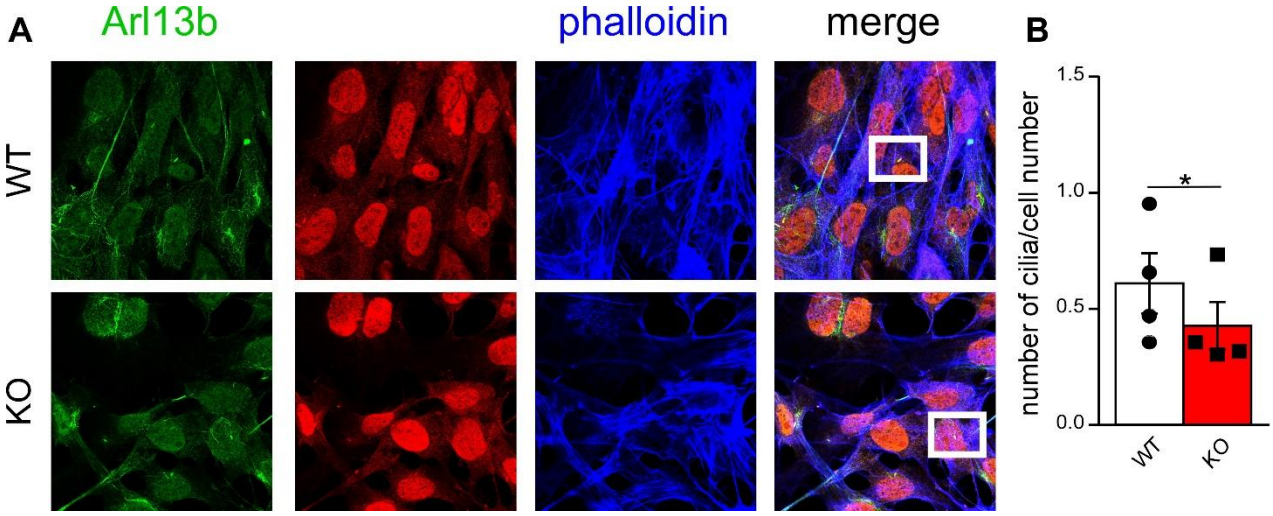

Figure 39: Immunostaining of cilia in BAs
(A) Representative immunofluorescence staining of cilia; merge: acetylated tubulin (green), Arl13b (red) and phalloidin (blue), magnification 63x. (B) Quantification of cilia number, data are represented in scatter plot bar graph, n=4 of independent cell culture experiments, N=10 pictures per experiment, mean ± SEM, *ANOVA*, *<0.05.

Immunofluorescence staining of cilia in BAs shows significant reduction of cilia number in KO cells (0,428 ± 0,103).

Taken together these data indicates that Gpr111 signaling is linked to cilia and HH signaling. These data are in line with previously shown *in vitro* results regarding to BA differentiation, because HH signaling negatively regulates differentiation of preadipocytes (Nosavanh et al., 2015b).

3.7.2. Interplay between GPR111, cAMP signaling and mechanical force

There are different molecular mechanisms for cells to sense force: 1) force sensing by adhesion complexes, 2) by actomyosin networks, 3) by the cell plasma membrane, 4) by change in cell geometry (Chanet and Martin, 2014). Adhesion complexes are the cell's front line for receiving mechanical stimuli and there are more than 100 different proteins such as integrin receptors, adhesion proteins/ receptors etc. (Chanet and Martin, 2014).

cAMP is a second messenger involved in different cellular processes. In BAT cAMP signaling promotes lipolysis, differentiation, proliferation and the expression of key regulators of thermogenesis in BAs (Reverte-Salisa et al., 2019). Besides, cAMP is involved in mechanosensation. Namely, it was shown that mechanostimulation decreases the cAMP concentration in mechanosensory neurons (Scholz et al., 2017). Moreover, cAMP is an important messenger in cilia related signaling (Sherpa et al., 2019).

To investigate the connection between Gpr111, cAMP signaling and mechanosensation, WT and KO BAs were mechanically stimulated for 1h on orbital plate shaker (8 Hz). After stimulation actin filaments were stained with phalloidin staining and intracellular cAMP levels were measured using cAMP ELISA (Figure 40).

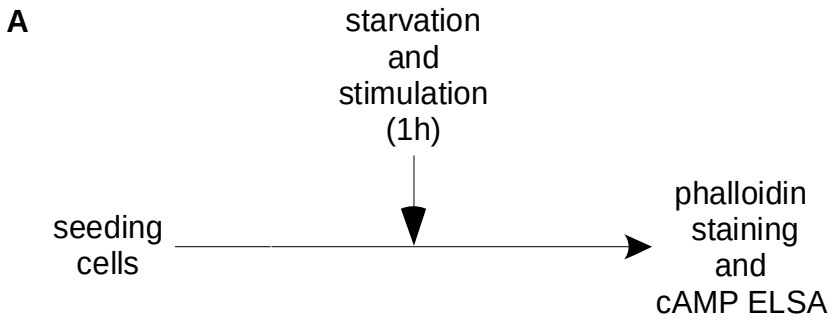

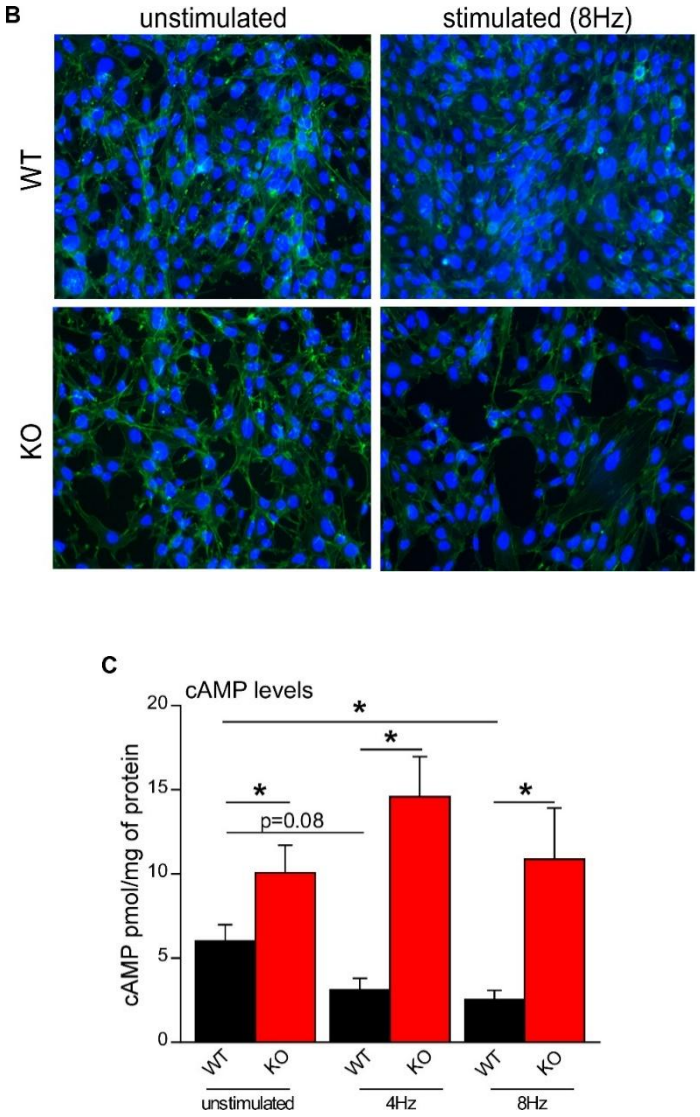

Figure 40: Interplay between GPR111, cAMP signaling and mechanical force
(A) Schematic representation of treatment. (B) Representative pictures of phalloidin staining, merge: phalloidin and DAPI, magnification 20x.(C) cAMP levels normalized to protein content in unstimulated, 4Hz and 8Hz stimulated WT and KO BAs respectively.

Phalloidin staining shows that applied mechanical stress causes complete disorganization of cellular network of KO BAs while WT network stayed stabile (Figure 40A).

cAMP levels were significantly increased in KO cell without stimulation (10,08 ± 1,631) and after applied mechanical stress of 4Hz (14,59 ± 2,395) or 8Hz (10,8 8 ± 3,044). Moreover, cAMP levels are significantly decreased in WT cells after the stimulation with

4Hz (3,12 ± 0,7) and 8Hz (2,54 ± 0,56) in comparison to unstimulated cells (Figure 40C). Reduction of cAMP in WT cells was gradual in contrast to KO cells.

To prove further involvement of Gpr111 in organization of cytoskeletal filaments, cells were serum starved for 24h, the next day cells were incubated for 30 min with 10% FBS to induce the formation of F-actin stress fibers (Figure 41).

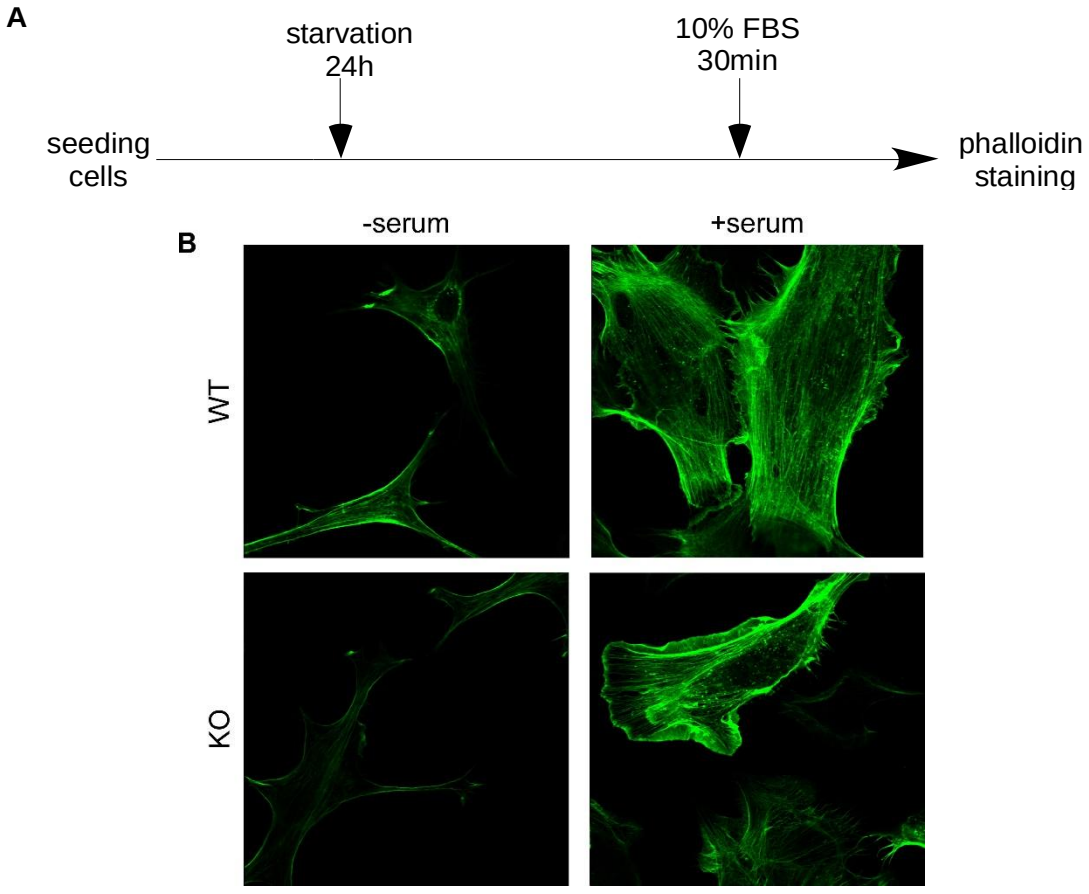

Figure 41: Gpr111 and stress fibers
(A) Scheme of treatment of BAs to visualize stress fibers (B) Representative phalloidin staining of stress fibers in Gpr111 WT and KO BAs.

Phalloidin staining of stress fibers show less stress fibers in KO cells in serum starved condition. Addition of serum strongly induced formation of stress fibers in WT cells, while in KO cells effect was lower. Changes is cytoskeletal organization are closely related to RhoA/ROCK signaling which could further indicate crosstalk between of RhoA Rock and Gpr111 signaling.

In summary, these results show that Gpr111 is involved in cytoskeletal organization. Additionally, less RhoA/ROCK signaling in KO BAs might be an explanation for better differentiation of KO cells.

4. Discussion

Obesity is a global health problem with a dramatically increasing incidence worldwide (Ng et al., 2014). Pathophysiology of obesity is multifactorial including epigenetic factors, reduced physical activity, increase of food intake, modern life style etc. (Must et al., 1999). Due to the effects of all these factors diet interventions as well as increase of physical activity are not enough to treat obesity. Hypocaloric diets initially lead to weigh loss but in the long term this reduced weight is very hard to maintain. As a consequence of the caloric restriction and negative energy balance, the body adapts by decreasing in whole-body energy expenditure (Rosenbaum 2008), which impairs the long-term maintenance of weight loss; this is also known as yo-yo effect or weight cycling. (Amigo and Fernández, 2007). Thus, it is necessary to find other solutions and novel treatments for obese patients (Rosenbaum et al., 2008).

GPCRs are the largest family of receptors that is targeted by approved drugs on the market (Sriram and Insel, 2018). They are very attractive targets in the field of obesity research, because many GPCRs play an important role in obesity and obesity related diseases (Riddy et al., 2018).

This thesis elucidated the role of adhesion GPCR Gpr111 in BAs and WAs, with the special focus on *in vivo* aspects of Gpr111 deletion.

4.1. Role of Gpr111 in differentiation, proliferation and function of brown and white adipocytes

The role of aGPCRs in AT is largely unknown. Only a few aGPCRs (EMR1, GPR97, CD97 (Shi et al., 2016)) were described to play a role in metaflammation (Kolehmainen et al., 2015). However, Gpr116, Gpr64, Gpr126 and Gpr56 are directly connected (Nie et al., 2012) with adipogenesis and adipocyte function which was shown using the 3T3-L1 adipocyte cell line, (Al Hasan et al., 2020), (Suchý et al., 2020). It was reported that knockdown of Gpr56 dramatically inhibits differentiation, proliferation, adhesion and abundance of extracellular matrix in 3T3-L1 cells via β-catenin (Al Hasan et al., 2020). Similarly, knockdown of six different aGPCRs (Lphn2, Gpr124, Gpr125, Gpr116, Gpr64, Gpr126) resulted in reduction of lipid accumulation and differentiation of 3T3-L1 cells. In contrast, I found that lipid accumulation was dramatically increased in GPR111 KO BAs and WAs. Additionally, the master regulator of adipogenesis (*Pparγ*) and the main marker of BAs (*Ucp1*) were upregulated on mRNA as well as on protein level in GPR111 KO BAs and WAs. The increase in differentiation was paralleled by enhanced adipocyte function with increased lipolysis and oxygen consumption. Interestingly, there was so far no evidence in literature which shows that knockdown of aGPCRs increases adipogenesis. As mentioned before all previous studies investigated aGPCRs using 3T3-L1 cell line, which does not represent all features of adipocytes and it was reported that Gpr111 is not expressed in this cell line (Suchý et al., 2020). In my study BAs and WAs, differentiated from SVF of BAT and WAT, respectively, were used. qPCR analysis

performed in those cells shows that Gpr111 is highly expressed in preadipocytes, especially WAs (Figure 18B). Interestingly, after the induction of adipogenesis, expression of Gpr111 is reduced and stays unchanged till end of the differentiation, while most of the other aGPCRs are preferentially expressed in later stages of adipocyte differentiation.

Based on expression data, which show that *Gpr111* is highly express in preadipocytes, one might speculate that Gpr111 is involved in early phase of differentiation of BAs and WAs. Lack of this receptor increases adipogenesis and improves adipocytes function. Some members of aGPCR family are involved in proliferation, migration/invasion of tumor cells and their role in these processes could be explained through the interaction of the receptor with integrins and/or ECMs (Kuhnert et al., 2010), (Scholz, 2018). Additionally, several aGPCRs have been shown to signal via small GTPases such as RhoA (Singer et al., 2013) and Rac1 (Lanoue et al., 2013). These downstream effectors are all involved in cell motility and activation of the cytoskeleton and proliferation. The only evidence of involvement of aGPCRs in proliferation of adipocytes was shown for Gpr56 in 3T3-L1 cells (Al Hasan et al., 2020). However, EdU proliferation assay using immortalized as well as primary BAs, didn't show any difference in proliferation between genotypes. On the other hand, Gpr111 KO WAs proliferate more than WT cells. This phenomenon could be explained through proliferation of beige progenitor cells (Taguchi et al., 2020). This observation is in concordance with *in vivo* results, where I could clearly observe the beiging effect in KO WAT. To further investigate difference in proliferation, EdU proliferation assay should be performed *in vivo*.

Beige adipocytes develop through two major mechanisms such as trans-differentiation of WAs into BAs and *de novo* differentiation from vascular precursors cells (Long et al., 2014). It is hard to determine which of these mechanisms plays the main role in proliferation and beiging of GPR111 KO cells.

4.2. Potential Gpr111 signaling

Studying signaling pathways of orphan receptors is difficult due to a lack of pharmacological tools (Tang et al., 2013). However, for some of aGPCRs signaling pathways as well as interactor with N-terminal fragment are clearly define and most of them signal via RhoA, Rac or cAMP signaling (Purcell and Hall, 2018).

In case of aGPCRs mechanical force can cause disruption of the heterodimers at GPS motif or allosteric modulation of the GAIN domain. In both situations, the receptor will be exposed to the *Stachel* sequence which will in the end activate the receptor. In the first scenario autoproteolytic cleavage is crucial for activation of the receptor, on the other hand, allosteric modulation doesn't require GPS cleavage for receptor activation (Scholz et al., 2017). As discussed before, Gpr111 does not undergo autoproteolysis and thus the second scenario is more likely when mechanical force activates this receptor. It was shown in dCIRL that autoproteolytic cleveage is not required for perception and

transduction of vibrational mechanical stimuli and probably that could be also the case for Gpr111 (Scholz et al., 2017).

Cilia are organelles involved in mechanosensation as well as aGPCRs and according to this fact I derived my hypothesis that Gpr111 signaling is linked to cilia.
The proposed signaling encloses cross-roads of three signaling pathways: HH, RhoA/ROCK and cAMP signaling.

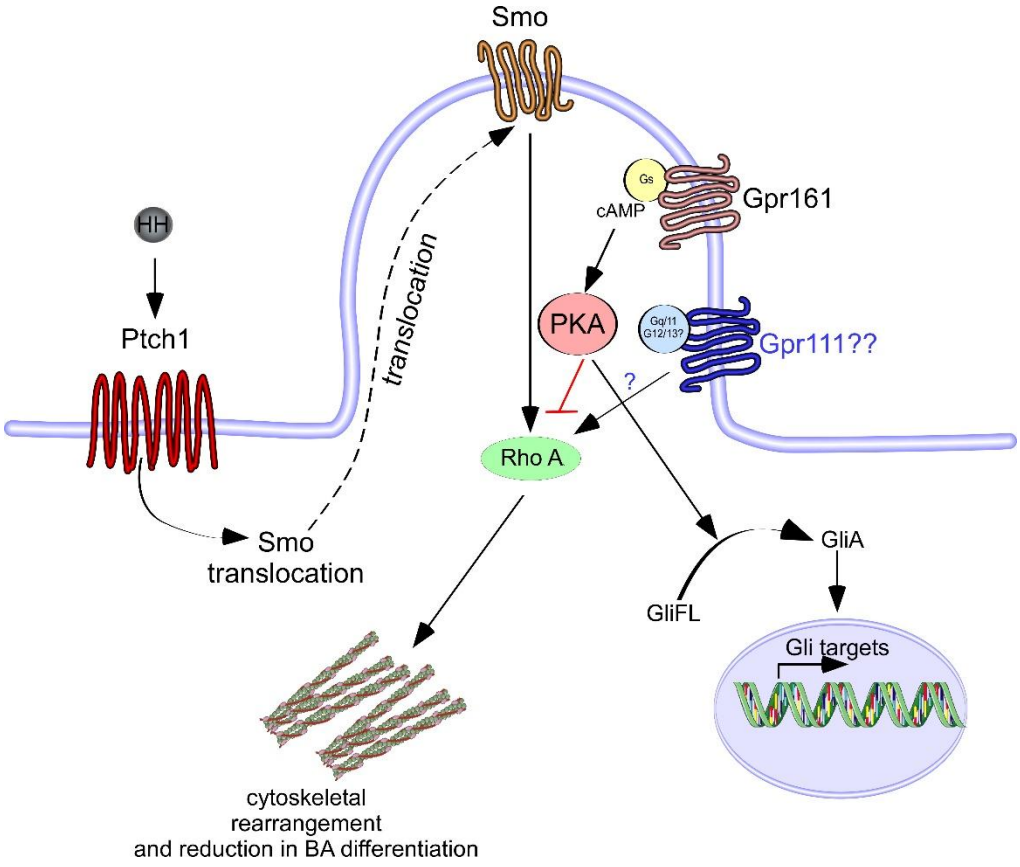

Figure 42: Proposed mechanism of Gpr111 signaling
Gli1F-full length (inactive), GliA-active form, PKA-protein kinase A.

Activation of HH signaling through stimulation of Ptch1 will cause a translocation of Smo. Activated Smo can directly activate RhoA. When HH is “on”, PKA phosphorylates and activates Gli, which translocate into the nucleus and induce transcription of Gli target genes. Also, it is well known that PKA can inhibit RhoA. My hypothesis is that Gpr111 - via Gq or G12/13 - activates RhoA. RhoA in turn has a negative effect on differentiation of BAs. Moreover, in KO cells which have altered cilia, HH is impaired which in turn leads to less RhoA signaling. Overall, differentiation of BA will be massively increased.

In this study, I found that the most important elements of HH signaling were downregulated in KO BAs. Similarly, reduction in HH related genes (*Smo*, *Ptch1* and *Gli1*) was observed in AT of KO mice. Also, expression of *Gli1* in KO cells was 27% lower than in WT after the stimulation with SAG. On the other hand, the major opponent of HH signaling is cAMP signaling and in my experiments, I observed an increase of intracellular cAMP, in KO cells at basal levels as well as after mechanical stimulation.

Several studies (Fredriksson and Nedergaard, 2002), (Kozak and Kozak, 1994) were described beneficial effects of cAMP on differentiation, proliferation and metabolism of brown adipocytes mainly in PKA-dependent manner. On the other hand, HH signaling negatively regulates BA differentiation through up-regulation of anti-adipogenic genes such as *GATA2* and *GATA3* binding proteins, *Pref1*, *Wnt1b*, *COUP-TFII* (Nosavanh et al., 2015a), (Fontaine et al., 2008b).
HH signaling mainly takes place in cilia and some studies (Mykytyn and Askwith, 2017) linked GPCR signaling and cilia; therefore, I speculated that the morphology of cilia might be affected by the loss of GPR111. Moreover, lower number of cilia or defected cilia are mainly related to non-canonical HH signaling (Razumilava et al., 2014) which is involved in cytoskeletal remodeling and operates via RhoA/ROCK signaling (Gu and Xie, 2015b).
In this study, immunofluorescence staining showed significantly lower number of cilia in KO BAs in comparison with WT cells. Therefore, I hypothesized that KO cells, due to defect in cytoskeletal organization especially under stress conditions have a defect in cilium function (Mirvis et al., 2018).
To investigate changes in cytoskeletal remodeling, I applied sheer stress using orbital plate shaker. Phalloidin staining showed disorganization of actin fibers in KO BAs after 1h of stimulation. Moreover, the experiment where serum was used to induce stress fibers shows less phalloidin staining in KO BAs, which is an additional indication that this hypothesis might be correct.
Taken together, in steady state, KO BAs differentiate better than WT cells and they develop normal cell-network, but after application of stress, the KO cells loose normal cytoskeletal organization.
In summary, impaired HH signaling together with defect in cytoskeleton and lead to inhibition of RhoA/ROCK signaling, which is a central inhibitor of differentiation, in KO BAs. Moreover, cAMP-PKA signaling also reduces RhoA/ROCK and additionally suppresses HH signaling (Figure 42). However, further studies using genetic modifications, electron and immunofluorescent microscopy are required to further elucidate the cilia-related phenotype of GPR111 KO cells.

4.3. Role of Gpr111 in AT of adult mice

When eight week old WT and KO mice were housed in metabolic cages at 23^0 C EE was increased in KO mice. Moreover, KO mice had 15% less fat mass, which was shown by NMR analysis and by post mortal tissue mass. Histological analysis of AT shows smaller adipocytes and more UCP1 staining in WAT of KO mice. Additionally,

UCP1 (protein levels) and *Pparg1cα* (mRNA) were elevated in AT of KO mice. AT of KO mice is fully active and shows a higher *ex vivo* oxygen consumption. Finally, pictures of WAT of KO mice clearly indicate browning phenotype.

Usually in WAT of animals kept at 23^0 C, there are relatively few beige adipocytes (Stine et al., 2016). However, I could observe massive browning phenotype in KO mice when they were kept at 23^0 C, especially in WATg. This observation is very important if it is taken on an account that recent studies have indicated that beige adipocyte activity affects systemic metabolism and contributes in a significant way to whole body insulin sensitivity (Cohen et al., 2014), (Qiu et al., 2014). The possible explanation for browning of WAT in KO mice might be related to high expression of Gpr111 in WATg.

Additionally, my finding of increased browning in WAT of KO mice is in line with *in vitro* results obtained using WAs isolated from WT and KO GPR111 mice.

An interesting question is whether the lack of Gpr111 drives the browning process trough trans-differentiation or *de novo* differentiation from vascular precursors cells (PDGFRα+). To answer this questions further experiments such as fluorescence-activated cell sorting (FACS) of beige cells and adipocytes progenitors has to be performed.

4.4. Metabolic changes of KO mice after cold exposure

It was reported that cold exposure can stimulate BAs to do thermogenesis (Brychta and Chen, 2017). Activated BAs as well as beige cells can burn energy and this leads to weight loss in mammals (Saito et al., 2020).

Gpr111 KO mice measured in metabolic cages for 7 days at 4^0 C have shown a higher EE. In the WAT after cold exposure it was easy to notice a strong browning effect in KO samples compared to WT. Histological analysis of AT shows smaller adipocytes area and more UCP1 in KO mice which is linked to a higher gene expression and protein levels of thermogenic and adipogenic markers observed in almost all AT of KO mice.

Apart from these data, which again confirmed the strong browning effect of cold stimulus in KO mice, some unexpected results were observed. Namely, KO mice moved much more, ate more and in the end they gained more weight in comparison to WT mice. Also NMR analysis has shown a significant increase of fat mass and muscle mass (7%).

All these results were unexpected because, mice during cold exposure are usually minimally physically active they eat same amounts of food and the body weight after measurement is the same or decreased. The possible explanation for the increase in motility and feeding behavior could be thermal stress. It could be that Gpr111 KO mice can’t cope with lower temperatures and they are trying to compensate it. Probably mice move more to warm up and they eat more to provide fuel for thermogenesis. Due to higher energy intake mice gain weight which was reflected as an increase of fat mass and muscle mass (7%).

To confirm this hypothesis further experiments with heterozygous, as well as with tissue specific KO mice are planned. Increased motility and food intake in KO mice, especially during cold exposure, could be reduced by using heterozygous mice.

By using tissue specific KO model, it would be possible to provide stronger evidence to explain the effects of Gpr111 in AT without additional effects that arise by the use of global KO model. Also, experiments in which mice are exposed to mild cold 16ºC and to short term cold (1 day, 4ºC) are planned. Behind these experiments stands a hypothesis that exposure of mice to 16ºC or 4ºC for a short time, would not cause huge thermal stress and additional effects such as high motility and food intake.

4.5. Changes in Gpr111 KO mice upon HFD

Results that were obtained in the experiment when HFD was used to induce obesity and diabetes were not in line with the postulated hypothesis. According to all previous results it was expected that Gpr111 KO mice would be resistant to DIO; however, that was not the case.

Gpr111 KO mice gained weight similarly like WT mice during 12 weeks of feeding with HFD/ND. Also, KO mice fed with HFD developed diabetes as WT mice and that is clearly shown as a result of GTT test. Interestingly, KO mice have a slightly higher EE at 23ºC as well as when they were exposed to cold (4ºC) for 1 hour. However, body mass as well as AT mass of KO and WT mice were similar and not significantly changed. This observation was even more interesting because KO mice took 20% more food in than WT mice. To find the reason why KO mice eat more, serum leptin ELISA was performed. Leptin is a hormone produced from AT that regulates appetite (Zhang et al., 1994). If mice or humans have an increased food intake, leptin will stimulate leptin receptors in hypothalamus to suppress appetite and further (over)feeding. My results show a slight reduction in serum leptin levels in KO mice and downregulation of LepR in those mice which could contribute to the increased food intake of KO mice. Furthermore, downregulation of LepR is a limiting factor in leptin signaling.

The phenotype of the BBS model might further indicate a connection between leptin signaling and Gpr111 signaling. Namely, BBS-induced obesity has previously been explained as inability of the hypothalamus to respond to leptin (Rahmouni et al., 2008).

To further investigate the reasons for the phenotype, further experiments were performed on explanted fat tissues. Even though, qPCR analysis did not show significant difference in expression of adipogenic and thermogenic markers in AT after HFD/ND between genotypes. Western blot analysis clearly showed that UCP1 protein was reduced almost in all fat tissues. Reduction in UCP1 and other parameters e.g. GTT were clear indicators of pathophysiological conditions in AT.

To study inflammation in AT, pro-inflammatory markers (*Ccl2* and *Tnfα*) were analyzed. Indicating reduced inflammation in AT in the absence of GPR111. Additional histological staining of crown-like structure is needed to clarified absence of inflammation in AT of KO mice.

To further clarify the the role of Gpr111 in AT, it is necessary to use a tissue-specific KO model.

5. Summary

Due to obesity pandemic and limited therapeutic approaches, novel targets of pharmaceutical treatments are urgently needed.
AT as a very important metabolic organ is an attractive target for combating obesity and obesity related metabolic diseases.
Humans possess two different types of adipose tissue: BAT and WAT. WAT is important as main energy storage, whereas BAT dissipates energy in the form of heat (Chen et al., 2016). Our research group has shown that among GPCRs, aGPCRs are highly represented in pre- and mature brown adipocytes. One of the identified receptors was the orphan GPR111, which belongs to F subgroup of aGPCRs.
The data presented in this study identified the role of Gpr111 in AT. *In vitro* data which were obtained using KO BAs and WAs, show that lack of Gpr111 promotes adipo- and thermogenesis. That was manifested through an increase of adipogenic and thermogenic markers, higher lipolytic rate and higher oxygen consumption in KO cells. Also, it is important to emphasise a massive browning effect that was observed in KO WAs.
Due to a lack of ligands for Gpr111, the detailed investigation of signalling pathways was difficult. However, I could show that Gpr111 probably signals into the cilium and is tightly linked to HH and cAMP signalling. Furthermore, I could demonstrate that Gpr111 is involved in cell adhesion and cell organization especially after mechanical sheer stress was applied. Lack of Gpr111 has a big impact on cilia number and important genes of HH signalling, which were downregulated in KO cells as well as in some ATs.
Adult Gpr111 KO mice showed a higher expression of adipogenic and thermogenic markers, higher EE and 15 % less fat mass. Measurement of oxygen consumption performed on explanted fat tissues was also higher in KO then in WT. Additionally, expression of UCP1 was increased in fat tissues of KO mice. According to these results I could conclude that a lack of Gpr111 induces browning phenotype in mice.
Apart from investigation of Gpr111 mice under basal condition, in this study I challenged Gpr111 WT and KO mice with cold exposure and feeding them with HFD.
Under cold stimulation KO mice show lightly higher EE *in vivo.* On the other hand, qPCR, Western blot and immunohistochemistry show massive browning in KO WAT, but unexpectedly KO mice had higher motility, food intake in comparison to WT and correspondingly more fat and muscle mass. As it was discussed before, possible reason for that is not related to AT, but to global deletion of Gpr111 and thermal stress. To reduce these unexpected results under cold stimulation the use of tissue specific KO model and exposing the mice to 4^0 C for shorter time were proposed.
The most important challenge is HFD and KO mice fed with HFD show minor increase in EE. They also developed diabetes, food intake in KO HFD was much higher than in WT HFD and Western blot analysis has shown less UCP1 on protein level. Probably KO mice are resistant to HFD in young age and later on they develop obesity in a similar

manner as WT mice. The HFD feeding at young age and tissue specific KO would give more explanations to this puzzle.

In conclusion, my study identifies a previously unknown role for Gpr111 in energy metabolism. I provided evidence that depletion of Gpr111 promotes browning of adipose tissue. Thus, Gpr111 may be a pharmacological target to combat obesity and associated morbidities given its selective impact on WAT browning.

6. References

Al Hasan, M., Roy, P., Dolan, S., Martin, P.E., Patterson, S., and Bartholomew, C. (2020). Adhesion G-protein coupled receptor 56 is required for 3T3-L1 adipogenesis. Journal of cellular physiology *235*, 1601-1614. https://doi.org/10.1002/jcp.29079.

Alcalá, M., Calderon-Dominguez, M., Serra, D., Herrero, L., and Viana, M. (2019). Mechanisms of Impaired Brown Adipose Tissue Recruitment in Obesity. Frontiers in physiology *10*, 94. https://doi.org/10.3389/fphys.2019.00094.

Amigo, I., and Fernández, C. (2007). Effects of diets and their role in weight control. Psychology, Health & Medicine *12*, 321-327. https://doi.org/10.1080/13548500600621545.

Antic, D., Stubbs, J.L., Suyama, K., Kintner, C., Scott, M.P., and Axelrod, J.D. (2010). Planar cell polarity enables posterior localization of nodal cilia and left-right axis determination during mouse and Xenopus embryogenesis. PloS one *5*, e8999. https://doi.org/10.1371/journal.pone.0008999.

Anvarian, Z., Mykytyn, K., Mukhopadhyay, S., Pedersen, L.B., and Christensen, S.T. (2019). Cellular signalling by primary cilia in development, organ function and disease. Nat Rev Nephrol *15*, 199-219. https://doi.org/10.1038/s41581-019-0116-9.

Araç, D., Boucard, A.A., Bolliger, M.F., Nguyen, J., Soltis, S.M., Südhof, T.C., and Brunger, A.T. (2012). A novel evolutionarily conserved domain of cell-adhesion GPCRs mediates autoproteolysis. The EMBO journal *31*, 1364-1378. https://doi.org/10.1038/emboj.2012.26.

Bangs, F., and Anderson, K.V. (2017). Primary Cilia and Mammalian Hedgehog Signaling. Cold Spring Harbor perspectives in biology *9*. https://doi.org/10.1101/cshperspect.a028175.

Bélanger, C., Luu-The, V., Dupont, P., and Tchernof, A. (2002). Adipose tissue intracrinology: potential importance of local androgen/estrogen metabolism in the regulation of adiposity. Hormone and metabolic research = Hormon- und Stoffwechselforschung = Hormones et metabolisme *34*, 737-745. https://doi.org/10.1055/s-2002-38265.

Bonaglia, M.C., Marelli, S., Novara, F., Commodaro, S., Borgatti, R., Minardo, G., Memo, L., Mangold, E., Beri, S., and Zucca, C., et al. (2010). Genotype-phenotype relationship in three cases with overlapping 19p13.12 microdeletions. European journal of human genetics : EJHG *18*, 1302-1309. https://doi.org/10.1038/ejhg.2010.115.

Brychta, R.J., and Chen, K.Y. (2017). Cold-induced thermogenesis in humans. Eur J Clin Nutr *71*, 345-352. https://doi.org/10.1038/ejcn.2016.223.

Cannon, B., and Nedergaard, J. (2004). Brown adipose tissue: function and physiological significance. Physiological reviews *84*, 277-359. https://doi.org/10.1152/physrev.00015.2003.

Chai, G., Zhou, L., Manto, M., Helmbacher, F., Clotman, F., Goffinet, A.M., and Tissir, F. (2014). Celsr3 is required in motor neurons to steer their axons in the hindlimb. Nature neuroscience *17*, 1171-1179. https://doi.org/10.1038/nn.3784.

Chan, Y.F., Jones, F.C., McConnell, E., Bryk, J., Bünger, L., and Tautz, D. (2012). Parallel selection mapping using artificially selected mice reveals body weight control loci. Current biology : CB *22*, 794-800. https://doi.org/10.1016/j.cub.2012.03.011.

Chanet, S., and Martin, A.C. (2014). Mechanical force sensing in tissues. Prog Mol Biol Transl Sci *126*, 317-352. https://doi.org/10.1016/B978-0-12-394624-9.00013-0.

Chang, G.-W., Stacey, M., Kwakkenbos, M.J., Hamann, J., Gordon, S., and Lin, H.-H. (2003). Proteolytic cleavage of the EMR2 receptor requires both the extracellular stalk and the GPS motif. FEBS Letters *547*, 145-150. https://doi.org/10.1016/S0014-5793(03)00695-1.

Chen, P.-L., and Clandinin, T.R. (2008). The cadherin Flamingo mediates level-dependent interactions that guide photoreceptor target choice in Drosophila. Neuron *58*, 26-33. https://doi.org/10.1016/j.neuron.2008.01.007.

Chen, Y., Buyel, J.J., Hanssen, M.J.W., Siegel, F., Pan, R., Naumann, J., Schell, M., van der Lans, A., Schlein, C., and Froehlich, H., et al. (2016). Exosomal microRNA miR-92a concentration in serum reflects human brown fat activity. Nature communications *7*, 11420. https://doi.org/10.1038/ncomms11420.

Cinti, S. (2012). The adipose organ at a glance. Dis Model Mech *5*, 588-594. https://doi.org/10.1242/dmm.009662.

Coelho, M., Oliveira, T., and Fernandes, R. (2013). Biochemistry of adipose tissue: an endocrine organ. Archives of medical science : AMS *9*, 191-200. https://doi.org/10.5114/aoms.2013.33181.

Cohen, P., Levy, J.D., Zhang, Y., Frontini, A., Kolodin, D.P., Svensson, K.J., Lo, J.C., Zeng, X., Ye, L., and Khandekar, M.J., et al. (2014). Ablation of PRDM16 and beige adipose causes metabolic dysfunction and a subcutaneous to visceral fat switch. Cell *156*, 304-316. https://doi.org/10.1016/j.cell.2013.12.021.

Cortijo, C., Gouzi, M., Tissir, F., and Grapin-Botton, A. (2012). Planar cell polarity controls pancreatic beta cell differentiation and glucose homeostasis. Cell reports *2*, 1593-1606. https://doi.org/10.1016/j.celrep.2012.10.016.

Demberg, L.M., Winkler, J., Wilde, C., Simon, K.-U., Schön, J., Rothemund, S., Schöneberg, T., Prömel, S., and Liebscher, I. (2017). Activation of Adhesion G Protein-coupled Receptors: AGONIST SPECIFICITY OF STACHEL SEQUENCE-DERIVED PEPTIDES. The Journal of biological chemistry *292*, 4383-4394. https://doi.org/10.1074/jbc.M116.763656.

Doyle, S.E., Scholz, M.J., Greer, K.A., Hubbard, A.D., Darnell, D.K., Antin, P.B., Klewer, S.E., and Runyan, R.B. (2006). Latrophilin-2 is a novel component of the epithelial-mesenchymal transition within the atrioventricular canal of the embryonic chicken heart. Developmental dynamics : an official publication of the American Association of Anatomists *235*, 3213-3221. https://doi.org/10.1002/dvdy.20973.

Duman, J.G., Tzeng, C.P., Tu, Y.-K., Munjal, T., Schwechter, B., Ho, T.S.-Y., and Tolias, K.F. (2013). The adhesion-GPCR BAI1 regulates synaptogenesis by controlling the recruitment of the Par3/Tiam1 polarity complex to synaptic sites. The Journal of neuroscience : the official journal of the Society for Neuroscience *33*, 6964-6978. https://doi.org/10.1523/JNEUROSCI.3978-12.2013.

Fontaine, C., Cousin, W., Plaisant, M., Dani, C., and Peraldi, P. (2008a). Hedgehog signaling alters adipocyte maturation of human mesenchymal stem cells. Stem cells (Dayton, Ohio) *26*, 1037-1046. https://doi.org/10.1634/stemcells.2007-0974.

Fontaine, C., Cousin, W., Plaisant, M., Dani, C., and Peraldi, P. (2008b). Hedgehog signaling alters adipocyte maturation of human mesenchymal stem cells. Stem cells (Dayton, Ohio) *26*, 1037-1046. https://doi.org/10.1634/stemcells.2007-0974.

Fredriksson, J.M., and Nedergaard, J. (2002). Norepinephrine specifically stimulates ribonucleotide reductase subunit R2 gene expression in proliferating brown adipocytes: mediation via a cAMP/PKA pathway involving Src and Erk1/2 kinases. Experimental cell research *274*, 207-215. https://doi.org/10.1006/excr.2002.5470.

Fredriksson, R., and Schiöth, H.B. (2005). The repertoire of G-protein-coupled receptors in fully sequenced genomes. Molecular pharmacology *67*, 1414-1425. https://doi.org/10.1124/mol.104.009001.

Galle, J., Sittig, D., Hanisch, I., Wobus, M., Wandel, E., Loeffler, M., and Aust, G. (2006). Individual cell-based models of tumor-environment interactions: Multiple effects of CD97 on tumor invasion. The American journal of pathology *169*, 1802-1811. https://doi.org/10.2353/ajpath.2006.060006.

Gesta, S., Tseng, Y.-H., and Kahn, C.R. (2007a). Developmental origin of fat: tracking obesity to its source. Cell *131*, 242-256. https://doi.org/10.1016/j.cell.2007.10.004.

Gesta, S., Tseng, Y.-H., and Kahn, C.R. (2007b). Developmental origin of fat: tracking obesity to its source. Cell *131*, 242-256. https://doi.org/10.1016/j.cell.2007.10.004.

Glenn, T.D., and Talbot, W.S. (2013). Analysis of Gpr126 function defines distinct mechanisms controlling the initiation and maturation of myelin. Development *140*, 3167-3175. https://doi.org/10.1242/dev.093401.

Gregor, M.F., and Hotamisligil, G.S. (2007). Thematic review series: Adipocyte Biology. Adipocyte stress: the endoplasmic reticulum and metabolic disease. Journal of lipid research *48*, 1905-1914. https://doi.org/10.1194/jlr.R700007-JLR200.

Gu, D., and Xie, J. (2015a). Non-Canonical Hh Signaling in Cancer-Current Understanding and Future Directions. Cancers (Basel) *7*, 1684-1698. https://doi.org/10.3390/cancers7030857.

Gu, D., and Xie, J. (2015b). Non-Canonical Hh Signaling in Cancer-Current Understanding and Future Directions. Cancers (Basel) *7*, 1684-1698. https://doi.org/10.3390/cancers7030857.

Hamann, J., Aust, G., Araç, D., Engel, F.B., Formstone, C., Fredriksson, R., Hall, R.A., Harty, B.L., Kirchhoff, C., and Knapp, B., et al. (2015). International Union of Basic and Clinical Pharmacology. XCIV. Adhesion G protein-coupled receptors. Pharmacological reviews *67*, 338-367. https://doi.org/10.1124/pr.114.009647.

Hamann, J., Vogel, B., van Schijndel, G.M., and van Lier, R.A. (1996). The seven-span transmembrane receptor CD97 has a cellular ligand (CD55, DAF). The Journal of experimental medicine *184*, 1185-1189. https://doi.org/10.1084/jem.184.3.1185.

Hashimoto, M., Shinohara, K., Wang, J., Ikeuchi, S., Yoshiba, S., Meno, C., Nonaka, S., Takada, S., Hatta, K., and Wynshaw-Boris, A., et al. (2010). Planar polarization of node cells determines the rotational axis of node cilia. Nature cell biology *12*, 170-176. https://doi.org/10.1038/ncb2020.

Ikeda, K., Maretich, P., and Kajimura, S. (2018). The Common and Distinct Features of Brown and Beige Adipocytes. Trends Endocrinol Metab *29*, 191-200. https://doi.org/10.1016/j.tem.2018.01.001.

Ishibashi, J., and Seale, P. (2015). Functions of Prdm16 in thermogenic fat cells. Temperature (Austin, Tex.) *2*, 65-72. https://doi.org/10.4161/23328940.2014.974444.

Jastrzebska, B. (2013). GPCR: G protein complexes--the fundamental signaling assembly. Amino acids *45*, 1303-1314. https://doi.org/10.1007/s00726-013-1593-y.

Jiang, Y., Ma, W., Wan, Y., Kozasa, T., Hattori, S., and Huang, X.Y. (1998). The G protein G alpha12 stimulates Bruton's tyrosine kinase and a rasGAP through a conserved PH/BM domain. Nature *395*, 808-813. https://doi.org/10.1038/27454.

Kamesh, N., Aradhyam, G.K., and Manoj, N. (2008). The repertoire of G protein-coupled receptors in the sea squirt Ciona intestinalis. BMC Evol Biol *8*, 129. https://doi.org/10.1186/1471-2148-8-129.

Kershaw, E.E., and Flier, J.S. (2004). Adipose tissue as an endocrine organ. The Journal of clinical endocrinology and metabolism *89*, 2548-2556. https://doi.org/10.1210/jc.2004-0395.

Khan, S.M., Sleno, R., Gora, S., Zylbergold, P., Laverdure, J.-P., Labbé, J.-C., Miller, G.J., and Hébert, T.E. (2013). The expanding roles of Gβγ subunits in G protein-coupled receptor signaling and drug action. Pharmacological reviews *65*, 545-577. https://doi.org/10.1124/pr.111.005603.

Kim, J.-J., Park, Y.-M., Baik, K.-H., Choi, H.-Y., Yang, G.-S., Koh, I., Hwang, J.-A., Lee, J., Lee, Y.-S., and Rhee, H., et al. (2012). Exome sequencing and subsequent association studies identify five amino acid-altering variants influencing human height. Human genetics *131*, 471-478. https://doi.org/10.1007/s00439-011-1096-4.

Klepac, K., Kilić, A., Gnad, T., Brown, L.M., Herrmann, B., Wilderman, A., Balkow, A., Glöde, A., Simon, K., and Lidell, M.E., et al. (2016). The Gq signalling pathway inhibits brown and beige adipose tissue. Nature communications *7*, 10895. https://doi.org/10.1038/ncomms10895.

Koh, J.T., Kook, H., Kee, H.J., Seo, Y.-W., Jeong, B.C., Lee, J.H., Kim, M.-Y., Yoon, K.C., Jung, S., and Kim, K.K. (2004). Extracellular fragment of brain-specific angiogenesis inhibitor 1 suppresses endothelial cell proliferation by blocking alphavbeta5 integrin. Experimental cell research *294*, 172-184. https://doi.org/10.1016/j.yexcr.2003.11.008.

Kolehmainen, M., Ulven, S.M., Paananen, J., Mello, V. de, Schwab, U., Carlberg, C., Myhrstad, M., Pihlajamäki, J., Dungner, E., and Sjölin, E., et al. (2015). Healthy Nordic diet downregulates the expression of genes involved in inflammation in subcutaneous adipose tissue in individuals with features of the metabolic syndrome. The American journal of clinical nutrition *101*, 228-239. https://doi.org/10.3945/ajcn.114.092783.

Kou, I., Takahashi, Y., Johnson, T.A., Takahashi, A., Guo, L., Dai, J., Qiu, X., Sharma, S., Takimoto, A., and Ogura, Y., et al. (2013). Genetic variants in GPR126 are associated with adolescent idiopathic scoliosis. Nature genetics *45*, 676-679. https://doi.org/10.1038/ng.2639.

Kozak, U.C., and Kozak, L.P. (1994). Norepinephrine-dependent selection of brown adipocyte cell lines. Endocrinology *134*, 906-913. https://doi.org/10.1210/endo.134.2.7905411.

Krishnan, A., Almén, M.S., Fredriksson, R., and Schiöth, H.B. (2012). The origin of GPCRs: identification of mammalian like Rhodopsin, Adhesion, Glutamate and Frizzled GPCRs in fungi. PloS one *7*, e29817. https://doi.org/10.1371/journal.pone.0029817.

Kuhnert, F., Mancuso, M.R., Shamloo, A., Wang, H.-T., Choksi, V., Florek, M., Su, H., Fruttiger, M., Young, W.L., and Heilshorn, S.C., et al. (2010). Essential regulation of CNS angiogenesis by the orphan G protein-coupled receptor GPR124. Science *330*, 985-989. https://doi.org/10.1126/science.1196554.

Langenhan, T., Aust, G., and Hamann, J. (2013). Sticky signaling--adhesion class G protein-coupled receptors take the stage. Science signaling *6*, re3. https://doi.org/10.1126/scisignal.2003825.

Lanoue, V., Usardi, A., Sigoillot, S.M., Talleur, M., Iyer, K., Mariani, J., Isope, P., Vodjdani, G., Heintz, N., and Selimi, F. (2013). The adhesion-GPCR BAI3, a gene linked to psychiatric disorders, regulates dendrite morphogenesis in neurons. Molecular psychiatry *18*, 943-950. https://doi.org/10.1038/mp.2013.46.

Lee, H., Song, J., Jung, J.H., and Ko, H.W. (2015). Primary cilia in energy balance signaling and metabolic disorder. BMB Rep *48*, 647-654. https://doi.org/10.5483/bmbrep.2015.48.12.229.

Lee, M.-J., Wu, Y., and Fried, S.K. (2013). Adipose tissue heterogeneity: implication of depot differences in adipose tissue for obesity complications. Molecular aspects of medicine *34*, 1-11. https://doi.org/10.1016/j.mam.2012.10.001.

Liebscher, I., Ackley, B., Araç, D., Ariestanti, D.M., Aust, G., Bae, B.-i., Bista, B.R., Bridges, J.P., Duman, J.G., and Engel, F.B., et al. (2014). New functions and signaling mechanisms for the class of adhesion G protein-coupled receptors. Annals of the New York Academy of Sciences *1333*, 43-64. https://doi.org/10.1111/nyas.12580.

Lizcano, F. (2019). The Beige Adipocyte as a Therapy for Metabolic Diseases. International journal of molecular sciences *20*. https://doi.org/10.3390/ijms20205058.

Long, J.Z., Svensson, K.J., Tsai, L., Zeng, X., Roh, H.C., Kong, X., Rao, R.R., Lou, J., Lokurkar, I., and Baur, W., et al. (2014). A smooth muscle-like origin for beige adipocytes. Cell metabolism *19*, 810-820. https://doi.org/10.1016/j.cmet.2014.03.025.

Louka, P., Vasudevan, K.K., Guha, M., Joachimiak, E., Wloga, D., Tomasi, R.F.-X., Baroud, C.N., Dupuis-Williams, P., Galati, D.F., and Pearson, C.G., et al. (2018). Proteins that control the geometry of microtubules at the ends of cilia. J Cell Biol *217*, 4298-4313. https://doi.org/10.1083/jcb.201804141.

Luo, R., Jeong, S.-J., Yang, A., Wen, M., Saslowsky, D.E., Lencer, W.I., Araç, D., and Piao, X. (2014). Mechanism for adhesion G protein-coupled receptor GPR56-mediated RhoA activation induced by collagen III stimulation. PloS one *9*, e100043. https://doi.org/10.1371/journal.pone.0100043.

Marion, V., Mockel, A., Melo, C. de, Obringer, C., Claussmann, A., Simon, A., Messaddeq, N., Durand, M., Dupuis, L., and Loeffler, J.-P., et al. (2012). BBS-induced ciliary defect enhances adipogenesis, causing paradoxical higher-insulin sensitivity, glucose usage, and decreased inflammatory response. Cell metabolism *16*, 363-377. https://doi.org/10.1016/j.cmet.2012.08.005.

Martyniak, K., and Masternak, M.M. (2017). Changes in adipose tissue cellular composition during obesity and aging as a cause of metabolic dysregulation. Experimental gerontology *94*, 59-63. https://doi.org/10.1016/j.exger.2016.12.007.

Meldrum, D.R., Morris, M.A., and Gambone, J.C. (2017). Obesity pandemic: causes, consequences, and solutions-but do we have the will? Fertility and sterility *107*, 833-839. https://doi.org/10.1016/j.fertnstert.2017.02.104.

Meseguer, A., Puche, C., and Cabero, A. (2002). Sex steroid biosynthesis in white adipose tissue. Hormone and metabolic research = Hormon- und Stoffwechselforschung = Hormones et metabolisme *34*, 731-736. https://doi.org/10.1055/s-2002-38249.

Mirvis, M., Stearns, T., and James Nelson, W. (2018). Cilium structure, assembly, and disassembly regulated by the cytoskeleton. The Biochemical journal *475*, 2329-2353. https://doi.org/10.1042/BCJ20170453.

Mogha, A., Benesh, A.E., Patra, C., Engel, F.B., Schöneberg, T., Liebscher, I., and Monk, K.R. (2013). Gpr126 functions in Schwann cells to control differentiation and myelination via G-protein activation. The Journal of neuroscience : the official journal of the Society for Neuroscience *33*, 17976-17985. https://doi.org/10.1523/JNEUROSCI.1809-13.2013.

Monk, K.R., Hamann, J., Langenhan, T., Nijmeijer, S., Schöneberg, T., and Liebscher, I. (2015). Adhesion G Protein-Coupled Receptors: From In Vitro Pharmacology to In Vivo Mechanisms. Molecular pharmacology *88*, 617-623. https://doi.org/10.1124/mol.115.098749.

Monk, K.R., Naylor, S.G., Glenn, T.D., Mercurio, S., Perlin, J.R., Dominguez, C., Moens, C.B., and Talbot, W.S. (2009). A G protein-coupled receptor is essential for Schwann cells to initiate myelination. Science (New York, N.Y.) *325*, 1402-1405. https://doi.org/10.1126/science.1173474.

Moran, C.M., Myers, C.T., Lewis, C.M., and Krieg, P.A. (2012). Hedgehog regulates angiogenesis of intersegmental vessels through the VEGF signaling pathway. Developmental dynamics : an official publication of the American Association of Anatomists *241*, 1034-1042. https://doi.org/10.1002/dvdy.23795.

Must, A., Spadano, J., Coakley, E.H., Field, A.E., Colditz, G., and Dietz, W.H. (1999). The disease burden associated with overweight and obesity. JAMA *282*, 1523-1529. https://doi.org/10.1001/jama.282.16.1523.

Mykytyn, K., and Askwith, C. (2017). G-Protein-Coupled Receptor Signaling in Cilia. Cold Spring Harbor perspectives in biology *9*, a028183. https://doi.org/10.1101/cshperspect.a028183.

Néchad, M., Kuusela, P., Carneheim, C., Björntorp, P., Nedergaard, J., and Cannon, B. (1983). Development of brown fat cells in monolayer culture. I. Morphological and biochemical distinction from white fat cells in culture. Experimental cell research *149*, 105-118. https://doi.org/10.1016/0014-4827(83)90384-1.

Nedergaard, J., and Lindberg, O. (1979). Norepinephrine-stimulated fatty-acid release and oxygen consumption in isolated hamster brown-fat cells. Influence of buffers, albumin, insulin and mitochondrial inhibitors. European journal of biochemistry *95*, 139-145. https://doi.org/10.1111/j.1432-1033.1979.tb12948.x.

Ng, M., Fleming, T., Robinson, M., Thomson, B., Graetz, N., Margono, C., Mullany, E.C., Biryukov, S., Abbafati, C., and Abera, S.F., et al. (2014). Global, regional, and national prevalence of overweight and obesity in children and adults during 1980-2013: a systematic analysis for the Global Burden of Disease Study 2013. Lancet *384*, 766-781. https://doi.org/10.1016/S0140-6736(14)60460-8.

Nguyen, A.M., Young, Y.-N., and Jacobs, C.R. (2015). The primary cilium is a self-adaptable, integrating nexus for mechanical stimuli and cellular signaling. Biology Open *4*, 1733. https://doi.org/10.1242/bio.014787.

Nie, T., Hui, X., Gao, X., Li, K., Lin, W., Xiang, X., Ding, M., Kuang, Y., Xu, A., and Fei, J., et al. (2012). Adipose tissue deletion of Gpr116 impairs insulin sensitivity through modulation of adipose function. FEBS Letters *586*, 3618-3625. https://doi.org/10.1016/j.febslet.2012.08.006.

Nishimura, T., Honda, H., and Takeichi, M. (2012). Planar cell polarity links axes of spatial dynamics in neural-tube closure. Cell *149*, 1084-1097. https://doi.org/10.1016/j.cell.2012.04.021.

Nosavanh, L., Yu, D.-H., Jaehnig, E.J., Tong, Q., Shen, L., and Chen, M.-H. (2015a). Cell-autonomous activation of Hedgehog signaling inhibits brown adipose tissue development. Proceedings of the National Academy of Sciences *112*, 5069. https://doi.org/10.1073/pnas.1420978112.

Nosavanh, L., Yu, D.-H., Jaehnig, E.J., Tong, Q., Shen, L., and Chen, M.-H. (2015b). Cell-autonomous activation of Hedgehog signaling inhibits brown adipose tissue development. Proc Natl Acad Sci U S A *112*, 5069-5074. https://doi.org/10.1073/pnas.1420978112.

Nygaard, M.B., Almstrup, K., Lindbæk, L., Christensen, S.T., and Svingen, T. (2015). Cell context-specific expression of primary cilia in the human testis and ciliary coordination of Hedgehog signalling in mouse Leydig cells. Sci Rep *5*, 10364. https://doi.org/10.1038/srep10364.

Park, S.M., Jang, H.J., and Lee, J.H. (2019). Roles of Primary Cilia in the Developing Brain. Frontiers in Cellular Neuroscience *13*, 218. https://doi.org/10.3389/fncel.2019.00218.

Petersen, S.C., Luo, R., Liebscher, I., Giera, S., Jeong, S.-J., Mogha, A., Ghidinelli, M., Feltri, M.L., Schöneberg, T., and Piao, X., et al. (2015). The adhesion GPCR GPR126 has distinct, domain-dependent functions in Schwann cell development mediated by interaction with laminin-211. Neuron *85*, 755-769. https://doi.org/10.1016/j.neuron.2014.12.057.

Pfeifer, A., and Hoffmann, L.S. (2015). Brown, beige, and white: the new color code of fat and its pharmacological implications. Annual review of pharmacology and toxicology *55*, 207-227. https://doi.org/10.1146/annurev-pharmtox-010814-124346.

Phillips, K.J. (2019). Beige Fat, Adaptive Thermogenesis, and Its Regulation by Exercise and Thyroid Hormone. Biology (Basel) *8*, 57. https://doi.org/10.3390/biology8030057.

Prömel, S., Waller-Evans, H., Dixon, J., Zahn, D., Colledge, W.H., Doran, J., Carlton, M.B.L., Grosse, J., Schöneberg, T., and Russ, A.P., et al. (2012). Characterization and functional study of a cluster of four highly conserved orphan adhesion-GPCR in mouse. Developmental dynamics : an official publication of the American Association of Anatomists *241*, 1591-1602. https://doi.org/10.1002/dvdy.23841.

Purcell, R.H., and Hall, R.A. (2018). Adhesion G Protein-Coupled Receptors as Drug Targets. Annual review of pharmacology and toxicology *58*, 429-449. https://doi.org/10.1146/annurev-pharmtox-010617-052933.

Putnam, N.H., Srivastava, M., Hellsten, U., Dirks, B., Chapman, J., Salamov, A., Terry, A., Shapiro, H., Lindquist, E., and Kapitonov, V.V., et al. (2007). Sea anemone genome reveals ancestral eumetazoan gene repertoire and genomic organization. Science (New York, N.Y.) *317*, 86-94. https://doi.org/10.1126/science.1139158.

Qiu, Y., Nguyen, K.D., Odegaard, J.I., Cui, X., Tian, X., Locksley, R.M., Palmiter, R.D., and Chawla, A. (2014). Eosinophils and type 2 cytokine signaling in macrophages orchestrate development of functional beige fat. Cell *157*, 1292-1308. https://doi.org/10.1016/j.cell.2014.03.066.

Qu, Y., Huang, Y., Feng, J., Alvarez-Bolado, G., Grove, E.A., Yang, Y., Tissir, F., Zhou, L., and Goffinet, A.M. (2014). Genetic evidence that Celsr3 and Celsr2, together with Fzd3, regulate forebrain wiring in a Vangl-

independent manner. Proceedings of the National Academy of Sciences of the United States of America *111*, E2996-3004. https://doi.org/10.1073/pnas.1402105111.

Rahmouni, K., Fath, M.A., Seo, S., Thedens, D.R., Berry, C.J., Weiss, R., Nishimura, D.Y., and Sheffield, V.C. (2008). Leptin resistance contributes to obesity and hypertension in mouse models of Bardet-Biedl syndrome. The Journal of clinical investigation *118*, 1458-1467. https://doi.org/10.1172/JCI32357.

Razumilava, N., Gradilone, S.A., Smoot, R.L., Mertens, J.C., Bronk, S.F., Sirica, A.E., and Gores, G.J. (2014). Non-canonical Hedgehog signaling contributes to chemotaxis in cholangiocarcinoma. Journal of hepatology *60*, 599-605. https://doi.org/10.1016/j.jhep.2013.11.005.

Reverte-Salisa, L., Sanyal, A., and Pfeifer, A. (2019). Role of cAMP and cGMP Signaling in Brown Fat. Handbook of experimental pharmacology *251*, 161-182. https://doi.org/10.1007/164_2018_117.

Rhee, S.G., and Bae, Y.S. (1997). Regulation of phosphoinositide-specific phospholipase C isozymes. The Journal of biological chemistry *272*, 15045-15048. https://doi.org/10.1074/jbc.272.24.15045.

Riddy, D.M., Delerive, P., Summers, R.J., Sexton, P.M., and Langmead, C.J. (2018). G Protein-Coupled Receptors Targeting Insulin Resistance, Obesity, and Type 2 Diabetes Mellitus. Pharmacol Rev *70*, 39-67. https://doi.org/10.1124/pr.117.014373.

Riobo, N.A., and Manning, D.R. (2007). Pathways of signal transduction employed by vertebrate Hedgehogs. The Biochemical journal *403*, 369-379. https://doi.org/10.1042/BJ20061723.

Rosen, E.D., and Spiegelman, B.M. (2014). What we talk about when we talk about fat. Cell *156*, 20-44. https://doi.org/10.1016/j.cell.2013.12.012.

Rosenbaum, D.M., Rasmussen, S.G.F., and Kobilka, B.K. (2009). The structure and function of G-protein-coupled receptors. Nature *459*, 356-363. https://doi.org/10.1038/nature08144.

Rosenbaum, M., Hirsch, J., Gallagher, D.A., and Leibel, R.L. (2008). Long-term persistence of adaptive thermogenesis in subjects who have maintained a reduced body weight. The American journal of clinical nutrition *88*, 906-912. https://doi.org/10.1093/ajcn/88.4.906.

Rosenwald, M., Perdikari, A., Rülicke, T., and Wolfrum, C. (2013). Bi-directional interconversion of brite and white adipocytes. Nature cell biology *15*, 659-667. https://doi.org/10.1038/ncb2740.

Saely, C.H., Geiger, K., and Drexel, H. (2012). Brown versus white adipose tissue: a mini-review. Gerontology *58*, 15-23. https://doi.org/10.1159/000321319.

Saito, M., Matsushita, M., Yoneshiro, T., and Okamatsu-Ogura, Y. (2020). Brown Adipose Tissue, Diet-Induced Thermogenesis, and Thermogenic Food Ingredients: From Mice to Men. Front Endocrinol (Lausanne) *11*, 222. https://doi.org/10.3389/fendo.2020.00222.

Sanchez-Gurmaches, J., and Guertin, D.A. (2014). Adipocyte lineages: tracing back the origins of fat. Biochimica et biophysica acta *1842*, 340-351. https://doi.org/10.1016/j.bbadis.2013.05.027.

Sari, I.N., Phi, L.T.H., Jun, N., Wijaya, Y.T., Lee, S., and Kwon, H.Y. (2018). Hedgehog Signaling in Cancer: A Prospective Therapeutic Target for Eradicating Cancer Stem Cells. Cells *7*. https://doi.org/10.3390/cells7110208.

Scholz, N. (2018). Cancer Cell Mechanics: Adhesion G Protein-coupled Receptors in Action? Front Oncol *8*, 59. https://doi.org/10.3389/fonc.2018.00059.

Scholz, N., Gehring, J., Guan, C., Ljaschenko, D., Fischer, R., Lakshmanan, V., Kittel, R.J., and Langenhan, T. (2015a). The adhesion GPCR latrophilin/CIRL shapes mechanosensation. Cell reports *11*, 866-874. https://doi.org/10.1016/j.celrep.2015.04.008.

Scholz, N., Gehring, J., Guan, C., Ljaschenko, D., Fischer, R., Lakshmanan, V., Kittel, R.J., and Langenhan, T. (2015b). The Adhesion GPCR Latrophilin/CIRL Shapes Mechanosensation. Cell reports *11*, 866-874. https://doi.org/10.1016/j.celrep.2015.04.008.

Scholz, N., Guan, C., Nieberler, M., Grotemeyer, A., Maiellaro, I., Gao, S., Beck, S., Pawlak, M., Sauer, M., and Asan, E., et al. (2017). Mechano-dependent signaling by Latrophilin/CIRL quenches cAMP in proprioceptive neurons. eLife *6*. https://doi.org/10.7554/eLife.28360.

Schulz, T.J., and Tseng, Y.-H. (2013). Brown adipose tissue: development, metabolism and beyond. The Biochemical journal *453*, 167-178. https://doi.org/10.1042/BJ20130457.

Shan, T., Liang, X., Bi, P., Zhang, P., Liu, W., and Kuang, S. (2013). Distinct populations of adipogenic and myogenic Myf5-lineage progenitors in white adipose tissues. Journal of lipid research *54*, 2214-2224. https://doi.org/10.1194/jlr.M038711.

Sherpa, R.T., Mohieldin, A.M., Pala, R., Wachten, D., Ostrom, R.S., and Nauli, S.M. (2019). Sensory primary cilium is a responsive cAMP microdomain in renal epithelia. Sci Rep *9*, 6523. https://doi.org/10.1038/s41598-019-43002-2.

Shi, J., Zhang, X., Wang, S., Wang, J., Du, B., Wang, Z., Liu, M., Jiang, W., Qian, M., and Ren, H. (2016). Gpr97 is dispensable for metabolic syndrome but is involved in macrophage inflammation in high-fat diet-induced obesity in mice. Scientific reports *6*, 24649. https://doi.org/10.1038/srep24649.

Singer, K., Luo, R., Jeong, S.-J., and Piao, X. (2013). GPR56 and the developing cerebral cortex: cells, matrix, and neuronal migration. Mol Neurobiol *47*, 186-196. https://doi.org/10.1007/s12035-012-8343-0.

Sriram, K., and Insel, P.A. (2018). G Protein-Coupled Receptors as Targets for Approved Drugs: How Many Targets and How Many Drugs? Molecular pharmacology *93*, 251-258. https://doi.org/10.1124/mol.117.111062.

Stacey, M., Chang, G.-W., Davies, J.Q., Kwakkenbos, M.J., Sanderson, R.D., Hamann, J., Gordon, S., and Lin, H.-H. (2003). The epidermal growth factor-like domains of the human EMR2 receptor mediate cell attachment through chondroitin sulfate glycosaminoglycans. Blood *102*, 2916-2924. https://doi.org/10.1182/blood-2002-11-3540.

Stephenson, J.R., Paavola, K.J., Schaefer, S.A., Kaur, B., van Meir, E.G., and Hall, R.A. (2013). Brain-specific angiogenesis inhibitor-1 signaling, regulation, and enrichment in the postsynaptic density. The Journal of biological chemistry *288*, 22248-22256. https://doi.org/10.1074/jbc.M113.489757.

Stine, R.R., Shapira, S.N., Lim, H.-W., Ishibashi, J., Harms, M., Won, K.-J., and Seale, P. (2016). EBF2 promotes the recruitment of beige adipocytes in white adipose tissue. Molecular Metabolism *5*, 57-65. https://doi.org/10.1016/j.molmet.2015.11.001.

Suchý, T., Zieschang, C., Popkova, Y., Kaczmarek, I., Weiner, J., Liebing, A.-D., Çakir, M.V., Landgraf, K., Gericke, M., and Pospisilik, J.A., et al. (2020). The repertoire of Adhesion G protein-coupled receptors in

adipocytes and their functional relevance. International journal of obesity (2005). https://doi.org/10.1038/s41366-020-0570-2.

Syrovatkina, V., Alegre, K.O., Dey, R., and Huang, X.-Y. (2016). Regulation, Signaling, and Physiological Functions of G-Proteins. Journal of molecular biology *428*, 3850-3868. https://doi.org/10.1016/j.jmb.2016.08.002.

Taguchi, K., Kajita, K., Kitada, Y., Fuwa, M., Asano, M., Ikeda, T., Kajita, T., Ishizuka, T., Kojima, I., and Morita, H. (2020). Role of small proliferative adipocytes: possible beige cell progenitors. J Endocrinol *245*, 65-78. https://doi.org/10.1530/JOE-19-0503.

Tang, X., Jin, R., Qu, G., Wang, X., Li, Z., Yuan, Z., Zhao, C., Siwko, S., Shi, T., and Wang, P., et al. (2013). GPR116, an adhesion G-protein-coupled receptor, promotes breast cancer metastasis via the Gαq-p63RhoGEF-Rho GTPase pathway. Cancer research *73*, 6206-6218. https://doi.org/10.1158/0008-5472.CAN-13-1049.

Tobaben, S., Südhof, T.C., and Stahl, B. (2002). Genetic analysis of alpha-latrotoxin receptors reveals functional interdependence of CIRL/latrophilin 1 and neurexin 1 alpha. The Journal of biological chemistry *277*, 6359-6365. https://doi.org/10.1074/jbc.M111231200.

Tönjes, A., Koriath, M., Schleinitz, D., Dietrich, K., Böttcher, Y., Rayner, N.W., Almgren, P., Enigk, B., Richter, O., and Rohm, S., et al. (2009). Genetic variation in GPR133 is associated with height: genome wide association study in the self-contained population of Sorbs. Human molecular genetics *18*, 4662-4668. https://doi.org/10.1093/hmg/ddp423.

Trayhurn, P., and Beattie, J.H. (2001). Physiological role of adipose tissue: white adipose tissue as an endocrine and secretory organ. The Proceedings of the Nutrition Society *60*, 329-339. https://doi.org/10.1079/pns200194.

Urano, T., Shiraki, M., Yagi, H., Ito, M., Sasaki, N., Sato, M., Ouchi, Y., and Inoue, S. (2012). GPR98/Gpr98 gene is involved in the regulation of human and mouse bone mineral density. The Journal of clinical endocrinology and metabolism *97*, E565-74. https://doi.org/10.1210/jc.2011-2393.

Vaisse, C., Reiter, J.F., and Berbari, N.F. (2017). Cilia and Obesity. Cold Spring Harb Perspect Biol *9*, a028217. https://doi.org/10.1101/cshperspect.a028217.

Vernia, S., Edwards, Y.J., Han, M.S., Cavanagh-Kyros, J., Barrett, T., Kim, J.K., and Davis, R.J. (2016). An alternative splicing program promotes adipose tissue thermogenesis. eLife *5*. https://doi.org/10.7554/eLife.17672.

Villarroya, F., Cereijo, R., Villarroya, J., and Giralt, M. (2017). Brown adipose tissue as a secretory organ. Nature reviews. Endocrinology *13*, 26-35. https://doi.org/10.1038/nrendo.2016.136.

Wandel, E., Saalbach, A., Sittig, D., Gebhardt, C., and Aust, G. (2012). Thy-1 (CD90) is an interacting partner for CD97 on activated endothelial cells. Journal of immunology (Baltimore, Md. : 1950) *188*, 1442-1450. https://doi.org/10.4049/jimmunol.1003944.

Wang, L., and Dynlacht, B.D. (2018). The regulation of cilium assembly and disassembly in development and disease. Development *145*, dev151407. https://doi.org/10.1242/dev.151407.

Wang, Q.A., and Scherer, P.E. (2014). The AdipoChaser mouse: A model tracking adipogenesis in vivo. Adipocyte *3*, 146-150. https://doi.org/10.4161/adip.27656.

Wang, T., Ward, Y., Tian, L., Lake, R., Guedez, L., Stetler-Stevenson, W.G., and Kelly, K. (2005). CD97, an adhesion receptor on inflammatory cells, stimulates angiogenesis through binding integrin counterreceptors on endothelial cells. Blood *105*, 2836-2844. https://doi.org/10.1182/blood-2004-07-2878.

Waters, A.M., and Beales, P.L. (2011). Ciliopathies: an expanding disease spectrum. Pediatric nephrology (Berlin, Germany) *26*, 1039-1056. https://doi.org/10.1007/s00467-010-1731-7.

Wettschureck, N., and Offermanns, S. (2005). Mammalian G proteins and their cell type specific functions. Physiological reviews *85*, 1159-1204. https://doi.org/10.1152/physrev.00003.2005.

Yates, L.L., Schnatwinkel, C., Murdoch, J.N., Bogani, D., Formstone, C.J., Townsend, S., Greenfield, A., Niswander, L.A., and Dean, C.H. (2010). The PCP genes Celsr1 and Vangl2 are required for normal lung branching morphogenesis. Human molecular genetics *19*, 2251-2267. https://doi.org/10.1093/hmg/ddq104.

Yona, S., Lin, H.-H., Siu, W.O., Gordon, S., and Stacey, M. (2008). Adhesion-GPCRs: emerging roles for novel receptors. Trends in biochemical sciences *33*, 491-500. https://doi.org/10.1016/j.tibs.2008.07.005.

Yuan, J.S., Reed, A., Chen, F., and Stewart, C.N. (2006). Statistical analysis of real-time PCR data. BMC bioinformatics *7*, 85. https://doi.org/10.1186/1471-2105-7-85.

Zhang, Y., Proenca, R., Maffei, M., Barone, M., Leopold, L., and Friedman, J.M. (1994). Positional cloning of the mouse obese gene and its human homologue. Nature *372*, 425-432. https://doi.org/10.1038/372425a0.

List of Figures

Figure 1: Activation of GPCRs 2
Figure 2: Simplified structure of aGPCRs and mechanism of autoprotolysis 4
Figure 3: Three potential mechanisms of aGPCRs activation 5
Figure 4: Simplified structure of Gpr111 6
Figure 5: Localization of AT in humans and in mice 9
Figure 6: Schematic representation of brown adipocyte 10
Figure 7: Schematic representation of thermogenesis in brown adipocytes 11
Figure 8: Schematic representation of white adipocyte 12
Figure 9: Schematic representation of beige adipocyte 13
Figure 10: Schematic representation of primary cilium 14
Figure 11: Schematic representation of Hedgehog signalling 15
Figure 12: Canonical and non-canonical HH signaling 16
Figure 13: Schematic representation of BAs isolation for newborn BAT 21
Figure 14: Schematic representation of BAs differentiation 22
Figure 15: Schematic representation of WAs isolation 23
Figure 16: Schematic representation of differentiation of WAs 24
Figure 17: Important parts of the OROBOROS® oxygraph 28
Figure 18: Expression pattern of Gpr111 46
Figure 19: Effects of Gpr111 ablation on differentiation of BAs 48
Figure 20: Effects of Gpr111 ablation on BAs function 50
Figure 21: Lack of Gpr111 has no effect on proliferation of BAs 51
Figure 22: Loss of Gpr111 promotes differentiation of WAs 52
Figure 23: Lack of Gpr111 promotes browning of WAs 53
Figure 24: Effects of Gpr111 deletion on function of WAs 55
Figure 25: Lack of Gpr111 increases proliferation of WAs 56
Figure 26: Adult Gpr111 KO mice housed at 23ºC have higher oxygen consumption 57
Figure 27: Lack of Gpr111 in adult mice promotes browning of WAT 59
Figure 28: Gpr111 deletion promotes ex vivo oxygen consumption of AT 60
Figure 29: Cold exposure of Gpr111-/- mice cause metabolic changes 61
Figure 30: Cold exposure of Gpr111-/- mice induces massive browning of WAT 63
Figure 31: Effect of HFD on body weight, body composition and glucose tolerance of Gpr111 mice 66
Figure 32: Effect of HFD on energy expenditure and motility of GPR111 WT and KO mice 67
Figure 33: Histological analysis of ATs of Gpr111 mice after 12 weeks of HFD 69
Figure 34: qPCR analysis of ATs of Gpr111 mice after 12 weeks of ND or HFD 70
Figure 35: Western blot analysis of ATs of Gpr111 mice after 12 weeks of ND or HFD 71

Figure 36: Serum leptin levels and expression of leptin receptor in GPR111 WT and KO mice after HFD 72
Figure 37: Expression of important genes of HH signaling 73
Figure 38: Treatment of BAs with SAG 74
Figure 39: Immunostaining of cilia in BAs 75
Figure 40: Interplay between GPR111, cAMP signaling and mechanical force 77
Figure 41: Gpr111 and stress fibers 78
Figure 42: Proposed mechanism of Gpr111 signaling 81

List of Tables

Table 1: Nomenclature of aGPCRs 3
Table 2: Body mass index 8
Table 3: Substances used in measurement of oxygen consumption 29
Table 4: List of antibodies for immunofluorescence staining of cilia 32
Table 5: Ingredients needed for separation and stacking gel 36
Table 6: List of antibodies for Western blot 38
Table 7: PCR cycling program used for genotyping 39
Table 8: qPCR program 41
Table 9: qRT-PCR primer list 42